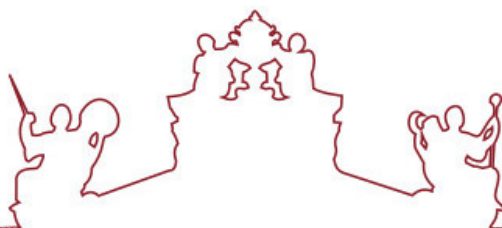




SAPIENZA
UNIVERSITÀ DI ROMA



ARISTOTLE
UNIVERSITY OF
THESSALONIKI



**Universidade de Évora - Instituto de Investigação e Formação Avançada
Università degli Studi di Roma "La Sapienza" Aristotle University of
Thessaloniki**

Mestrado em Ciência dos Materiais Arqueológicos (ARCHMAT)

Dissertação

Application of Portable XRF to Human Osteological Series from Evora and Porto

Athulya Nalini Rajan

Orientador(es) | Anne-France Maurer

Ana Curto

Francisca Alves Cardoso

Évora 2025

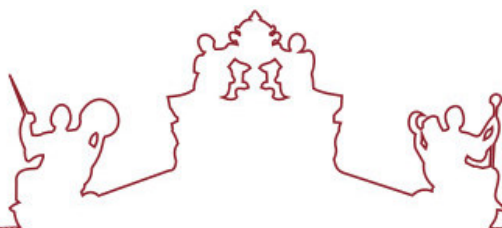




SAPIENZA
UNIVERSITÀ DI ROMA



ARISTOTLE
UNIVERSITY OF
THESSALONIKI



**Universidade de Évora - Instituto de Investigação e Formação Avançada
Università degli Studi di Roma "La Sapienza" Aristotle University of
Thessaloniki**

Mestrado em Ciência dos Materiais Arqueológicos (ARCHMAT)

Dissertação

**Application of Portable XRF to Human Osteological Series
from Evora and Porto**

Athulya Nalini Rajan

Orientador(es) | Anne-France Maurer

Ana Curto

Francisca Alves Cardoso

Évora 2025

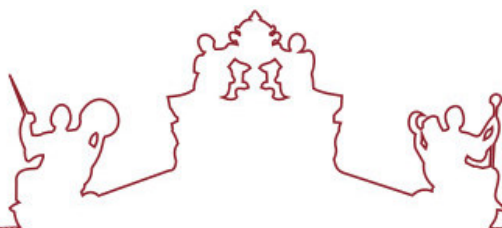




SAPIENZA
UNIVERSITÀ DI ROMA



ARISTOTLE
UNIVERSITY OF
THESSALONIKI



A dissertação foi objeto de apreciação e discussão pública pelo seguinte júri nomeado pelo Diretor do Instituto de Investigação e Formação Avançada:

Presidente | Nicola Schiavon (Universidade de Évora)

Vogais | Anne-France Maurer (Universidade de Évora)
Cristina Barrocas Dias (Universidade de Évora) (Arguente)
Donatella Magri (Università degli Studi di Roma "La Sapienza")
Federico di Rita (Università degli Studi di Roma "La Sapienza")
Ioannis Kozaris ()
Panagiotis Spathis (Aristotle University of Thessaloniki)

Abstract

The aim of the presented work is to evaluate the scope of portable XRF as a non-invasive compositional analytical tool for the investigation for human remains from archaeological context. In relation to the study, individual from two archaeological sites (I) Necropolis at Church Third Order of our Lady of Carmo, Porto and (ii) Church of Espírito Santos and Collection of identified skeletons of Évora, dated to the time frame of 15th- 19th century AD were quantitatively analysed to examine the elemental distribution within the individual. Concentration of elements such as Ca, P, Mn, Ni, Fe, Zn and Sr in archaeological bones were accurately detected. As per the obtained values, possible intra variation is observed for all individual studied from the sites. An intra -skeletal variability is observed within the individual was comparatively low for various elements. A comparative approach performed on the site ways to analyse variability among individuals from same locality and different sites indicating possibilities of variation for Ca and Zn. A positive relation among the values Ca, P and Ni indicating for individuals irrespective of pathological condition.

Key words: p-XRF, Evora, Porto, intra-bone variability, intra-skeletal variability, diet, diagenesis

Resumo

O objetivo do trabalho apresentado é avaliar o alcance do XRF portátil como uma ferramenta analítica de composição não invasiva para a investigação de restos humanos a partir do contexto arqueológico. Em relação ao estudo, indivíduos de dois sítios arqueológicos (I) Necrópole da Igreja Terceira Ordem de Nossa Senhora do Carmo, Porto e (ii) Igreja do Espírito Santos e Coleção de esqueletos identificados de Évora, datados do período temporal dos séculos 15-19 d.C. foram analisados quantitativamente para examinar a distribuição elementar dentro do indivíduo. A concentração de elementos como Ca, P, Mn, Ni, Fe, Zn e Sr em ossos arqueológicos foi detetada com precisão. De acordo com os valores obtidos, observa-se uma possível variação intra para todos os indivíduos estudados a partir dos locais. Uma variabilidade intra-esquelética é observada dentro do indivíduo foi comparativamente baixa para vários elementos. Uma abordagem comparativa realizada no local forma de analisar a variabilidade entre indivíduos da mesma localidade e diferentes.

Palavras-chave: p-XRF, Évora, Porto, variabilidade intraóssea, variabilidade intra-esquelética, dieta, diagénese

Acknowledgments

I would like to express my sincere gratitude to Professor Anne-France Maurer, supervisor of this thesis, Professor Ana Curto and Professor Francisca Alves Cardodso, co supervisors of the thesis for their systematic guidance, unwavering patience, motivation and immense knowledge, which consistently inspired the successful completion of this work.

I would also like to acknowledge Dr. Massimo Beltrame for his immense help and advices received during the course of analysis.

I extend my gratitude to Dr. Celia Lopes and BeFrail Project and associated members for providing human remains to conduct the analysis as part of the study.

I also thank Biological Anthropology Laboratory of Department of Biology of University of Evora for providing space to conduct a safe and successful analysis.

My gratitude extends to all the faculties of the HERCULES Laboratory, University of Evora and Biological Anthropology Laboratory of Department of Biology of University of Evora for their support and guidance.

I am also grateful to HERCULES Laboratory, University Evora for the resources and support provided for the completion of this work.

I would also like acknowledge to Erasmus Mundus Association for funding the project and providing an insightful academic opportunity.

Last but not the least, a special thanks to all my friends and family, for providing a stimulating, encouraging and fun environment in which to learn and grow throughout this journey.

TABLE OF CONTENTS

LIST OF TABLES	III
LIST OF FIGURES	V
CHAPTER 1: INTRODUCTION	1
CHAPTER -2: PORTABLE XRF: AN OVERVIEW	4
2.1. History of p-XRF as an analytical tool	4
2.2. Principles of p-XRF	6
2.3. Production of characteristic fluorescence radiation	7
2.4. Instrumentation	9
2.5 Elemental detection limits of p-XRF	10
2.6 p-XRF in archaeology and cultural heritage	11
2.7 Archaeological human remains	14
2.8 p-XRF application for archaeological human remains	17
[(i)] Methodological studies for analysis of human remains	17
(ii) Dietary studies	18
(iii) Evaluation of taphonomic alteration affecting osseous tissues	18
(iv) Resolving commingled human remains	19
(v) Pathological examination of archaeological bones	21
(vi) Toxicity or medical treatment detection	23
2.9 Limitation of p-XRF for the analysis of human remains	23
CHAPTER-3: ARCHAEOLOGICAL BACKGROUND OF HUMAN REMAINS	29
3.1 Hospital of Third Order of Our Lady of Mount Carmo: excavation and historical background	30
3.2 Brief history of necropolis at Hospital of Third Order of Our Lady of Mount Carmo, Porto	32
3.3 Burial context of specimen recovered from church of Espírito Santo, Évora	37
3.4 Collection of Identified Skeletons of Évora	34
CHAPTER -4: METHODS AND MATERIALS	39
4.1 Human remains under study	39
4.2 Pre-treatment of samples	40
4.3 Bone element selection	40
4.4 Device and parameter included for the analysis	41

4.5 Safety precautions for scanning with p-XRF	42
4.6 Method creation using ARTAX software for quantification of elements	43
CHAPTER-5: RESULTS AND DISCUSSION	45
5.1 Precision	45
5.2 Accuracy	48
5.3 Reliability of measurement- from the analysis of human remains	50
5.4 Intra- bone variability	51
5.5 Intra -skeletal variability	56
5.6 Inter -individual variability within the individuals from Porto	58
5.7 Inter -individual variability within the individuals from Évora	59
5.8 Variation between individuals from Évora and Porto	66
5.9 Ca, P, and Ca/ P	67
5.10 Pathological evaluation of individuals	70
5.11 Diet and diagenesis from the analysis	75
CHAPTER 6: CONCLUSION	76
6.1 Practical suggestions for non-invasive p-XRF analysis of human bone tissues	79
REFERENCES	81
APPENDIX	93
A.1: List of analysed individuals and bone types from all archaeological contexts	93
A.2: ANOVA results for intra-bone variation	95
A.3 ANOVA and post-hoc analysis results from cranial bone of necropolis at Hospital of Third Order of Our Lady of Carmo, Porto	97
A.4 Cranium from Ossuary of the church of Espírito Santo, Évora-Normality Check	98
A.5 Shapiro-Wilk test result for cranial bones from the church of Espírito Santo, Évora(IESE)	98
A.6: T -test result for cranial bones from the church of Espírito Santo, Évora	99
A.7: Results of ANOVA and post- hoc analysis on measurements of individuals from the church of Espírito Santo (IESE) and Collection of identified Skeletons of Évora	99
A.8: ANOVA and post-hoc analysis results on individuals from Porto and Évora	100
Measurements from analysis of human remains	101
Images of analysed human remains	129

LIST OF TABLES

Table 1: Factors affecting reproducibility and replicability of p-XRF studies	21
Table 2: Summary of reviewed articles on analysis of human remains with p-XRF from	23
Table 3: Archaeological human remains, chronology, and burial context	27
Table 4: Historical sequence of occupation identified from excavation at necropolis at Hospital of Third Order of Our Lady of Mount Carmo, Porto	28
Table 5: Description of individual remains excavated from the crypt of Church of Espírito Santos, Évora collected from excavation report	32
Table 6: Details of individuals selected from Collection of Identified Skeletons of Évora(CEIE)	35
Table 7: Details of analysed human remains	36
Table 8: General parameter set up for TRACER handheld XRF Unit	39
Table 9: Mean and SD obtained for NIST 1400 Bone Ash	46
Table 10: Comparison of verified element concentrations with three different techniques	46
Table 11: Frequency table for RSD% measurements for bones	47
Table 12: ANOVA results for Intra-skeletal Variability	55
Table 13: Mean concentration and SD for cranial bones from Porto	56
Table 14: Concentration of various elements reported in archaeological and modern human bones	60
Table 15: Mean concentration and SD for various bones from ossuary and crypt of Church of Espírito Santos, Évora	61
Table 16: Mean concentration and SD for various bones from collection of identified skeletons of Évora (CEIE)	61
Table 17: Correlation matrix for cranial bones from Church of Espírito Santo, Évora	63
Table 18: Mean and standard Deviation between individual from IESE and CEIE	64
Table 19: Mean and SD from the cranial bones Measurements from Porto and Évora	65
Table 20: Ca/P Ratio reported in literature	67
Table 21: Mean and SD of Ca and P and Ca/P	67
Table 22: Elemental concentration reported from palaeopathological studies	70
Table 23: Mean concentration calculated for individual with pathology and no pathology and female and male Individuals	72
Table 24: Correlation matrix for measurement of elements in individual	

LIST OF FIGURES

Figure 1: William Cohnrad Rontgen	4
Figure 2: Charles Barkla	4
Figure 3: Henrey Mosley	5
Figure 4: First spectrometer by Henrey Moseley	5
Figure 5: Hanford nuclear reserve handheld XRF for U (1982)	6
Figure 6: Tracer II Unit- 1st X-ray tube with silver (Ag) anode from key master(2001)	6
Figure 7: Pictorial representation of X-ray interaction with matter	7
Figure 8: Characteristic X-ray production	8
Figure 9: Schematic representation of p-XRF device and components within	9
Figure 10: Element detection range of p-XRF	11
Figure 11: Number of publications in archaeology with the application of HH-XRF	12
Figure 12: Different fields for application of HH-XRF within archaeology	13
Figure 13: Structure of cortical and trabecular bone sections	15
Figure 14: Epiphyseal, metaphyseal, and diaphyseal region of a long bone	16
Figure 15: Location of different archaeological sites of analysed human remains	29
Figure 16: Individual burial from first phase of excavation, Porto	32
Figure 17: Collective burial from first phase of excavation, Porto	32
Figure 18: Remains of burial from second phase	34
Figure 19: IESE/21-1 Skeleton in coffin	34
Figure 20: IESE/21-2 and IESE/21-2	33
Figure 21: IESE/21-4 Skeleton completely covered with lime	37
Figure 22: IESE/21-5 Skeleton partially covered with lime	37
Figure 23: Analysed spots in cranial bone of SKL1	41
Figure 24: Analysed spots in femur of SKP1	41
Figure 25: Machine set up for analysis	43
Figure 26: Homogenised mean concentration of routine measurement of SRM NIST1400 bone ash	46
Figure 27: Relative standard deviation from measurement of SRM NIST 1400 Bone Ash	47
Figure 28: Elements with less than 30% of relative standard deviation from measurement of SRM NIST 1400 Bone Ash	47
Figure 29: Intra-bone mean and standard deviation for Fe and Zn content in individuals	

from Porto and Évora	54
Figure 31: Intra-bone mean and standard deviation for Ni content in individuals from Porto and Évora	55
Figure 32: Intra-bone mean and standard deviation for Mn and Sr content in individuals from Porto and Évora	55
Figure 33: Intra-skeletal homogenised mean and SD of element concentration in individuals from the Church of Espírito Santo and collection of identified skeletons of Évora (in ppm)	56

CHAPTER- 1

INTRODUCTION

Bone is a dynamic, living tissue that plays a crucial role in various physiological functions within the human body. It supports the maintenance of blood vessels, provides a storage facility for fat, and serves as a repository of certain elements such as calcium, and phosphorous. At the molecular level, bone comprises both organic and inorganic components (Zimmerman, 2015). During primary mineralization, actively forming skeletal regions incorporate major and minor elements. The absorption of these chemical elements into various bone regions is influenced by turnover rates, which are tissue- and bone-specific (Simpson et al., 2021). For example, among the two bone sections, trabecular (cancellous) bone has a higher rate of turnover than cortical bone, which in turn results in varying thickness and density along the external layer of the bone. Similarly, bone types such as ribs and phalanges experience faster renewal than long bones like the femur and humerus (White et al., 2012). Owing to its renewal over time, bone is considered an archive for analysing major and minor elements that provide relevant information on diet, mobility, pathology, and diagenesis in bioarchaeological studies (Lachowicz et al., 2017). Traditionally, bioarchaeological studies on bone compositional analysis rely on different analytical techniques such as ICP-MS, AAS-MS, which are invasive in nature. This study explores the potential of portable XRF, a non-destructive analytical technique to examine major and minor elements in the human bones collected from diverse archaeological contexts.

As mentioned earlier, key elements such as calcium (Ca), phosphorous (P), zinc (Zn), copper (Cu) are significant for the growth and remodelling process in bones. Similarly, elements like strontium (Sr), barium (Ba), iron (Fe) can form part of the archaeological bones composition through diet, diagenesis, and via other pathways (Giblin, 2004). Elemental concentrations vary among individuals due to differences in diet, environmental exposure, and pathological conditions (Skytte & Rasmussen, 2013; Arroyo et al., 2008; Rasmussen et al., 2019). For instance, the presence of Zn and Cu in archaeological human bones has been linked to diets rich in animal and marine resources (Allmae et al., 2012). The Ba/Ca and Sr/Ca ratios serve as proxies for differentiating marine and terrestrial diets, given the lower Sr/Ba ratios observed in seawater (Szostek, 2009). Elemental compositions are also connected to palaeopathological conditions, reflecting metabolic and pathological changes in human physiology. Elements such

as Mg, Zn, Fe, and Cu, essential for health, can indicate pathological states when their levels deviate from the norm (Zdráhal et al., 2021). Accurate interpretations of dietary and palaeopathological findings depend on understanding diagenetic processes, which involve chemical, physical, and microbial interactions affecting bone's mineral and organic components (Loyl et al., 2023; Moroni et al., 2014). The elements from groundwater and burial soil may infiltrate the bone matrix through cracks and voids via ionic exchange (Carvalho et al., 2007). Elemental mapping and quantification provide critical insights into how different elements integrate into bones.

This work aims at evaluating portable XRF as a non-invasive analytical tool for exploring human skeletal remains collected from various archaeological contexts. Portable XRF, a compact version of laboratory XRF, has proven effective for analysing the composition of various artefacts, including biological remains such as bones and teeth. Although p-XRF is widely used in archaeometry, its application in studying archaeological human remains is less explored. With the developed methodology, this study will focus on analysing chemical composition of human remains acquired from three archaeological sites within Portugal. The archaeological sites considered are (i) necropolis associated with Hospital of Third Order of Our Lady of Carmo, Porto (19th century AD), in association with BeFRAIL Project, as results of this work may be helpful to narrate the context of Porto in Times of Cholera and War (DOI: 10.54499/2022.02398.PTDC) (ii) crypt and ossuary connected to the Church of Espírito Santo, Évora (15th -19th century AD) and individual skeletons selected from the collection of Identified Skeletons of Évora (CEIE) housed in Biological Anthropology Laboratory of Department of Biology of University of Évora (19th century AD).

The selected cluster of human remains included four cranial bones from the necropolis at Porto, five individuals cranial bones from the ossuary and multiple bones of five individuals from the crypt of the Church of Espírito Santo, Évora. In addition, three individuals with pathological lesions in their skeletal remains and three individuals with no visible pathological alterations are also included in this analysis. Apart from anthropological examination, compositional analyses were not performed on these bioarchaeological remains. With this proposed study, a focus will be given to examine intra-individual and inter-individual variability based on elemental concentration. Parallely, the study will evaluate how the quantified elements can address various aspects concerning these individuals such as diet,

environment, affected pathology, and state of these remains in terms of diagenesis. To accomplish the aforementioned aim, the following objectives will be sought:

1. Evaluate which elements can be measured in bones using p-XRF and develop an appropriate sampling strategy.
2. Evaluate intra-bone and the intra-skeletal variabilities of the measured elements.
3. Evaluate the differences in the measured elements observed within individuals from Évora.
4. Evaluate the differences in the measured elements observed within individuals from Porto.
5. Evaluate the differences in the measured elements observed between individuals from Porto and Évora.
6. Evaluate the influence of bone pathologies on the concentration of measured elements.
7. Evaluate the how elemental concentrations are related to bone diagenesis, diet, health, environment.

CHAPTER -2

PORTABLE XRF: AN OVERVIEW

The rapid and simultaneous multi-elemental analysis conducted on-site has significantly broadened the utilisation of portable X-ray fluorescence (p-XRF) across various disciplines, including geology, pharmaceuticals, geochemistry, industrial science, and archaeometry. p-XRF facilitate both in situ and laboratory-based compositional analysis of prepared and unprepared solid samples. Studies highlighting the utility of p-XRF emphasize its compact design, low power consumption, minimal weight, operational capacity at varying voltages (40 keV to 60 keV), and microampere-range currents. These characteristics make p-XRF particularly advantageous for site prospection of raw materials and the analysis of immobile artifacts (Potts and Sargent, 2022). Furthermore, Barago et al. (2022) notes that the miniature size and battery-powered operation of p-XRF help in in-situ analysis.

2.1. History of p-XRF as an analytical tool

The discovery of unidentified radiation emanating from gas-filled discharge tubes, by Wilhelm Conrad Rontgen in 1895 gave birth to X-rays (see Figure 1). He named it by adopting the same notation used for an unknown variable in mathematical expression (Piorek, 1997; Panchbhai, 2015). Rontgen also used X-rays to produce the first radiograph of the human palm in the same year. This has been a turning point in delineating the structure of DNA double helix later.



Figure 1: William Cohnrad Rontgen (Britannica, 2024)



Figure 2: Charles Barkla (Britannica, 2024)

Charles Barkla, a Nobel prize awardee physicist discovered that each element has a characteristic spectrum when scattered by gas (See figure 2). This led to the finding of polarization of X-rays, gaps in the atomic absorption, and X-ray series such as K, L, M which form the characteristic radiations. The phenomenon of X-ray diffraction by Max von Lue also took place during the same duration. Later Sir William Bragg formulated Bragg's Law of Diffraction. The utilization of X-ray in World War I led to the development of a mobile X-ray unit by Madam Curie, which was used to create imaging of soldiers in war fields (Gancz, 2019). In 1913 Henrey Moseley was the first to use X-ray for analysis (see figure 3). The instrument he built was the primitive form of what is used today (see Figure 4)(Gancz, 2019).

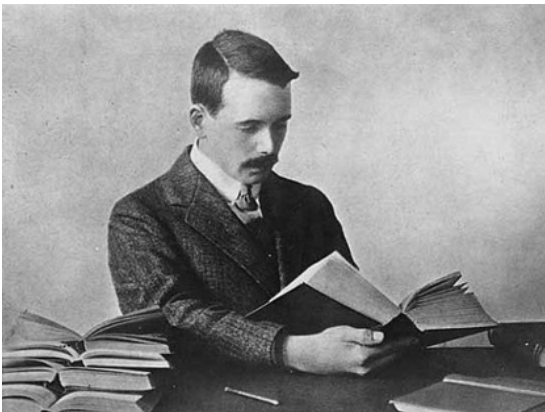


Figure 3: Henrey Mosley
(History of Science Museum, n. d)



Figure 4: First spectrometer by Henrey Moseley
(History of Science Museum, n. d)

Commercial X-ray spectrometers for industrial applications were introduced in 1948. R. Clocker and H. Schreiber were the first to apply this technique for quantitative analysis. However, it took several more years to develop detector technology to catch up, allowing it to be applied in a practical setting. Prototypes of p-XRF became widely available for explorations in the late 1970s and early 1980s. The first p-XRF weighing 31 kg was created in 1982 with a measurement head connected to a trolley to display the data electronically (see Figure 5). The use of radon technology was another main feature in early p-XRF machines. In 1994, the first p-XRF with a real-time digital signal processing feature and a silicon PIN diode was created. The lightest element that was possible to detect by the tool was titanium (Portable Spectral Service, n. d).

Between 1984 and 2000, Chinese scientists developed an IEP-2000P p-XRF machine incorporating ^{238}Pu isotopes (Lemiere, 2013; Potts and West, 2008). The radioisotope excitation used in earlier machines was replaced with advanced X-ray tube technology around

2000. The X-ray tubes offered improved safety, faster analysis time, and lower detection limits compared to the radioisotopes. Additionally, it weighed 2-3 kg and the lightest element that was measurable by the new tool was magnesium. Traditionally used Si(Li) detectors and HPGe are replaced with non-cryogenic detectors to manage the limitations arising from liquid cooling nitrogen and portability (Longoni et al., 1998). The first TRACER II p-XRF is illustrated in Figure 6, which is the earliest prototype of the machine selected for the current analysis.



Figure 5: Hanford nuclear reserve handheld XRF for U (1982) (Portable Spectral Service, n.d)



Figure 6: Tracer II Unit- 1st X-ray tube with silver (Ag) anode from key master(2001) (Portable Spectral Service, n.d)

2.2. Principles of p-XRF

The fundamental principle behind p-XRF and laboratory XRF is the measurement of the energy of photons emitted by a material irradiated with X-rays. This helps in detecting the elemental composition and their respective concentration within the examined material. X-rays are a type of electromagnetic radiation with a wavelength between 0.01nm-10.0nm and of energy in the range of 125keV-0.125keV (Brouwer, 2003). These radiations are generated by electrons slowed down in the outer space of the atomic nucleus or by a change in bound states of electrons in the electronic shell of an atom (Ribeiro et al., 2017). When a beam of X-ray photon is directed towards a material, three phenomenons take place (i) a fraction of the beam will be transmitted through the material (ii) another fraction of the radiation is absorbed by the material resulting in fluorescence, and (iii) the remaining is scattered (see Figure 7). Here, scattering can occur in two ways: (i) Compton scattering which involves an energy loss associated with scattering, and (ii) Rayleigh scattering, which happens without any energy

loss. These mentioned phenomena can be influenced by the energy of photons, thickness, density, and composition of the material that is investigated (Brouwer, 2003).

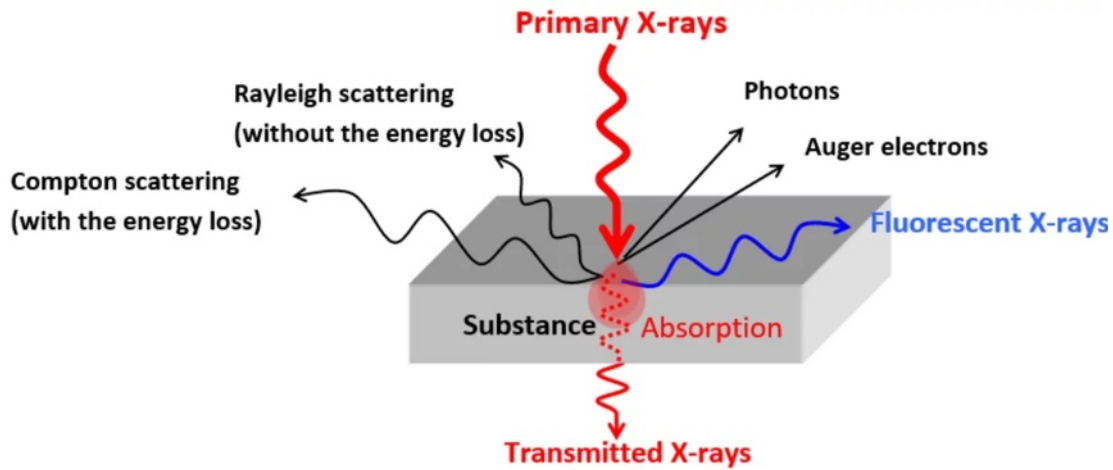


Figure 7: Pictorial representation of X-ray interaction with matter (HORIBA SCIENTIFIC, n. d)

2.3. Production of characteristic fluorescence radiation

High-energy X-ray beams can eject electrons from the innermost shells of an atom in the object they strike. On incidence, the photons transfer the energy to the electron, causing it to gain energy greater than that of its binding energy. As a result, electrons are expelled from the atom, putting it in an unstable excited state with a higher energy. This leads to several phenomena including fluorescence. An electron from outer most shell of the atom replaces the hole created in the innermost shell by the result of the aforementioned events. The energy difference between these two shells can result in X-ray emission, since the outermost shell has more energy than that of the shell to which the electron is added. Each atom has specific energy levels, so the emitted radiation is characteristic of that atom. An atom can emit more than a single energy (or line) because different holes can be produced and different electrons can fill these holes, as depicted in Figure 8 (Brouwer, 2003).

The collection of emitted lines is characteristic of the element and are considered as the fingerprint of the atom. The characteristic frequency of the atom is proportional to the difference in the binding energy between two electrons involved in the fluorescence emission and to the atomic number of the nucleus (Pinto, 2018). To expel an electron within an atom, the

energy of the X-rays must be higher than the binding energy of the electron (energy required to remove an electron from an atom). Electrons in the inner shells have higher binding energy than electrons in the outer shells. An electron is expelled when it absorbs incoming radiation. If the energy of incoming radiation is too high, photons will pass through the atoms without being absorbed, leading to fewer ejections of electrons. This process reduces absorption and consequently lowers the fluorescence. Conversely, if the energy of an incoming photon is lower and comes closer to the binding energy of the shell, higher absorption will occur. The highest yield is reached when the energy of the incoming photon is just above the binding energy of electrons to be expelled (Brouwer, 2003).

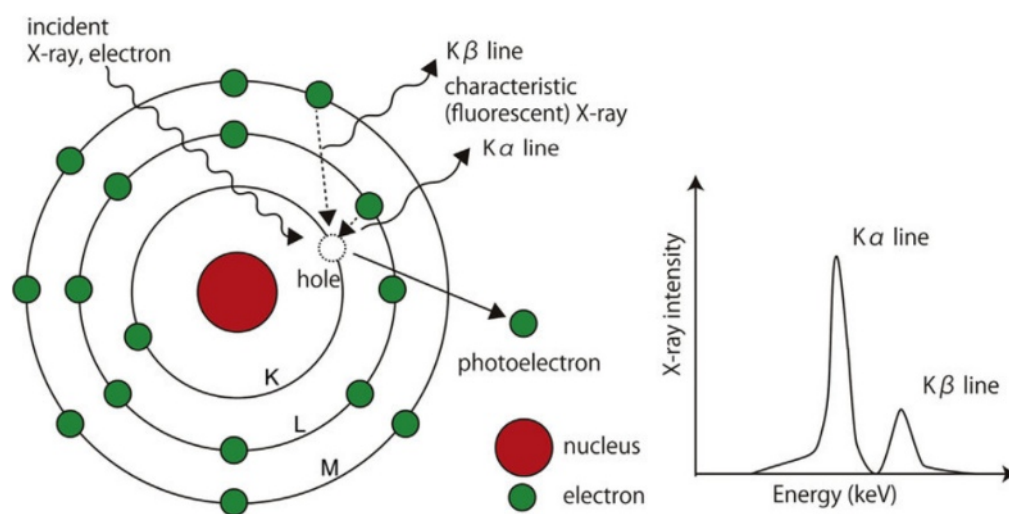


Figure 8: Characteristic X-ray production (Radiology Star, 2022)

There are instances, when the initial vacancies created by incoming radiation do not result in fluorescence. This scenario can give rise to Auger electron emission, where the atom readjusts itself to a more stable state by ejecting one or more electrons instead of giving out photons. Another phenomenon associated with fluorescence is a jump, which happens when the energy is too low to expel electrons from the corresponding shell but high enough to expel electrons from the lower shell. This will result in a jump or edge in the spectrum. Fluorescence yield is the measure to assess the success of the phenomena. It is defined as the ratio of the emitted fluorescent photons to the number of initial vacancies created. Yield is usually low for light elements, making it difficult to measure (Brouwer, 2003).

2.4. Instrumentation

A portable XRF machine consists of mainly six prominent parts: (i) X-ray source (ii) preamp (iii) detector (iv) digital signal processor (v) CPU which includes USB port, and (vi) wireless and storage part, as illustrated in Figure 9.

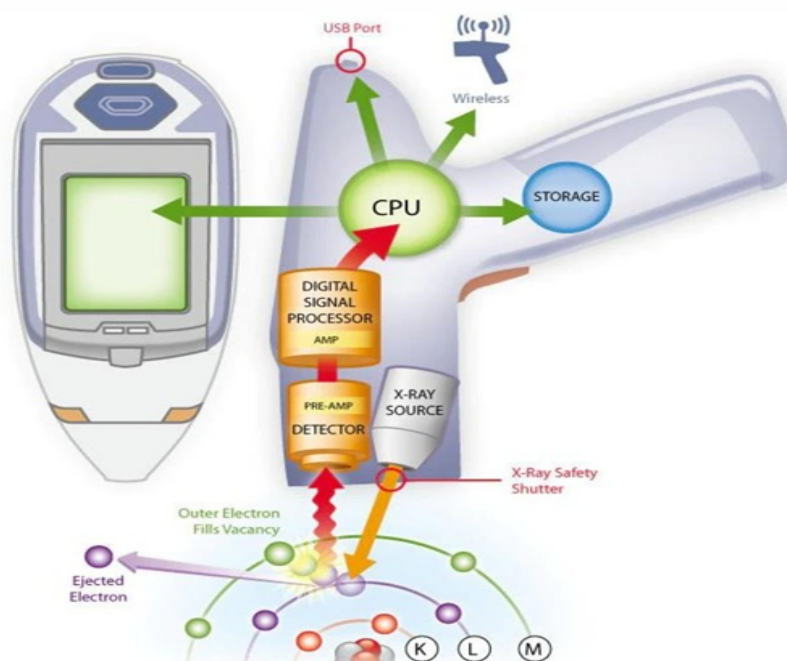


Figure 9: Schematic representation of p-XRF device and components within (Portable Analytical Solutions, n. d)

The X-ray excitation source emits radiation that interacts with the sample to generate secondary X-ray fluorescence. The emitted photons can be high-energy X-rays or gamma rays. Portable instruments such as p-XRF use gamma rays due to low energy requirements. There are mainly two different configurations for radioactive isotopic excitation sources, that are used in some devices such as ^{55}Fe , ^{109}Cd , and ^{241}Am . Nowadays, a miniature X-ray tubes dissipating lesser watts are widely in use instead of radioisotopes (Thompson, 2009).

Fluorescence X-rays generated as the result of excitation are detected by an energy-dispersive system, which forms the fundamental part of the p-XRF machine. Over time, several types of detectors were used in the p-XRF instrument and have been modified to make adjustments in its designs. So that the upgraded features support easy handling, detection level, and power consumption. The choice of detectors also depends on specific applications and energy ranges.

The two types of detectors mainly employed in modern p-XRF technology are as follows:

(i) SDD/Silicon Drift Detectors are used in high-count rate applications. A larger extent of the active area of the detector can facilitate efficient gathering and processing of X-ray counts. Instruments with SDD are applied in investigations that need extreme sensitivity. It can also be utilized for the detection of light elements such as Magnesium (Mg), Aluminium (Al), Silicon (Si), Phosphorous (P), and Sulphur (S) (Portable Analytical Solutions, n. d).

(ii) PIN detectors: High-performance and high-resolution capable detectors conventionally used for different applications. Instruments with Silicon PIN detectors are sensitive to X-rays from elements with higher atomic numbers than those of sulphur and are less expensive and robust than SDD (Portable Analytical Solutions, n. d).

The characteristic X-rays received by detector are converted into electronic pulses. These electronic pulses are sent to the preamp, which amplifies the signal and transfers it to the digital signal processor (DSP). The DSP collects and digitizes the X-ray events by sorting counts from each element through the DSP channel and sends the spectral data to the main CPU for further processing. The CPU contains algorithms for calculating the concentration of each element from their count rate data (Portable Analytical Solutions, n. d). Hence, from the data processed in the CPU, we derive detailed compositional data, which includes qualitative and quantitative information regarding the elements within the sample. CPU displays and stores these data in the memory for further review (Bloch, 2015)

2.5 Elemental detection limits of p-XRF

The p-XRF equipment, with the inbuilt features can detect and quantify elements primarily from medium to higher range of atomic numbers (see Figure 10). The detection level of the element range varies as per the machines, and additional factors such as the voltage of the X-ray tube, anode, detector technology, and filter used (Piorek, 1997; Lemiere, 2018). Filter selection can be done manually based on the type of material that needs to be analysed. This helps in eliminating the Rh and Pd L-lines from the spectra, as the p-XRF spectrometer includes a Rh X-ray tube and Pd slits. These elemental peaks of Rh and Pd can also interfere with the peaks of S and Cl in the spectra. The combination of appropriate tube powers with filters can also facilitate more sensitive detection (Bruker, 2024).

H	Elements for pXRF analysis															He	
Li	Be											B	C	N	O	F	Ne
Na	Mg											Al	Si	P	S	Cl	Ar
K	Ca	Sc	Ti	V	Cr	Mn	Fe	Co	Ni	Cu	Zn	Ga	Ge	As	Se	Br	Kr
Rb	Sr	Y	Zr	Nb	Mo	Tc	Ru	Rh	Pd	Ag	Cd	In	Sn	Sb	Te	I	Xe
Cs	Ba	La	Ce	Pr	Nd	Pm	Sm	Eu	Gd	Tb	Dy	Ho	Er	Tm	Yb	Lu	
			Hf	Ta	W	Re	Os	Ir	Pt	Au	Hg	Tl	Pb	Bi	Po	At	Rn
Fr	Ra	Ac	Th	Pa	U	Np	Pu	Am	Cm	Bk	Cf	Es	Fm	Md	No	Lr	

	cannot be analysed by pXRF, or out of scope of field analysis
	may be analysed with specific pXRF technologies
	may be analysed according to contents and matrix with current equipment
	can be analysed by pXRF in most cases
	detected but cannot be analysed individually by current equipment

Figure 10: Element detection range of p-XRF (Lemiere, 2018)

2.6 p-XRF in archaeology and cultural heritage

Application of p-XRF in archaeometric investigations surged in the last three decades. An increased reliability and applicability of the technique for archaeological investigation have been reported from 1991 onwards (Johnson et al., 2024) (see Figure 11). Early applications of this technique in archaeology include copper smelting site prospection in Oman, followed by archaeo-metallurgical studies carried out in Turkey. Roberts (1960) mentions the effects of corroded metal on artefacts surface based on the results obtained using p-XRF analysis, which also implies the emergence of p-XRF technology in archaeological studies around 50 years ago. Remarkably, this technique is mainly attributed to site surveys, fieldwork, and excavations, due to the instantaneous feedback of the system and its portability. These features help in conveniently designing a sampling strategy by reducing the need for extensive logistic transport, as well as for creating a framework for the field surveys, taking into account both time and cost involved (Frahm and Doonan, 2012). Similarly, p-XRF to analyse soil chemistry to reconstruct and detect the pattern of settlement, occupational levels, and stratigraphic prospection are some other aspects discussed in archaeological studies (Gauss et al., 2012). This tool is applied to the conservation studies on pigments and inorganic materials, mostly in situ manner. Elemental determination using p-XRF can identify the compositions of pigments containing cobalt, chromium, lead, etc. On the other hand, artworks with the combined use of synthetic and organic paintings as well as in complex mixtures pose limitation in the use of p-XRF (Capobianco et al., 2018). Zoo-archaeological studies have used p-XRF to differentiate

different animal bones found across the archaeological contexts, discussed in the works by Nganvongpanait et al. (2016).

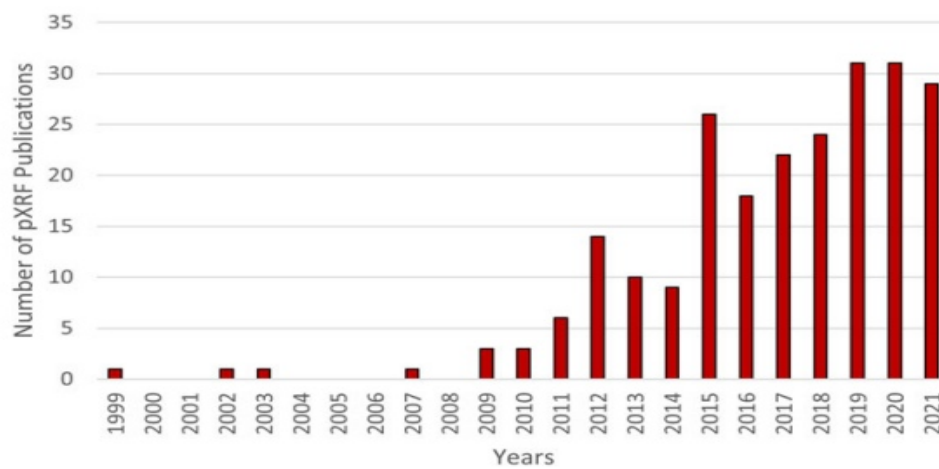


Figure 11: Number of publications in archaeology with the application of HH-XRF (adapted from Johnson et al., (2024))

Frahm and Doonan (2021) mention a few devices that appeared in the research publications as portable XRF because of their portability. These include (i) small bench top XRF, which is also portable and widely used in museum studies or conservation, (ii) set up of XRF components that can be transported and reassembled into the form for fieldworks and museum analysis, and (iii) hand-held XRF or Field-portable XRF, which is the specific one applied for this work and is of interest. Hence reviewing the literature gives glimpses of these three types of XRF machines. Comparing the studies done with handheld XRF in archaeology to that of above mentioned portable XRF tools, an increasing use of the former is visible. Frahm and Doonan (2012) propose an estimation of the handheld XRF publications so far appeared in archaeological studies as in Figure 12. This indicates the technique's suitability for in situ analysis, which popularised its use in museums, churches, memorials, and cemeteries. Similarly, studies also mention technique development and testing to assess the compatibility and performance of this method on archaeological and experimental findings. Further, chemostratigraphic analysis to build human settlement patterns or identifying potential excavation area has made use of p-XRF. For instance, Gauss et al. (2013) conducted a study at a multilayer Early Bronze Age site, Fidvar in Western Slovakia. The main focus of this study was to analyse the potential and limits of portable XRF in examining anthropogenic sediments, thereby proposing an effective strategy for fieldwork, by integrating multi-elemental analysis. Hence, they compared the soil sample obtained through drilling the core with p-XRF and AAS. Another

study that provides a different outlook on fieldwork and excavation using handheld XRF was conducted by Davis et al. (2012). The authors performed direct analyses on excavated wall profiles with HH-XRF, to link artefact-bearing sediments to the lithographic layer. This study stands as a unique excavation framework combined with soil chemometrics.

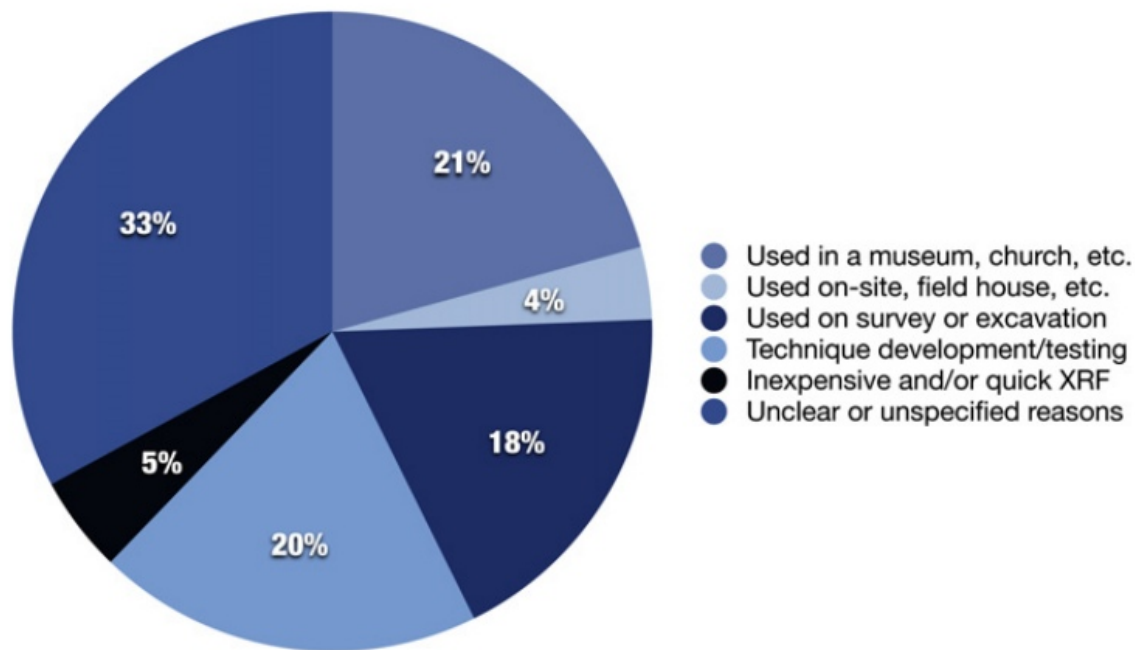


Figure 12: Different fields for application of HH-XRF within archaeology (adapted from Frahm and Doonan(2012))

Similarly, quantitative information from Figure 12 indicates HH-XRF as an alternative to lab XRF, later often requires rigorous sample preparation. Frahm and Doonan (2012) give an overall estimate of different materials studied using handheld XRF. Studies on obsidian and lithic artifacts are at the forefront, where the method helps in geo sourcing and provenance detection, thereby reducing the load of fieldwork involved. Clay and ceramic objects were also analysed with p-XRF in large quantities. Other frequently explored cultural materials are paintings and pigments, mostly in situ manner. Hence this technique enable working at museums, churches or even in remote areas with prehistoric paintings.

In addition, utilisation of p-XRF extends to diverse fields such as forensic science, bioarchaeological and bio-anthropological sciences, environmental science, primatology, and palaeontology. Forensic science employs this technique to evaluate biological fluids, blood clots, and saliva apart from bones, teeth, and hair fibres. Non-invasive nature of this technique

aids in the analysis of evidence in direct mode without causing any damages to its original state. Another aspect studied using p-XRF is environmental and forensic toxicology. Investigations of elemental concentration in bones due to toxic elemental exposure in the past and present are discussed in the context of the aftermath of industrialization and metallurgy (Kobylarz et al., 2023; Bamford et al., 2004). Similar to this, research were done to evaluate poisoning due to heavy metals (like mercury and lead) which can be indicative of chronic conditions using the technique (Specht, 2019). Primatology and palaeontology are other disciplines where the handheld XRF was applied for reconstructing patterns of primates inhabiting remote areas by evaluating the ecological and physiological factors (Schwartz, 2021).

2.7 Archaeological human remains

Human bone tissues are frequently recovered and studied within archaeological contexts. A comprehensive understanding of their structural and functional characteristics is essential for interpreting the analytical results concerning these tissues. This section will be focusing on a detailed explanation on bone tissues.

Bone is a dynamic mineralized tissue that aids in locomotive functions of the human body. It also plays a key role in maintaining mineral homeostasis, facilitating blood cell formation, and providing protection to soft organs such as the brain within cranial bone. Bone is composed of mainly three components such as (i) organic matrix (osteoid) (25%), (ii) inorganic mineral content (50%), and (iii) water (25%) (Bartl and Bartl, 2017). The organic matrix consists of collagen fiber (type I), and proteins including glycoprotein, osteocalcin, and proteoglycan. Mineral salts are initially deposited around the collagen fibres, which eventually crystallize and lead to the hardening of the tissue. This process is known as ossification. The degree of hardness of bone tissues depends on the type and quantity of minerals available, with hydroxyapatite being one of the major minerals present in bones. On the other hand, collagen fibres provide tensile strength and flexibility to the bones. Consequently, increased mineralization of collagen fibres or impaired collagen production can lead to brittleness of bones (walker, 2020).

The structure of bone includes two types of tissues (i) cortical bone and (ii) trabecular bone. Cortical bone is the dense outer layer that supports and protects the inner trabecular tissues. It consists of three consecutive layers, which are (i) periosteum, (ii) intra-cortical area, and (iii)

endosteum (Figure 13). The periosteum is a rigid and fibrous vascularised membrane forming the outer cover of the bone. Tendons and ligaments of the human body were attached to the outer surface of the periosteum. Osteoblasts and osteoclasts are responsible for bone remodelling and constitute the inner layer of the periosteum. The sensory fibers and Volkmann's canal connect blood vessels, lymph vessels, and nerves through the periosteum of cortical bones to the inter-cortical area. The intra-cortical area of cortical bone is formed by concentric cylindrical lamellar structures called osteons or Haversian system (Walker, 2020). Osteocytes or mature bone cells occupy the small space between these lamellar structures (lacunae). The blood vessels, lymph vessels, and nerves pass through the centre of osteons through the Haversian canal. The third structural unit of cortical bone endosteum is a thin layer of connective tissues arranged linearly across the cortical surface. Trabecular or cancellous bone is an irregular lamellar arrangement that replicates the structure of a honeycomb. The porous spaces within the cancellous bone make it lighter and easier to mobilize. The closer trabecular space arrangement indicates higher stability and structure of bone. In addition, red or yellow marrow is also embedded in these spaces, facilitating haemopoietic activities (Bartl and Bartl, 2017).

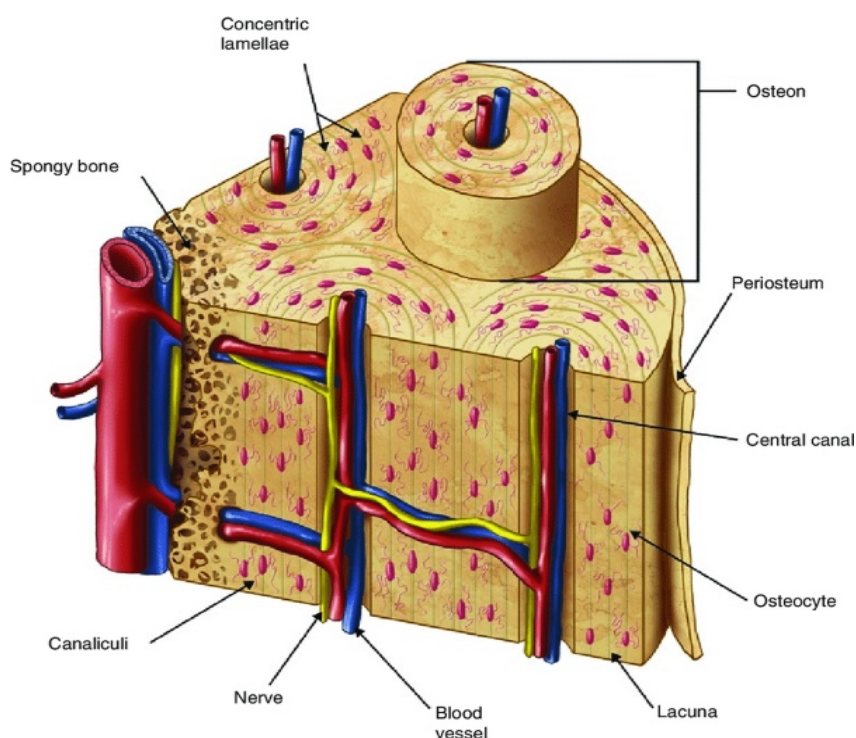


Figure 13 : Structure of cortical and trabecular bone sections (kumar et al., 2021)

According to the shape, bones of human skeletons are classified into five categories (i) long bones, (ii) short bones, (iii) flat bones, (iv) irregular bones, and (iv) sesamoid bones. As the name suggests, long bones such as the femur, humerus, tibia, radius, and ulna are longer than their wide cross-section (walker, 2020). The longitudinal division of long bones includes epiphysis, which forms the shaft, and diaphysis, the proximal and distal portions of the bones. Metaphysis forms the joining region of epiphysis and diaphysis and is the primary growth region of growing bones (Figure 14). These bones aid mainly in movements of human body (Setiawati and Rahardjo, 2018). Short bones appear in cuboidal shape with more cancellous tissues covered within narrow cortical layers as seen in tarsal and carpal bones of feet and hands. Skulls, ribs, and scapula are examples of flat bones with more flat and slightly curved surfaces. Flat bones are of thin layers of trabecular tissues within slender cortical outer surfaces. Long bones and flat bones form axial skeletal portions. The irregular bones such as the vertebral bones and pelvis, do not have a definite shape. These bones contain cancellous tissues rather than the cortical bone tissues forming the outer layer. Sesamoid bones are usually round or oval and are attached to the tendons (e.g. patella) (Setiawati and Rahardjo, 2018).

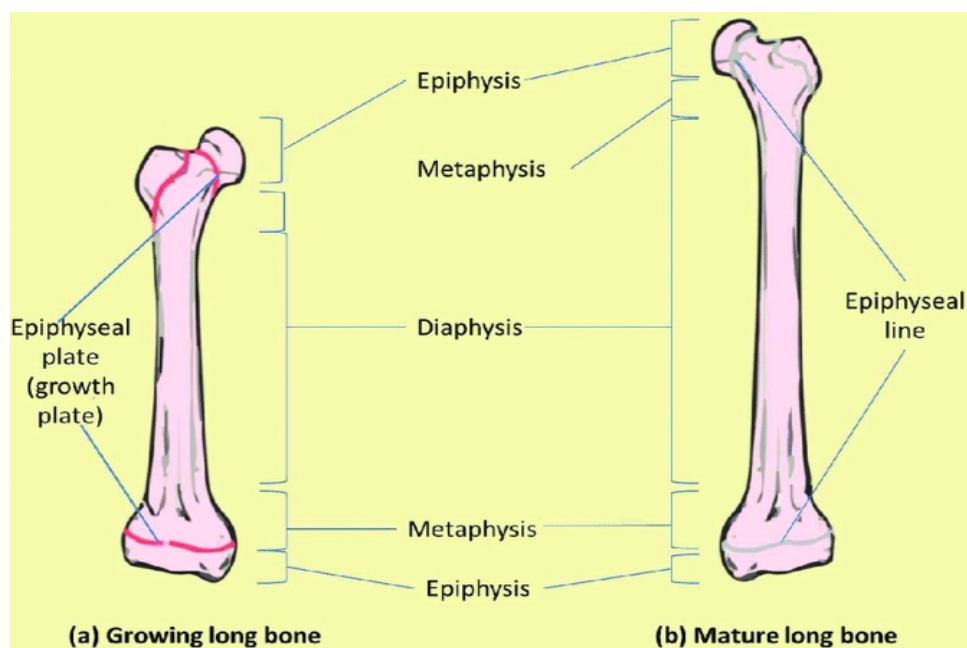


Figure 14: Epiphyseal, metaphyseal and diaphyseal region of a long bone (Setiawati and Rahardjo, 2018)

Bones are not fully developed at birth and will continue to grow until the skeletal maturity is attained. Active bone growth occurs at the end of adolescence, and skeletal maturity reaches

between 20-25 years. However, this can vary with the geographic location and socio-economic conditions. Besides, bone tissues also undergo constant remodelling after maturation and is facilitated by two types of cells namely osteoclasts and osteoblasts. During the remodelling old bone tissues are replaced with new tissues. Bone remodelling involves the mobilization of calcium and other minerals from skeletal system to optimize serum homeostasis, which allows replacing of old tissues, repairs damaged tissues and helps the body to adapt to the new loads and stress applied to the skeleton (Florencio-Silva et al., 2015). Portable -XRF applied studies on human remains are mostly focused on bone tissue compared to other human tissues such as bone. The following section gives a review of those studies mentioning the application of p-XRF to human bone tissues.

2.8 p-XRF application for archaeological human remains

Application of handheld XRF for the study of human remains from archaeological contexts can be divided into six categorical studies. This classification is based on their primary focus of investigation, as mentioned by Ganscz (2019), such as analysis concerning:

- (i) methodological studies for analysis of human remains,
- (ii) dietary studies,
- (iii) evaluation of taphonomic and diagenetic alteration affecting archaeological human remains,
- (iv) studies on resolving commingled human remains,
- (v) pathological examination of archaeological bones,
- (vi) toxicity or medical treatment detection.

[(I)] Methodological studies for analysis of human remains

Methodological studies compare the accuracy, reproducibility, sample preparation, and similar aspects of p-XRF. These studies mention concerns and problems arising in the course of analysis and provide guidelines for better results. One recent study by Gomes et al. (2024) describes aspects from sample preparation to data treatment that should be considered during the analysis of dry bones. Byrne and Bush (2016) suggest that the depth of X-ray penetration in and out of the bone varies in non-uniform bone samples due to the effect of diagenesis or soil matrix attached to the surface of the bone. The authors mention that the penetration depth of incident radiation entering the bone matrix is 1.9mm and it will result in the cortical bone

composition of the bone. Thereby, determining area of analysis for a particular element detection needs to consider the cortical bone thickness and the emission energies of the element of interest.

(ii) Dietary studies

Archaeological studies on elemental analysis to examine the diet using p-XRF are limited in the literature. The existing studies use complementary techniques such as ICP-MS or AAS to determine the accuracy of retrieved values. Gilbertson (2015), attempts to utilize p-XRF as an alternative to ICP-MS analysis for evaluating ancient Peruvian coastal diet. The author collected data using p-XRF from 208 cranium and correlated it with the data obtained from subsample isotopic information. Based on the bivariate statistical measures, the author confirms the validity of p-XRF for the analysis of strontium, barium, and iron for dietary analysis. Additionally, the study indicates that p-XRF cannot replace sensitive analytical techniques such as ICP-MS or ICE-AES. Bergmann (2018) analysed the diet of Peruvian sites in coastal areas and highlands to establish trade relations between the communities, using the elemental composition of bone. As part of this work, the author established a calibration with matrix-matched standards for elements such as Ba, Sr, and Ca to evaluate the reliability p-XRF method. Calibration was created using reference standards made from human and animal bones obtained from four archaeological sites in Peru (Cardal, Chokepukio, Pacopampa, and Tablada de Lurín), one archaeological site in Italy, and modern animal bones from Florida. These reference values are confirmed by assessing the elemental concentration obtained from the analysis using p-XRF and ICP-MS. Hence, this was a pioneer study done solely based on matrix-matched standards.

(iii) Evaluation of taphonomic alteration affecting osseous tissues

Bone is a heterogeneous material composed of inorganic and organic constituents, that determine its density and strength. Prolonged exposure to various environmental and burial conditions distorts physical and chemical status of bone. Taphonomic examination dealing with post-mortem alteration indicates that several factors such as soil composition, pH of the soil, precipitation, and human land use can influence the original chemical nature of these tissues (Caruso et al., 2020; Lopez-Costas et al., 2016). Pankowska and Monik (2018) discuss a

scenario that aim at differentiating intentional and accidental burn burials, also known as cenotaphs, found across central Bohemia during the late Bronze Age and Early Iron Age period. They employ p-XRF as one of the prime techniques to differentiate intentional burial from accidentally burnt burial by analysing their infill. Based on concentrations of elements such as P, Ca, Mn, Zn, V, and Pb, they were able to differentiate soil from infill with bone and without the presence of bone. The boneless infill soil showed similarity with the subsoil sample collected from the surroundings of burials, indicating in fills devoid of buried bones. The study implies that elemental changes of a decomposed body will result in an increased concentration of elements such as calcium, phosphorous, manganese (Mn), copper, boron (B), zinc, sodium (Na), Zn, and magnesium (Mg). Burning can shift the crystalline structure of skeletal tissues, particularly when temperature exceeds 500°C (Mamede et al., 2017). Gomes et al. (2024) also suggest that elements such as Pb and Fe, which can be indicative of diagenesis, should be monitored by their elemental levels in the soil. Lead (Pb) in the cortical and trabecular bone portions was evaluated in a skeleton dated to the medieval period by Rebocho et al. (2006). The study suggests influence of lead coffin induced the post-mortem alteration of the skeletons kept in it. The lead concentration across the bone cross-section was found to be higher in the cortical bone, gradually decreasing towards the trabecular portions.

(iv) Resolving commingled human remains

Mixed skeletal remains of different individuals often appear in archaeological burial contexts as a result of anthropogenic and natural actions. Osterholtz (2014) proposes three types of anthropogenic reasons which lead to commingling of remains. This division includes (a) long-term commingling, as a result of long-term usage a burial location or tomb, resulting in higher degree of commingling and fragmentation, (b) episodic commingling, which produces lesser degree of commingling, and occurs as a result of epidemic, warfare or catastrophic situations, and (c) poor handling in lab or during transportation.

In addition to morphometric and molecular analysis, several studies explored p-XRF as a chemometric tool to resolve commingling scenarios. Smith (2019) discusses how inter-individual differences can be applied to address this issue. The author creates a medium-scale commingling scenario with measured chemical element concentrations from multiple individuals. The study showed a moderate variation within bones for elements such as Fe, Pb, and Ba. In contrast, elemental variation at individual level was less significant for successfully resolving the commingling scenario. The element distribution within an individual was consistently evaluated for S, Ba, Mn, Fe, Sr, zirconium (Zr), and Pb. Additionally, strontium was

identified as one of the most significant elements for substantiating commingling in the mentioned study.

A similar approach was applied to five skeletons from a medieval cemetery dated between the 12th and 16th centuries AD in Lincoln by Gonzalez-Rodrigues and Fowler (2013). Based on the concentrations of Fe, Zn, P, and Ca, they successfully differentiated these five individuals. Additionally, the study introduced elemental ratios such as Zn/Fe, associated with metabolic activities, and K/Fe, related to blood flow into the bone, for the first time in anthropology. Perrone et al. (2014) mention inter-individual variability exceeds intra-individual variability based on a compositional evaluation done on twenty individuals. The authors state p-XRF as an effective tool to segregate commingled human remains, despite the possibility of overlapping of chemical concentration, which can lead to erroneous conclusions. Identically, Gancz (2019) also denotes limitation of p-XRF to resolve commingling scenarios involving large number of individuals.

Relatively, another study on commingled skeletons of two individuals indicates that both quantitative and qualitative analysis complement each other. However, qualitative analyses were found to be more beneficial in the resolution of small-scale commingling to determine secondary sexual characteristics that differentiating male from female skeletons (Wilburn et al., 2017). In this study, qualitative analysis distinguishes the skeletons from one another and that turned out to be of one male and one female. The application of quantitative analysis using p-XRF failed to support the same finding. Hence, the authors noted the possibility of disparity in differentiating male and female individuals using p-XRF.

Besides commingling, fragmentation or damage of skeletal remains can also pose a hindrance to morphological analysis. Shape and measurement of certain bones were considered for the sex determination of an individual in bioarchaeological studies. When such skeletal parts were absent or damaged, indeterminate sexual orientation was assigned to the studied individual. Nganvongpanit et al. (2015), studied whether p-XRF can be used as an alternative to morphometrical analysis for determining sex. The authors evaluated elemental concentrations within the coaxial bones, femur, and humerus, of male and female skeletons, as these bone types depict greater degree of dimorphism at corporal level for both sexes. Findings from the study imply differences across male and female bones based on element concentration, but

only S in females and Pb in males were consistently higher for all the three bones. The authors estimated 60- 67% accuracy for this technique in successful sex determination, which was lower than that of morphometric or molecular evaluation. Besides, combined analysis including all the three bones resulted variation in P, S and Ca among males and females for specific bones. Thereby, the study points out that sexual identity and external factors such as age, diet and environmental exposure can also influence elemental profile of human bones.

In addition to all aforementioned scenarios, fire induced changes such as warping, shrinking or fragmentation, can obscure the qualitative identification on bones. Heat exposure can vary based on the duration of exposure, intensity, oxygen supply and fire management and local weather (McGarry et al., 2021). Hence, the degree of burning may or may not vary within and among the individuals. McGarry and colleagues (2021) attempted an experimental study to assess the utilization of p-XRF for various modes of alteration in bone composition due to fire. A training set consist of 70 randomly selected fragments of sheep bones (selected despite human bones due to restriction) were burned. Using the detected elemental concentration, unburned and variably burned bones of lamb individuals were differentiated with 86% and 98.6% accuracy. The authors states that, heat exposure does influence discrimination of individual but the changes within bone will not affect the discrimination using their elemental status.

(v) Pathological examination of archaeological bones

Pathological assessment in archaeological contexts examines apparent changes or lesions discovered on bone surfaces. For example, porous lesions found on the orbital roof (*cribra orbitalia* - CO) and in the cranial vault (*cribra cranii*- CC) are most likely related with anaemic conditions (Gauss, 2019). Paleopathological studies using p-XRF focus on evaluating the relationship between element concentration and pathological condition observed on skeletal surface. Cirak et al. (2006) performed earliest study on elemental analysis on two females diagnosed with anaemia from the ancient Byzantine period. This study specially focused on Fe, Pb, Cu and Zn, revealed a lower levels of iron in the studied individuals with *porotic hyperostosis* than the normal limit. A decreased amount of Fe with elevated S was detected by Gomes et al. (2024) in a non-adult population (younger than 10 years old) of 100 individuals, who suffered anaemic conditions (18th and 19th century CE). The authors assert the need to analyse soil

samples associated with burials to differentiate the influence of diagenesis on the concentration of certain elements such as Pb and Fe. Kuccera et al. (2023) observed increased Ca/Fe ratio among children regardless of the pathological condition like *cribra orbitalia* (CO), from a combined analysis using p-XRF and ICP-MS.

Gomes et al. (2021) investigated the variation in elemental concentration of Fe among both male and female individuals whose cause of death was registered as chronic or acute anaemia. Their study points out higher Fe and lower S in patients with *cribra cranii* (CC). A difference in P and Ca observed in female and male individuals, was associated with age and physiological functions. Additionally, lower concentration of P, Ca, and Pb in older individuals were linked to the effect of ageing. Elevated level of Fe in population with CC was also noted by Maya (2020) complementing the finding of Gomes et al. (2021). Author examined cranial bones with and without *cribra orbitalia* and *cribra cranii* in males, females and from a non-adult. An increased amount of Fe found in the non-adult individual, was associated with the possibility of active and increased red blood cell production in cranial vault. All these studies indicate the presence of elements such as K and Si as possible indicators of diagenesis.

Other palaeopathological studies included rickets and scurvy, two diseases which can co-occur, particularly in infants and young children as evidenced from Chalcolithic Spain and 16-18th century France (Castilla et al., 2014; Schattmann et al., 2016). Some main diagnostic features of these conditions include abnormal porosity, new bone formation, and long bone deformation (Schattmann et al., 2016). A population constituted by seventy-three individuals (adults and non-adults) affected by CO, scurvy and rickets, was studied by Kilburn and team (2021). The non-adults skeletons were found to have pathological lesions associated with these conditions. Similarly, presence or absence of residual rickets and CO was also recorded for the adult individuals. The results indicates no distinctions exist between the elemental ratios of pathological and non-pathological states for rickets, scurvy and CO. Hence, no significant differences were identified between these conditions. The authors suggest that influence of a number of other factors such as diagenesis, periosteal bone formation, individual bodily response to stress, and age can influence elemental concentration in these studied bones.

Osteoporosis is a progressive skeletal disease characterized by low bone mass and deterioration of bone tissue, leading to increased fracture risk. It is found to be more prevalent in old age

group, mainly in women (Staff, 2011; Kawalkar, 2015). Decreasing mass of the bone is proportional to disintegration taking place in bone composition, leading to structural alteration. Zdrak et al. (2021) suggests a higher concentration of S and Ca/P ratio within the female femoral bones of individuals affected by osteoporosis. This study also elucidates a positive linear relationship between bone mineral density (BMD) and concentration of Fe and P. In addition, the analysis also showed a negative correlation of BMD with sulphur(S) indicating weak bone quality and osteoporosis associated with old age.

In different to the above discussed pathological conditions, Magalhães and colleagues (2021) assessed an individual cranium (cranium 226) exhibiting sclerosis and elevated levels of Zn associated with cranium overgrowth. Examined cranium (cranium 226), which displayed thickening, was studied using p-XRF in comparison to the craniums of similar age groups. The examined cranium 226 exhibited lead (Pb) concentration three times higher than the control group, suggesting influence of Pb on increased bone density. Similarly, high concentration of Cu detected on the skull is proposed as a possible cause of death of individual.

(vi) Toxicity or medical treatment detection

Bioarchaeological analysis on toxicity or pollution are primarily studied via highly sensitive techniques such as AAS and ICP-MS. Few examples from the literature denote p-XRF as a useful investigative tool to determine the concentration of elements indicating environmental or pollutant conditions. In addition, consumption of medications with high concentration of certain elements as an intentional uptake against epidemics or diseases are also included in this section. For example, heavy metal like mercury (Hg) in bones, associated with its systematic use as a medical aid for syphilis in early modern England was studied using p-XRF (Zuckermann, 2010). The study by Specht et al. (2019) support the findings of Byrne and Bush (2016) by measuring the lead (Pb) in individuals. These studies indicate the measurements acquired using p-XRF as concentration from cortical bone surface. Additionally, the former study also notes the concentration of lead in tibia and cranium varies slightly.

2.9 Limitation of p-XRF for the analysis of human remains

Apart from the discussed merits, the method has certain drawbacks. The number of elements falls within the limit of detection of this technique are comparatively fewer. Those elements

with atomic number below sodium ($Z=11$) are hard to detect using p-XRF. Range of element detection varies with respect to the machines used, due to associated mechanical features. These features include tube voltage and anode (Rh, Ag, W), detector technology (a better range is achieved with large area Silicon Drift SDD detectors than with traditional Si-PIN detectors), beam collimator, and filtration (Lemiere, 2018). Another limitation for analysing bones as well as organic materials is the lack of calibration standards (Zhou et al., 2022). Factory calibration standards associated with the p-XRF machine does not yield optimal results. Therefore, the use of matrix matched calibration standards such as SRM NIST1400 Bone Ash are preferred for p-XRF analysis of human bones (Gomes et al., 2024).

On surveying above 200 articles published on handheld XRF for different materials of archaeological and cultural significance, Johnson et al. (2024) put forward key elements which affects the reproducibility and replicability of this technique (Table 1).

Table 1: Factors affecting reproducibility and replicability of p-XRF studies (adapted from Johnson et al., 2024)

Project Design	Material analysed Number of samples analysed Way of selection of samples for study
Preparation of Sample	No preparation Grounded or pellet form
Instrument Conditions	Instrument model Counting Time for Analysis Voltage for each scan Ampere /Current Power Source for the machine functioning(Battery /Electricity) Standard used for Calibration Calibration being used to analyse the results of each scan Software used to process the spectra Diameter of the beam Type of filter used
Analysis: Object Considerations	Size of the samples Location(s) on the object that were scanned Number of scans of the same object Whether objects were repositioned between scans (if multiple scans)

Non-uniform bone morphology and shape can affect the elemental detection, due to the concave and convex surfaces of bones. This in turn results in an air gap between the detector window and the bone, leading to dissipation of emitted X-rays (Gonzalez-Rodriguez and Fowler, 2013). Though the discussed works selected all kind of skeletal elements including ribs, vertebrae, sacrum etc., it was most advisable to select bone with flat surface to reduce air attenuation (Gomes et al., 2024). Another aspect that needs to be considered is the excitation depth, which can often be limited by the adhered matrix potentially compromising reliability of measurement. Based on the experimental analysis performed by Byrnes and Bush (2016) on archaeological bones, the X-rays can enter up to a depth of 1.9 mm into the cortical bone. Hence, the results can be influenced by cortical thickness as well as poor preservation of archaeological bones. Element emission energy and the density of the material being analysed also impact the depth of X-rays penetrating to bone matrix.

As stated, p-XRF serves as a compositional tool for examining various aspects of human remains. Some scholars argue that this widening popularity challenges the decades of developed laboratory protocols for XRF analysis (Shackley, 2010). This demands careful comparisons as well as treatments principally, since lack of understanding can lead to errors (Grave et al., 2012). Compared to other archaeological materials, published sources on p-XRF applied to human remains are less. To develop an understanding as well as to establish a protocol for improved analysis, transparency and dissemination of research findings are essential. A comprehensive table is given as follows based on the reviewed p-XRF publication for elemental analysis on archaeological bones (Table 2).

Hence this work is a comprehensive study which aims at analysing the methodological aspects of p-XRF applicable for archaeological human remains with a focus on palaeopathology, diet as well as diagenesis.

Table 2: Summary of reviewed articles on analysis of human remains with p-XRF from various academic publishing platforms (Academia. edu, Google Scholar, Semantic Scholar, Science Direct)

Author&Year	Machine Type	Preparation of Sample	Study Area	Voltage keV	Current μ A	Counting Time (sec)	Filter Used	Elements Quantified	Complementary Methods
Bergmann, 2018	Bruker Tracer III-SD	Powdered Sample	Palaeo diet	40	11	120	12 mil Al, 1 mil Ti, 6 mil Cu filter	Ba, Ca, Fe, Sr	ICP -MS
Gomes et al., 2021	Thermo Scientific Niton XL3t900	No alteration	Palaeopathology	Not mentioned	Not mentioned	120	Not mentioned	Si, P, S, Cl, Ca, Mn, Fe, Cu, Zn, Sr, Ba	No other methods used
Gonzalez-Rodriguez and Fowler, 2013	Niton XL3t	No alteration	Commingling	Not mentioned	Not mentioned	Not mentioned	Not mentioned	Pb, Sr, Zn, Fe, Ca and K	No other methods used
Zdral et al., 2021	Thermo Scientific Niton™ XL3t	No alteration (Femoral bones)	Palaeopathology	Not mentioned	Not mentioned	Not mentioned	Not mentioned	P, S, Ca, Fe, Zn, Sr, Pb ,Ca/P	No other methods used
Gomes et	Thermo	Cranial	Methodological&	Not	Not	120 and 240	Not	Si, P, K, Ca,	No other

al,2024	Scientific Niton™ XL3t		Palaeopathology	mentione d	mentione d		mentioned	Fe, Zn,Sr	methods used
Maya, 2020	Nil	Cranial Bones	Palaeopathology	10 and 40	Nil	120	Not mentioned	Fe, K, Si	No other methods used
Nganvongpani t et al., 2016	DELTA Premium; Olympus	Tibia, Vertebrae	Commingling (comparison with animal bones)	Not mentione d	Not mentione d	120	Not mentioned	Al, Si, P, S, K, Ca, Ti, V, Cr, Mn, Fe, Ni, Cu, Zn, Zr, Mo, Ag, Cd, Sn, Sb, W, and Pb	No other methods used
Smith, 2021	Olympus Innov- X Delta-Pro		Commingling	Not mentione d	Not mentione d	9	Not mentioned	Ca, P, S, K, Cr, Mn, Fe, Cu, Zn, As, Rb, Sr, Zr, Sb, Ba, Hg, and Pb.	No other methods used
Magalhaes et al., 2021	Thermo Scientific Niton™ XL3t	Cranial Bone	nil	Not mentione d	Not mentione d	Not mentioned	Not mentioned	P, K, Mn, Ca, Cu, Pb, Zn	No other methods used
Zuckerman, 2004	Bruker Tracer III-V/III-SD	Gently abraded Bone surface	Detection Study	Not mentione d	Not mentione d	300	Not mentioned	Hg	No other methods used
Winburn et al., 2017	Bruker Tracer III-V		commingling	12-15	35	Not mentioned	no filter,	Si, P, K, Ca, Mn, Fe, Co	No other methods

									used
Janos et al., 2006	SPECTRO XEPOS XEP01	Bone surface	Detection/ Elemental Status	35	Not mentioned	Not mentioned	Not mentioned	Na, Mg, Al, P, K, Ca, P	No other methods used
Rodriguez and Fowler, 2012	Niton XL3t	Powdered Form	Palaeopathology	Not mentioned	Not mentioned	Not mentioned	Not mentioned	Pb, Sr, Zn, Fe, Ca and K	No other methods used
Zimmerman et al., 2015	nil	Bone surface	Commingling	Not mentioned	Not mentioned	Not mentioned	Not mentioned	Al, Ba, Cu, Fe, Mg, Mn, Pb, Sr, and Rb	No other methods used
Granite, 2021	Innov-X Alpha Series analyser	Bog bodies Not altered	Detection studies	Not mentioned	Not mentioned	Not mentioned	Not mentioned	Br, Cu, Fe, Mn, Mo, Pb, Rb, Zn, Sr, Ca and Zr	No other methods used
Byrnes and Bush, 2016	Innov-X Systems Alpha-2	Bone surface (abraded and non-abraded)	Methodological studies	40	10	60	Not mentioned	Sr	No other methods used
Specht et al., 2019	Niton XL3t GOLDD +	Different Bones Not altered	Detection of Lead	50	40	180	Not mentioned	Pb	No other methods used

CHAPTER-3

ARCHAEOLOGICAL BACKGROUND OF HUMAN REMAINS

A holistic approach to the analysis of bioarchaeological remains includes the integration of both analytical techniques along with contextual information. This chapter will present a brief narration on the historical background and burial context of human remains examined for the work. The analysed human remains were retrieved from two different regions, dated to the medieval and post-medieval periods, and are located in the Portuguese mainland (Figure 13).

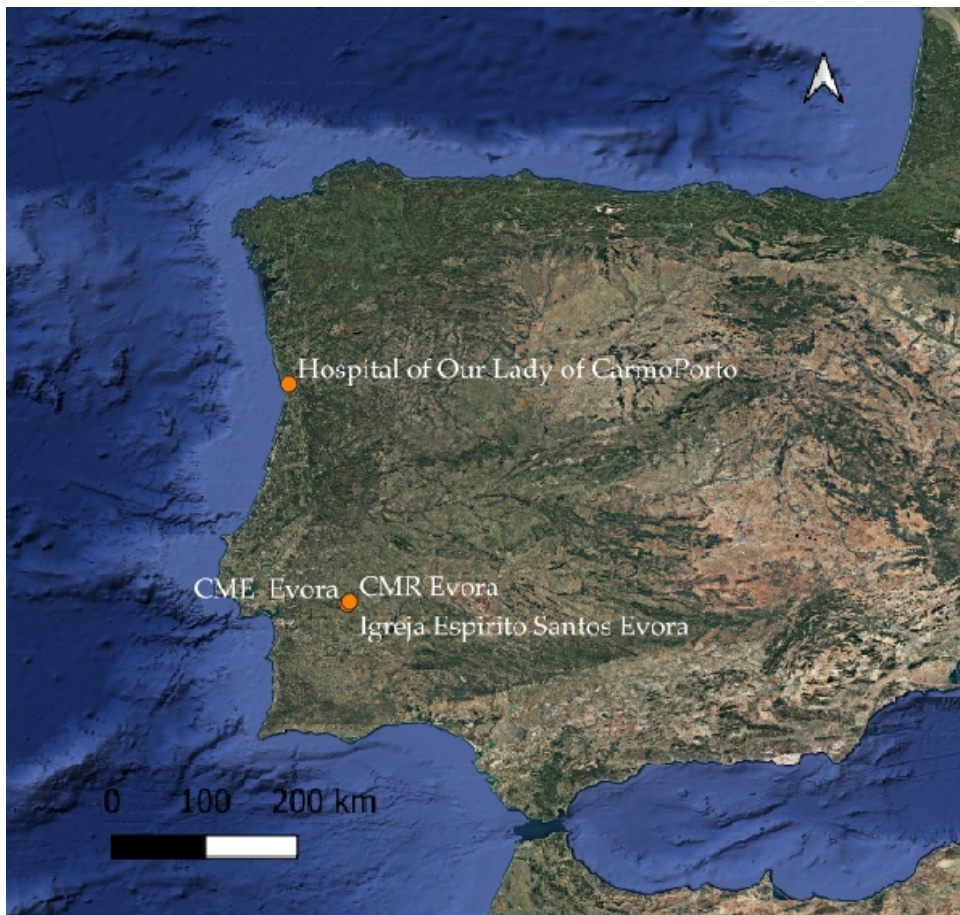


Figure 15: Location of different archaeological sites of analysed human remains

The human remains selected to answer the archaeological queries include both fully and partially preserved individuals. The remains and their respective archaeological context are listed in the table below (Table 3)

Table 3: Archaeological human remains, chronology, and burial context

Site	Chronology	Type of bone analysed	No of individuals
Necropolis at Hospital of Third order Our Lady of Carmo, Porto	19 th century AD	Cranial bones	4
Church of Espírito Santo, Évora (ossuary and crypt)	15-19 th century AD	Cranial bones	5
		Individual with multiple bones (Cranium, Femur, Humerus, Tibia, Ribs)	5
Collection of Identified Skeleton of Évora	19 th century AD	Individual with multiple bones (Cranium, Femur, Humerus, Tibia)	6

3.1 Hospital of Third Order of Our Lady of Mount Carmo: excavation and historical background

The hospital of Third Order of Our Lady of Carmo was constructed at the end 18th century and is located in the square previously known as Lagos dos Ferradores in Porto. This square was the beginning of Rua de Cedofeita, located in an area known as Horta do Olival. In the 14th century, this was part of an old route that connected the cities of Viana and Braga. Urban settlements were occupied this portion of the city during the time of hospital construction. An excavation was carried out to construct a new block for the same hospital. The excavation took place under the direction of Nicolas Marques Grant and Javier Naranjo from the company of Oxford

Archaeology. It revealed the existence of a 200-square-meter cemetery and archaeologically significant structures. A three-meter stratigraphical depth revealed eleven phases from the end of the 18th century when the hospital construction started, up to the present (see Table 4). This has shed light on the historical evolution of excavated parts of the city.

A total of 480 burials were unearthed from two levels of this cemetery space and were ascribed to the time frame between 1801 and 1869 (Menendez and Teixeira, 2008). This period of necropolis represents a time when the city of Porto was under turmoil of war and epidemic outbreaks, such as cholera in 1832. The first case of cholera outbreak in Porto was carried by troops from Ostend who arrived to help the liberal army in the civil war. As per the reports, this outbreak had a devastating effect on the population at the time due to the poor hygiene in the city and streets, as well as an uncontrolled number of patients and narrow spaces in hospitals (Almeida, 2019; Davis, 2022).

Table 4: Historical sequence of occupation identified from excavation at necropolis at Hospital of Third Order of Our Lady of Mount Carmo, Porto (Menendes and Silva, 2008)

Phases	Time period	Excavated features
Phase 1	Before 1791	Urban settlement (prior to the hospital Construction)
Phase 2	1791-1800	Construction of hospital Extraction and filling ditches for construction
Phase 3	1801-1832	Necropolis with north-south orientation, organized around stone pavement that functioned as a central axis
Phase 4	1832-1833	Burial levels related to the cholera epidemic period recorded during siege of Porto
Phase 5	1833-1869	Abandonment of necropolis Reuse of necropolis oriented east-west directions
Phase 6	1869-Last 20 th	Last quarter of 20th century construction of

	century	warehouses cutting through the necropolis
Phase 7	Last quarter of 20 th century- present	Use of area as a parking space

3.2 Brief history of necropolis at Hospital of Third Order of Our Lady of Mount Carmo, Porto

The space associated with the hospital of the Third Order of Our Lady of Mount Carmo Porto was converted into a cemetery following the order of Francisco Luis Galvao, after the completion of hospital's construction in 1800 AD. Graves discovered from the first phase of the burial location were dug in a simple pit approximately 2m long and 60cm wide and are oriented north-south direction as depicted in figures 14 and 15 below.



Figure 16: Individual burial from first phase of excavation, Porto (Menendes and Silva, 2008)



Figure 17: Collective burial from first phase of excavation, Porto (Menendes and Silva, 2008)

These graves were of average depth of 2m and yielded identification of 6-7 stratigraphic layers and the burials resulted in both sexes and different age groups. The oldest burial levels in each grave represented individual or coffin burials. Excavation also points out to a scenario of collective burial, where two to seven bodies were buried within each grave at the same time or in an interval of a short period, without any coffin in subsequent layers. In certain cases, the

deposited bodies appeared to be placed carefully to minimize the space utilization of the tombs. A collective burial during this phase is related to the great mortality that happened at the time of the siege of Porto, and the epidemic spread of typhus and cholera, which all together led to hunger and scanty supplies (Menendez and Silvia, 2008). A heavy mortar round found in these levels of the cemetery, indicates the radical change that appeared in the political and social context of the city during 1832 and 1833. Material evidence found within the burial ground, like canon balls and bullets indicates the invasion and firing took place under Miguelist forces from Vila Nova de Gaia (Menendez and Silvia, 2008).

Historical sources mention a couple of cholera outbreaks that affected the city of Porto during the same time. The most fatal one among these was the outbreak which was worsened by the poor economy and living conditions at the time of civil war. This conditions was spread through the soldiers who were coming back from Asian territories such as West Bengal which affected by cholera in 1826 (Pollitzer, 1954). Cascao (1993) mentions the number of people who were affected by the effect of cholera in Porto was more than that of people who were affected by war. As per the records, 40000 people perished with the epidemic effect. The intensity of this outbreak was accelerated by famine during the siege of the city by troops of King Miguel along with poor sanitation and an unhygienic environment existing at the time. The four individuals, who will be analysed in this study were part of the population that lived in Porto during the period of political and social distress (DOI:10.54499/2022.02398.PTDC).

The necropolis continued to be in use during the subsequent period (1833-1869CE), which was observed in excavation with a different orientation in an east-west direction. This phase has resulted in 300 burials deposited in pits with dimensions 2m*0.5m*1.5m. These were graves separated by a few centimetres and the burials were laid inside coffins. Unlike the necropolis dated before 1833, there was no mingling of individuals from different periods were visible. Remains of wooden coffins lined with fabrics and foliage which were used to bury the bodies were retrieved from the context along with iron nails, padlocks, fabric and rope fragments. Individuals buried in this phase were belonged to different age and sex groups. The preservation of the skeletons on top layers was hampered by 19th-century construction activities that took place at the site. While skeletons at a lower level of the phase were with

intact remains of hair, traces of clothing, shoe soles, rosaries, crossbars, and tomb remains (Figure 16).



Figure 18: Remains of burial from second phase (Menendes and Silva, 2008)

3.3 Burial context of specimen recovered from church of Espírito Santo, Évora

The Church of Espírito Santo located in Évora Municipality of Portugal was constructed during 1567- 1574. The first scientific intervention at the chapel, dedicated to São Sebastião took place in 2012, which led to the discovery of the burial of three male individuals and additional bones indicating the burial of a minimum of 11 individuals in the ossuary. Later in 2020, an excavation was conducted under the guidance of anthropologist Dr. Ana Curto at the Chapel of São João, as part of rehabilitation work to build a new crypt. Followed by, the second phase of this excavation conducted by anthropologist Dr. Célia Lopes in 2021 (Curto and Lopes, 2022).

These two seasons of excavation at the chapel of São João revealed fully and partially preserved skeletal remains. Excavation of the crypt associated with the chapel led to the discovery of five individual burials, including a coffin burial. The coffin burial was located in the middle of the crypt and two other burials were found with the coffin in the sediments. The other two burials were found above the crypt, under the floor of the chapel, one on each side of the crypt. The

coffin was attached with handles, decorative ribbons, and fabrics which remained along with the burial inside. The state of preservation of coffin wood was also observed to be non-uniform, with a darker hue appearance indicating wood degradation resulted from prolonged exposure to the closed space as well as body fluid (Curto and Lopes, 2022). A solidified deposit of lime around the coffin assuming its shape has been observed within context, pointing out typical characteristics of medieval burials.

The preservation of these bones recovered from ossuary appeared good, except the crystal growth found on their skeletal surface, which were attached to the wall. Similarly, the deformed shape of bones was observed as the result of skeletons laid attached to the walls (Curto and Lopes, 2022). Since the position of the skeleton and their association with various features differs within the same context, are illustrated in figures (17, 18, 19, 20) along with the tabular description (see Table 5) as follows.

Apart from these, completely intact loose bones were also found at the peripheral part of the crypt and ossuary (both interior and exterior). The bones obtained from the exterior of the crypt are quantified to a minimum number of 24 individuals based on the right radii (Curto and Lopes, 2022). A sample population from outside of the crypt including nine males, one female, and one undetermined were found from anthropological examination of hip bones. The present work includes different skeletal portions such as the humerus, cranium, tibia, femur, and ribs from five individuals mentioned in the above Table 5, in addition to the five cranial bones recovered from the context of ossuary within the chapel (Curto and Lopes, 2022).

Table 5: Description of individual remains excavated from the crypt of Church of Espírito Santo, Évora collected from excavation report (Curto and Lopes, 2022)

Individual	Age and sex	Description of burial and burial context
IESE /21-1 Coffin Burial (Figure 17)	16-21 years Male	No visible pathological remarks Lime deposit with description found along the coffin Associated findings: Shroud rosaries, shoes
IESE/21-2 Burial Found Right of coffin	Male 50 years old	Visible pathological symptoms of arthrosis on vertebral bodies Decubitus position and is oriented Southwest to north-west direction. Except ribs all other bone elements were intact

(Figure 18)		
IESE/21-3 Burial found at left of coffin (Figure 18)	Male 20-30 years	No visible pathological remarks Well maintained anatomical connection and preservation of individual All bone elements were preserved intact
IESE/21-4 (Figure 19)	Male 20-30 years	Entire rib cage and bone at the abdominal parts were covered by lime Long bones and cranial bones preserved well Findings of fragmentary bone with in lime is observed
IESE/21-5 (Figure 20)	Male 17-19 years	A congenital condition called spina bifida occulta was visible in the vertebral bones of individual. Upper part of the skeleton starting from pelvic girdle to the cranium was covered with thick deposit of lime Parts of leg bones are well preserved Slight periosteal reaction was also noted in the anterior shaft of tibia.



Figure 19: IESE/21-1 Skeleton in coffin (Curto and Lopes, 2022)



Figure 20: IESE/21-2 and IESE/21-2 (Curto and Lopes, 2022)



Figure 21: IESE/21-4 Skeleton completely covered with lime (Curto and Lopes, 2022)



Figure 22: IESE/21-5 Skeleton partially covered with lime (Curto and Lopes, 2022)

3.4 Collection of Identified Skeletons of Évora

This study includes six individuals selected from the Collection of Identified Skeletons (CEIE) in Évora, housed in the Biological Anthropology Laboratory of the Department of Biology at the University of Évora. CEIE is one of several reference collections in Portugal, consisting of identified individuals with known sex and age at death. The six individuals analysed belonged to a larger group of 201 adults (including both sexes) and seven non-adults. These individuals were born between 1790 and 1969 and died between 1870 and 1993, with most of them having

their life histories linked to the Alentejo region. This underscores the collection’s significance in the anthropological history of the region (Lopes and Fernandes, 2019).

The human remains were obtained from two municipal cemeteries in Évora: Nossa Senhora dos Remédios Municipal Cemetery (CMR) and Espinheiro Municipal Cemetery (CME). CMR, has been in use since 1840. The human remains from CMR are representative of the population from the nineteenth and early twentieth centuries. The lifestyles and living conditions of these individuals make them comparable to archaeological populations, and their lifespans predate the invention of antibiotics and vaccines. This population, primarily of low socio-economic status was mainly engaged in farming. Additionally, the collection includes remains from CME, inaugurated in 1984, and was the newer of the two cemeteries (Lopes and Fernandes, 2019). Among the six individuals analysed, three exhibited visible pathological lesions on their skeletal surfaces. A summary of these individuals and their pathological lesions is provided in Table 6.

Table 6: Details of individuals selected from CEIE (Collection of Identified Skeletons of Évora)






SPECIMEN LABEL	SEX	AGE	PATHOLOGY/
CEIE-123	FEMALE	81	Neoplasm/ Anaemia
CEIE-141	FEMALE	86	Possible Twin Sister of CEIE-123
CEIE-94	MALE	94	Neoplasm (Cancer)
CEIE-40	MALE	79	No pathology (Control Group)
CEIE-43	FEMALE	79	No pathology (Control Group)
CEIE-25	FEMALE	59	No pathology (Control Group)

CHAPTER -4
METHODS AND MATERIALS

4.1 Human remains under study

Human remains studied include both partial and full bone types which were accessed from different archaeological contexts. Table 7 gives a new nomenclature to all the samples included in the analysis for easy interpretation and graphical illustration. Expanded information on naming with excavation labels is included in appendix Table A1.

Table 7: Details of analysed human remains

Site	Individual Label	Analysed bone elements
Necropolis at Hospital of Third Order of Our Lady of Carmo, Porto	PC- PC1 PC2 PC3 PC4	Cranial Bone 
Church of Espírito Santos, Évora (from ossuary)	EC- COS1 COS2 COS3 COS4 COS5	Cranial Bone 
Church of Espírito Santos, Évora (from crypt)	SKRC- C, F, H, T, R SKLC- C, F, H, T, R SKL1- C, F, H, T, R SKL2- F, H, T, R SKC*- C, H	Cranium Femur Humerus Tibia Ribs 
CEIE- Individuals with pathology	SKP1- C, F, H, T, SKP2- C, F, H, T, SKP3-C, F, H, T,	Cranium Femur Humerus Tibia 
CEIE- Individuals with out pathology	SKNP1- C, F, H, U SKNP2- C, F, H, T SKNP3-C, F, H, T	*Ulna 

The analysed cranial bones were devoid of the mandible, hence selected portions for p-XRF scans were concentrated on the upper cranial surface. Morphological examination of these

cranial bones indicates a varying state of preservation. The two cranial bones from Porto (PC3 and PC4) have a disintegrated cortical surface. Greenish patches appeared along with the soil matrix on the surface of PC4, indicating possible association with brass or copper objects or Cu-enriched soil. The same can be noted in archaeological bone surfaces deposited with copper salt (Muller et al., 2011; Ferrand et al., 2014). Similarly, some of the cranial bones from the crypt and ossuary of Church were found to have small layers of white soil deposit. The skeleton of five individuals unearthed from the crypt includes both completely and partially preserved bone elements. Both long bones and pieces of long bones were included in the scanning. Human skeletal remains from CEIE constitute three individuals with clearly visible pathological lesions all over the scanned bones. The same subset also consists of three individuals with no visible alterations on their skeletal surface.

4.2 Pre-treatment of samples

Prior to the analysis, the selected points on bone surfaces were subjected to gentle cleaning using distilled water and then kept at room temperature to dry. The method of cleaning was adapted from Gomes et al. (2024) and Maya (2019). This procedure helps to remove adhered soil matrix or dust on the bone surface.

4.3 Bone element selection

Bone selection was carried out based on the guidelines for dry human bone analysis using p-XRF proposed by Gomes et al. (2024). Bones with irregular and curved surfaces often create a gap with the detector window. Similarly, large bones used for the analysis cannot be closed within the detector chamber. Both scenarios can give rise to air attenuation, as a result of the created gap. Therefore, special attention is given to the bone selection and setting of the bones for analysis (Zdral et al., 2021).

In this study, preference was given to the cranium and long bones (femur, humerus, tibia), which have flat surfaces. In the absence of tibia in one individual (SKNP1), the ulna was selected (see Table 7). Additionally, bone surfaces with writing or ink marks were excluded from scanning. Some rib portions were included for individuals from Evora. Analysed spots on

cranial bones were mainly chosen in parietal, temporal, and occipital regions from the available areas with intact cortical bones (Figure 21). A few cranial bones were scanned on randomly selected spots to avoid the possibility of obstruction from visible soil encrustations. Scanning spot of long bones mainly concentrated at diaphysis and metaphysis regions (Figure 22). Epiphyseal regions were avoided due to the lower count rate.



Figure 23: Analysed spots in cranial bone of SKL1



Figure 24: Analysed spots in femur of SKP1

4.4 Device and parameter included for the analysis

The analysis of the skeletal remains was performed with a Bruker Tracer III SD -handheld XRF spectrometer. The analysis was conducted at the bioarchaeology lab of Mitra, University of Evora. This device is a wide-range elemental analyser, based on energy-dispersive X-ray fluorescence technology. It includes an X-ray tube as its excitation source to irradiate the studied bones. The X-ray tube of the machine uses a bulk rhenium (Re), rhodium (Rh), or silver (Ag) target. This device combines a high-resolution Petlier, cooled Silicon PIN(Si-PIN) diode detector.

The TRACER III SD p-XRF analyser is fully equipped with a PC and an integrated Personal Digital Assistant (PDA) computer, which offers a user interface for operating the instrument by opting the required parameters. It also contains the Bruker S1 analytical program, which enables the user to choose analytical modes suitable for the sample, view spectra, and save the data using fingertip or stylus. The device is factory-calibrated for the measuring certain alloys such as nickel (Ni), aluminium (Al), cobalt (Co), and titanium (Ti) (Bruker AXS handheld Manual, 2008). The general operating parameters of Tracer Handheld III SD XRF are outlined in Table 8 below.

Table 8: General parameter set up for TRACER handheld XRF Unit

X-ray tube	Rh or Re, Pd, Ar
Filter	Manually selectable
Voltage selection	0-45kV, variable
Current selection	0-60 μ A, variable
Scan length	Manually selectable
Optimal Pulse Density	15000 max cps(PIN) 150000 max cps SDD
Environment	Air or Vacuum
Detector channel	1023PIN/2048SDD

The parameters adopted for the current analysis are as follows (i) voltage: 40 keV, (ii) amperage: 11 μ A, (iii) duration: 180 seconds. No filter mode was found suitable for yielding an optimal spectrum after a comparison with the working mode using Ti -Al filter.

4.5 Safety precautions for scanning with p-XRF

The scanning of bones was conducted at a place devoid of people and machine set up in such a way that it faces towards the wall. The machine was mounted on a tripod considering safety

and convenience. This also helps to stabilize instrument while measuring, since the movement of the sample or machine can affect the detection (Figure 23) (Gomes et al., 2024).



Figure 25: Machine set up for analysis

4.6 Method creation using ARTAX software for quantification of elements

The raw spectral data obtained from point scans on bones will appear in *.pdz* format. To derive elemental concentration from the bones, the obtained data in *.pdz* format (measured in count per second and intensity) need to be converted. This conversion can be performed with the help of ARTAX software, which is associated with the Bruker Tracer III SD p-XRF machine. ARTAX software helps in detecting spectral peaks and creating an appropriate method for calibration with its built-in user interface. Using the created calibration method, quantification of the elements can be obtained by converting raw intensity data to their corresponding concentration. Henceforth, the created method will be used as a base to calculate valid concentrations. Previous works mention that standard factory calibration does not affirm the optimal results. Therefore, matrix-matched internationally accepted standards are used for calibration (Hall et al., 2014; Lemiere, 2018).

As part of the current analysis, two reference materials SRM NIST 1400 Bone Ash and Microanalytical Phosphate Standard MAPS-4 were used to create an empirical calibration to

estimate the concentrations of elements. As the first step, two separate calibration methods were created using both standards. Further, concentrations were calculated with the created methods and were compared with each other to determine the more accurate method. The calibration method created with SRM NIST 1400 Bone Ash resulted in more accuracy and was subsequently used for the routine precision tests, accuracy check, and to evaluate the system conditions. As a preliminary assessment, SRM MAPS- 4 was scanned and quantified with the calibration method created using SRM NIST 1400 Bone ash. This resulted in the detection of elements such as: P, Ca, Fe, Zn and Sr with more than 90% accuracy. Additionally, Ba and Pb were detected with 83% and 85% accuracy, respectively.

CHAPTER-5

RESULTS AND DISCUSSION

5.1 Precision

Precision can be examined mainly in two ways (i) repeatedly testing international standards or inbuilt standards and (ii) measuring an unknown material that is not an international standard (Craig et al., 2007; Hughes, 1998). Routine scanning of standards facilitates monitoring operation conditions and assessing accuracy and precision. In addition, usage of the standard will allow the assessment of different equipments and the same equipment over time (Sheppard et al., 2011). Daily scanning of standards also facilitates the observation of instrumental conditions.

As part of the analysis, precision was ensured by scanning international standard NIST1400 Bone Ash three times, twice a day. This helped to evaluate the machine conditions over the progress of analysis and standardize the analysis over time. All the measurements were converted to quantitative data using the calibration method created with ARTAX 7 software. A total of nineteen elements were quantified by measuring NIST1400 Bone Ash. The values for these elements are presented as homogenized mean concentrations in Figure 24. Furthermore, the relative standard deviation percentage (RSD%) was calculated for each element for their per-day measurement and was considered as a mean to establish precision.

$$\text{Relative Standard Deviation in \% (RSD\%)} = (\text{Standard Deviation} / \text{Mean}) * 100$$

RSD% obtained for elements such as Al, K, Ca, P, Fe, Ni, Sr, and Zn was less than 15%, considered a good precision in p-XRF analysis (Saki 1991; Bergmann 2019)(See Figure 26). Elements such as manganese (Mn), tin (Sn), arsenic (As), rubidium (Rb), and cobalt (Co) range up to 40% in terms of RSD%. The remaining elements were noted to have a high RSD% (See Figure 25).

HOMOGENISED MEAN OF MEASUREMENT OF STD1400

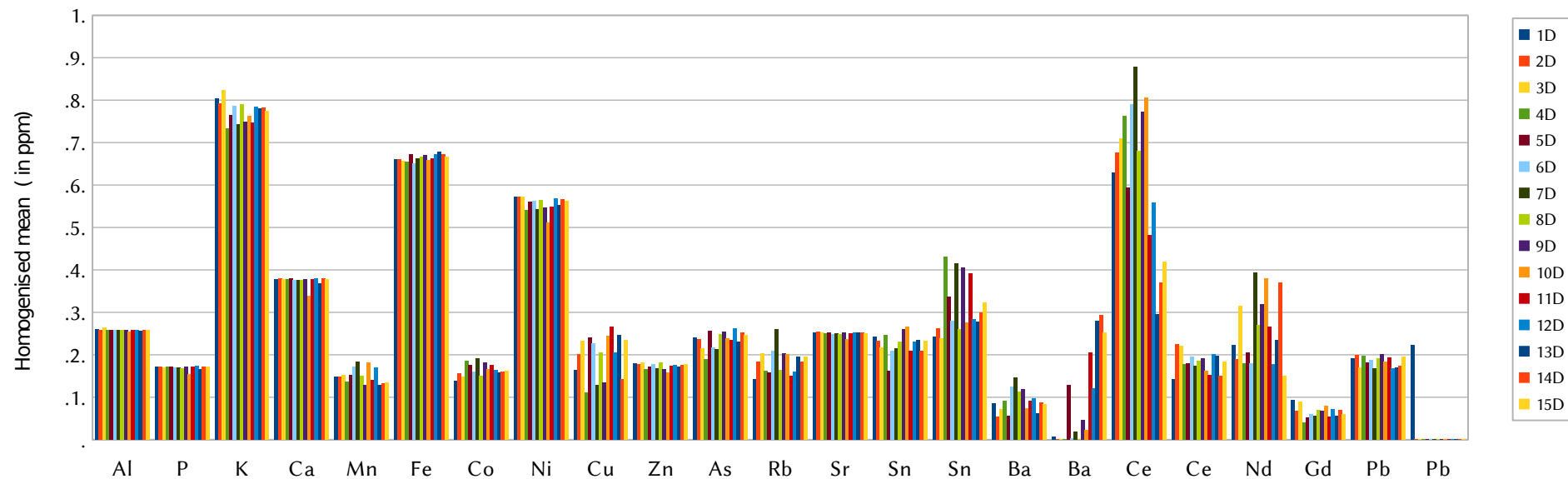


Figure 26 : Homogenised mean concentration of routine measurement of SRM NIST1400 bone ash

Unit of conversion for homogenised mean concentration					
Al*10000	P*1000000	K*1000	Ca*1000000	Mn*100	Fe*1000
Ni*10	Cu*10	Zn*1000	As*10	Rb*10	Sr*1000
Ba*10000	Ba*100000	Ce*10000	Pb*100	Pb*10	

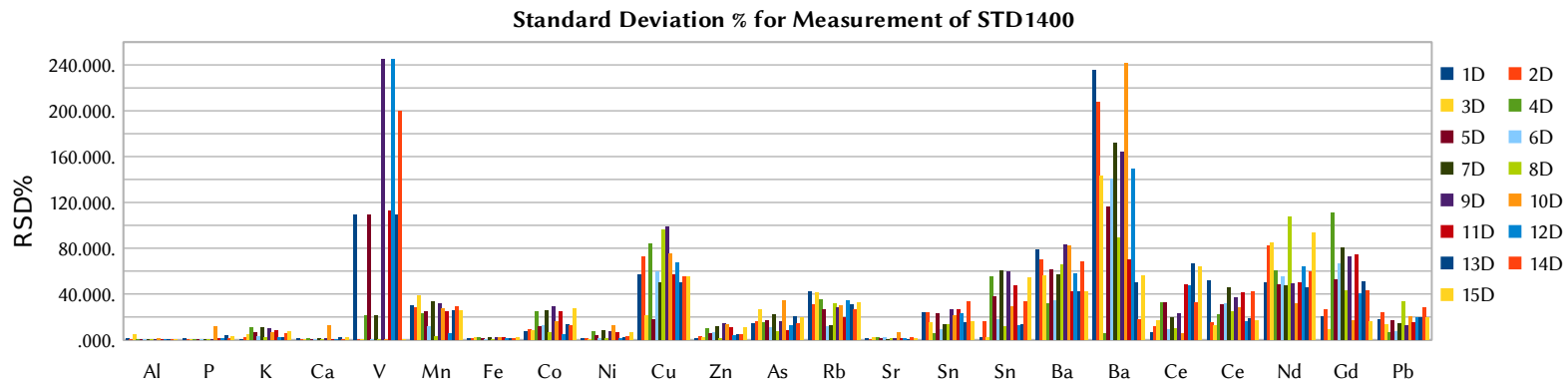


Figure 27: Relative standard deviation from measurement of SRM NIST 1400 Bone Ash (from per Day Routine Check)

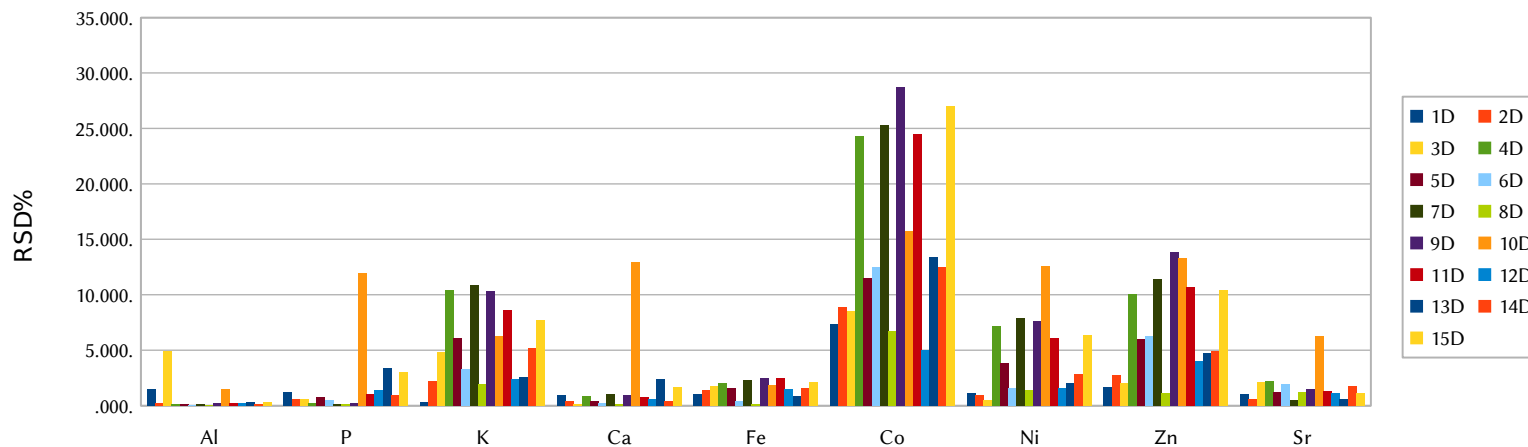


Figure 28: Elements with less than 30% of relative standard deviation from measurement of SRM NIST 1400 Bone Ash

5.2 Accuracy

Accuracy of measurement involves the proper calibration of instruments to yield results that agree with accepted standards (Pyrzszak and Tcherni-Buzzeo, 2018). Accuracy can be evaluated by assessing the difference between the true value and the measured value of a quantity (Zaichick et al., 2011). In order to ensure accuracy, Bergmann (2019) proposed a comparative measurement strategy involving more than one technique in her study involving analysis using p-XRF and ICP-MS. As part of this analysis, a standard reference material was measured during the scanning period to ensure accuracy. As outlined in the previous chapter, a method of calibration was developed to obtain a concentration of elements (see section 4.7). The estimated concentration for seven elements (Ca, P, Sr, Fe, Zn, Mn, and Ni) showed over 90% accuracy, which were used for further analysis and interpretation (see table 9). Additionally, the mean element concentrations obtained from routine checks of the reference materials were compared with the certified values as a standard procedure to assess instrument performance (Gomes et al., 2024).

A comparative approach to identify the instrumental performance between two different p-XRF devices (Thermo Scientific Niton XL3t 900 GOLDD+ and TRACER III SD) was attempted. This was done by comparing the mean values for SRM NIST 1400 Bone Ash from literature to the values derived in the current analysis (see Table 9). A difference was observed in the measurements gathered for Ca and P using TRACER III SD, compared to the values obtained by Gomes et al. (2024). In addition, SRM NIST 1400 Bone Ash measurements in this study indicate a high variability for Ca and P. On the other hand, values of elements such as Zn, Mn, and Fe show greater accuracy in this analysis compared to the values mentioned in the work of Gomes et al. (2024).

Similarly, a second comparison was performed to evaluate the variability and sensitivity of different techniques applied in the analysis of human remains. This involved a comparison of the values obtained for SRM NIST 1400 using the techniques such as ICP-MS and ED-XRF, as reported in literature, and the values obtained in the current analysis with Tracer III SD p-XRF (see Table 10). The results show higher precision and accuracy for the measurements gathered from analyses using laboratory XRF and ICP-MS than p-XRF for elements such as P, Ca, Fe, Ni, and Zn. Conversely, Sr yielded more accurate values using p-XRF, though this cannot be

generalised. Similarly, previous studies mention variability noted in the mean concentrations obtained for the same materials using p-XRF and laboratory XRF (Sheppard et al., 2011). Additionally, the number of elements that can be detected and quantitatively analyzed by the techniques mentioned in Table 10 cannot be matched by p-XRF analysis.

Table 9: Mean and SD obtained for NIST 1400 Bone Ash (from analysis and from literature)

Element	Certified value for STD 1400	Thermo Scientific Niton XL3t 900 GOLDD+ (Gomes et al., 2024)				Tracer III SD Measurement from all Analysis 180sec	
		Mean and SD-120 sec	RSD%	Mean and SD-240 sec	RSD%	Mean and SD (180 sec)	RSD%
P	17.91 ± 0.19	17.49± 0.4	2.3	17.11± 1.7	9.9	16.85 ± 0.9	5.3
Ca	38.18 ± 0.13	38.99 ± 0.3	0.8	39.27± 1.5	3.8	37.28± 0.2	0.5
Fe	660 ± 27	578.4 ± 26.6	4.6	1018.6± 148.6	14.6	665.27±9	1.3
Zn	181±3	190.3± 5.9	3.1	172.1± 7.4	4.3	173.06±9.2	5.3
Sr	249±7	233.5± 2.7	1.1	201.5± 35.7	17.7	250.53± 6	2.41
Ni	5.75 ±0.3565 (Hinneret.al.,1998)	Nil		Nil		5.56 ±0.16	2.9
Mn	17	Nil		Nil		15.03 ±1.8	12.3

Table 10: Comparison of verified element concentrations with three different technique

Element	Certified Value	ICP-MS Shafer et al., 2017	ED-XRF Lopes-Costas et al., 2016	TRACER III SD p-XRF
P	17.91 ±0.19	17.61 ± 0.7	17.5 ± 2.1	16.85±0.9
Ca	38.18 ±0.13	38.2± 0.6	38.6 ± 4.9	37.28± 2
Fe	660±27	590 ± 700	620 ± 40	665.27±9
Zn	181±3	249 ± 7	181 ± 7	173.06±9.19
Sr	249±7	181 ± 3	247 ± 15	250.53±6.04
Mn	17	15 ± 10	15.5 ± 0.6	15.03 ±1.85

5.3 Reliability of measurement- from the analysis of human remains

Analysis detected the presence of elements such as Ca, P, Al, K, Si, S, As, Pb, Cu, Se, Nd, Sn, V, Ti, Ce, Ba, Rb, Re, Ba, Nd, Mn, Co, Ni, Cu, V from human remains. Considering the accuracy and precision (as noted in previous sections 5.1 and 5.2), a quantitative analysis focusing on seven elements was adopted for further discussion. These elements include calcium (Ca), phosphorous (P), nickel (Ni), iron (Fe), manganese (Mn), zinc (Zn), and strontium (Sr). The concentrations of elements measured in this study are expressed in part per million (ppm) except for Ca and P (in wt%). The quantification of minimal number of elements can be attributed to the lower sensitivity and limited element detection of this method (Byrne and Bush, 2016).

Measurements were obtained from randomly selected five spots in cranial bones and in long bones across their flat surfaces. Mean concentrations and standard deviation were calculated for each bone as well as for each individual (taking values from multiple bone elements). In addition, RSD% was calculated for the element concentration (Ca, P, Mn, Fe, Zn, Ni, and Sr) in each bone and is given as a frequency table (see Table 11).

Table 11: Frequency table for RSD% measurements for bones

(RSD%)/Elements	0% -20%	20% -40%	40% -60%	60% -80%	80% - more
P	35	16	3	0	0
Ca	45	8	1	0	0
Mn	5	6	12	16	15
Fe	5	18	14	8	9
Ni	45	8	0	0	1
Zn	3	18	15	6	12
Sr	40	11	1	1	1

**each column indicate number of measured bone with reliability falls in the particular interval of RSD%*

Based on the table, RSD% exceeds 20% for Mn, Fe, and Zn in numerous bones. Higher consistency and reliability were noted in the concentration of elements such as Ca, P, Ni, and Sr. The analytical performance of the machine was ensured by the SRM measurement. Thereby,

higher RSD % for elements such as Fe, Mn and Zn indicate the possible contamination that have affected the human remains. Additionally, irregular surface morphology leading to air attenuation can also lead to higher deviation (Gomes et al., 2021). Mn which showed a RSD% ranges up to 40% on measuring SRM NIST Bone Ash (see table 11).

5.4 Intra- bone variability

Intra-bone variability was verified by comparing the measurements taken across diaphysis and metaphysis sections of long bones (for completely preserved long bone), and the frontal, parietal, occipital, and temporal regions in cranial bones (for completely preserved cranium). These are expressed as graphical representations with mean values and standard deviations per bone in Figures 27-29.

Elements such as Mn, Zn and Fe depict a large standard deviation within the majority of the bones. A higher deviation was noted in the values of Mn, Zn, and Fe in bones obtained from the crypt of the Church of Espírito Santo, Évora. However, the cranial bones from the ossuary of the church do not show high variability for these elements. In particular, a high deviation for Fe concentration was observed within the tibia of individual SKL1, the humerus of individual SKRC, and multiple bones of individual SKRL2.

Similarly, Zn concentration varied greatly within the tibia of individual SKNP3 (5502 ± 9554 ppm) from CEIE, compared to the other bones. A higher variability in concentration of manganese was visible among the cranium of SKC (915 ± 553 ppm), humeri of SKRC (444 ± 330 ppm), and SKNP2 (755 ± 254 ppm). In general, the bones of individuals from pathological and non-pathological categories of identified collection (CEIE) showed a higher intra-bone variability for manganese concentration.

To assess the statistical significance of intra-bone variation, one-way ANOVA analysis was performed with JASP software on quantified elemental concentrations. For the analysis, three measurements taken from each spot within the same bone were considered as a single group. Thereby, each of these groups represents different regions scanned in a single bone. This enabled the comparison of various regions within cranial and long bones. Hence, ANOVA analysis included a total of fifty-four bone elements from the entire collection of human

remains. As a result, a non-uniform element distribution within the same bone was observed for the majority of the analysed bone samples (see Appendix Table A.2).

Statistically non-significant mean concentrations ($p > 0.05$) were noted for few bones indicating a uniform distribution of elements across their surface. These specific bones from various individuals and the elements with uniform distribution are as follows: cranial bones – COS2 (P, Sr, Mn, Zn, Fe), SKLC (Ca, P, Sr, Ni), SKL1C (Mn, Zn, Fe), SKP2C (Sr, Ni), PC2 (Ca, P, Sr, Ni, Zn, Fe); long bones- femur from SKRC (Ni) and SKP2F (Mn, Fe), tibia of SKLC (Ni), humerus of SKLC (Ni), SKP2 (Mn), and SKNP1 (Ca, P, Ni).

As seen from the overall analysis, the measured elements and bone types show a lack of pattern for intra-bone variability. However, the non-significant mean concentrations for various bones and elements listed above indicate that the cranial bones exhibit less intra-bone variability compared to long bones. Similarly, a less significant variation was observed for the concentration of Sr and Ni, compared to remaining elements such as Ca, P, Mn, Fe, and Zn. Sr as a less variable element across archaeological bones was also noted in previous studies (Smith, 2021).

The results of the statistical analysis suggest that variations are likely to occur within bones between the sampling locations on the dense cortical bone and those containing more trabecular bone structures across the cranium and long bones. Macrostructural components of the bone, (i) porous inner trabecular bone and (ii) dense cortical bone, have a differential turnover ratio across the skeletal regions. For long bones, a significant difference in the turnover rate was noted for new bone formation and healing across diaphysis and metaphysis (Inoue et al., 2017). Similarly, the distribution of Zn is higher across cement lines of cortical bones compared to the surrounding matrix (Pemmer et al., 2013). Consequently, the variation in the bone composition can also be influenced by irregular morphological patterns of the bones. Therefore, the intra-bone variability noted in the measurements from the diaphysis and metaphysis of long bones and different outer cranial bone surfaces was possibly influenced by the aforementioned factors. Besides, influences of age and diet can also result in heterogeneous elemental concentration within a bone. For instance, a difference in the distribution of major elements such as Ca and P within the same bone can be altered with age and pathological conditions along with a negative effect on bone mineral density (Zdrav et al., 2021). Greater

variability within bones implies that the individual is more likely to show significant differences (Smith, 2016).

In addition, intra-bone heterogeneity in elemental concentration can also be linked to differential diagenesis of buried bones (Lebon et al., 2010). Taphonomic alteration and air attenuation are another two factors that can lead intra-bone variability (Gomes et al., 2024). The reviewed p-XRF studies indicate different procedures for quantifying concentration of different elements within the skeleton. It involves either considering one bone as a representation of an individual or with an assumption that one measurement per bone can represent the individual elemental composition (Kilburn et al., 2021; Perrone et al., 2014). Hence, such sampling can lead to the possibility of error by extrapolation from one sampling locus to another within a bone element and the error magnitude depends on the loci from where the sample is taken (Thompson et al., 2009; Snoeck et al., 2014).

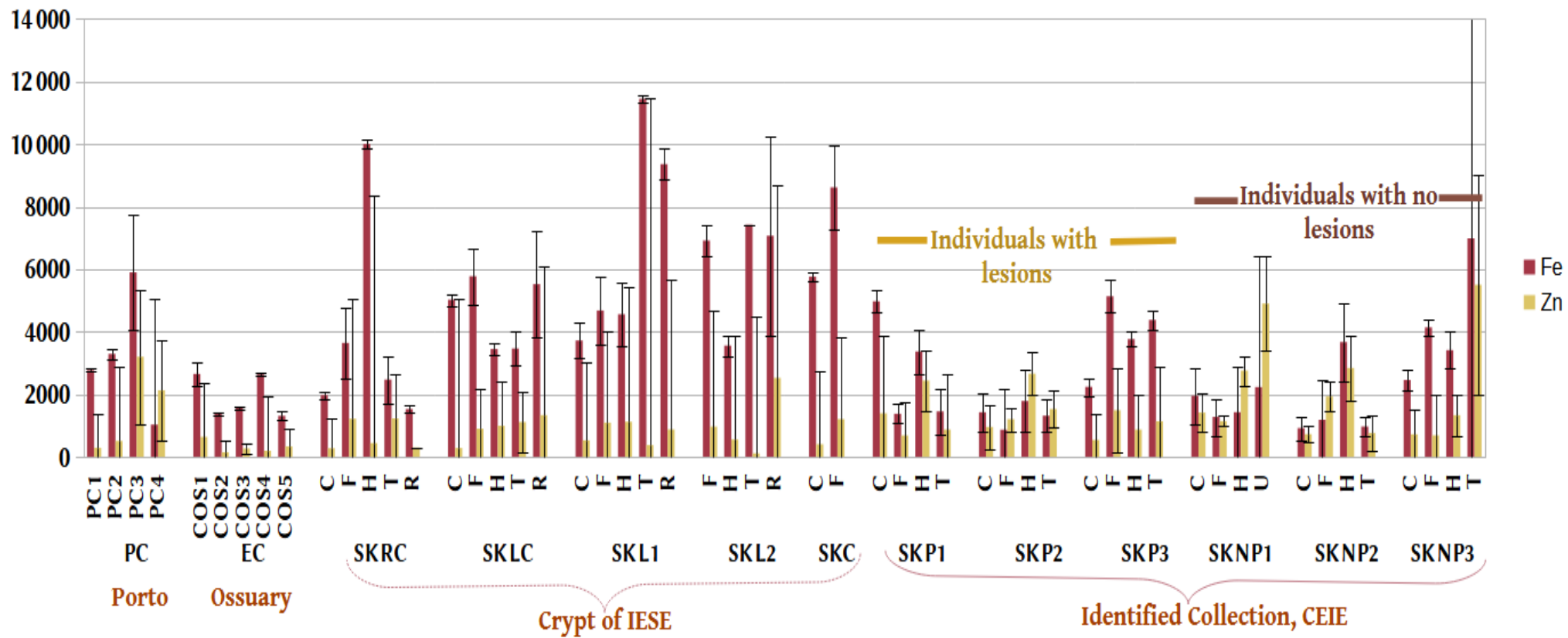


Figure 29: Intra-bone mean and standard deviation for Fe and Zn content in individuals from Porto and Evora (in ppm)

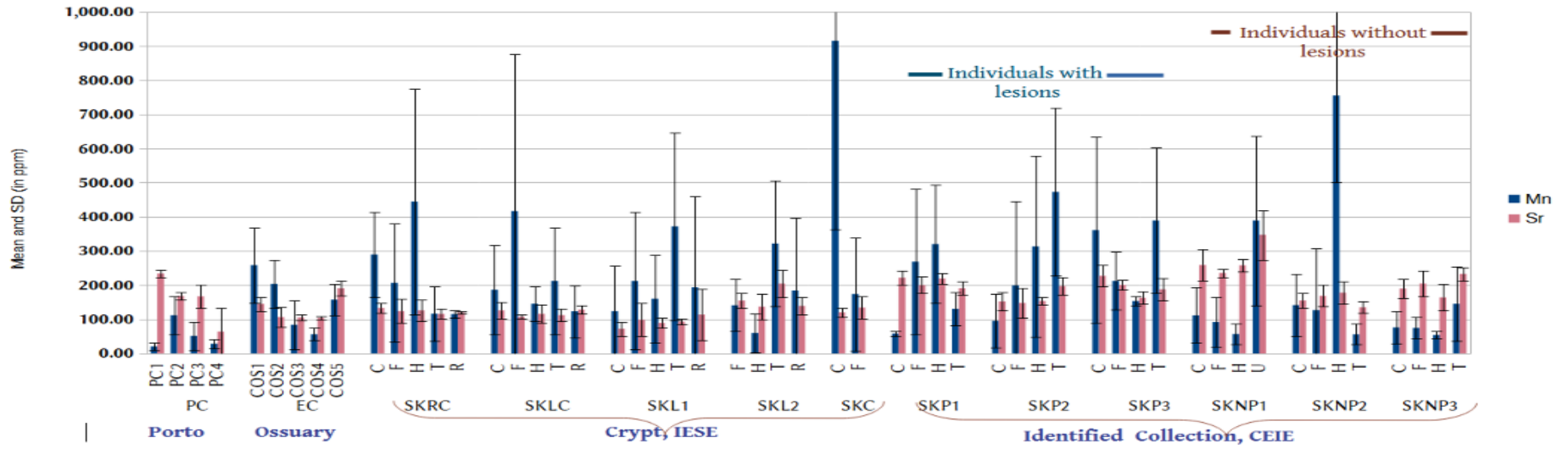


Figure 30: Intra-bone mean and standard deviation for Mn and Sr content in individuals from Porto and Evora

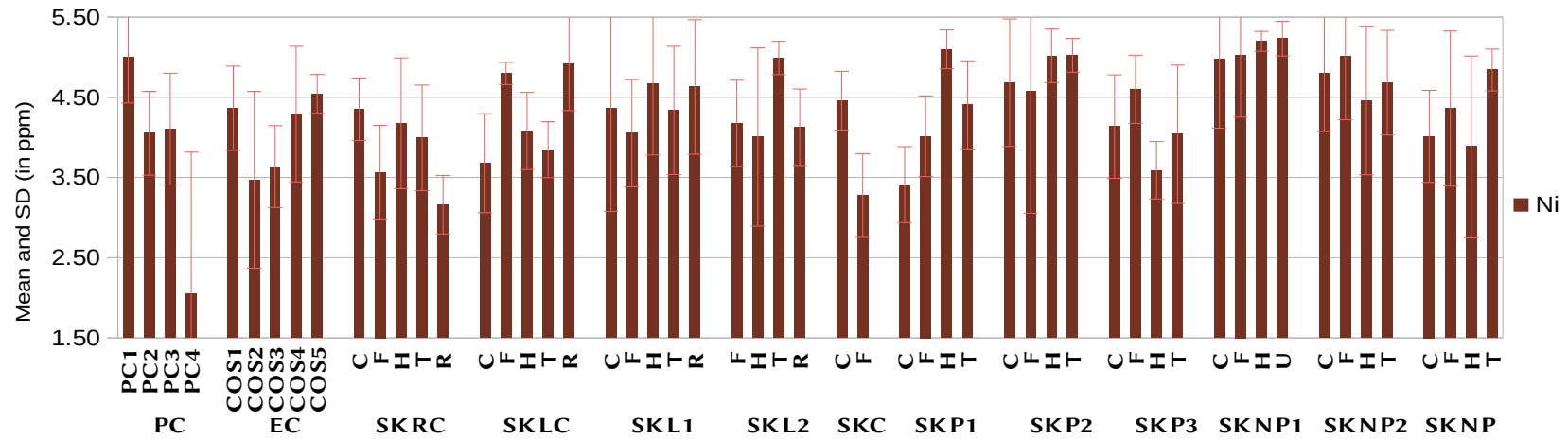


Figure 31: Intra-bone mean and standard deviation for Ni content in individuals from Porto and Evora (in ppm)

5.5 Intra -skeletal variability

Evaluation of intra-skeletal variability included only those individuals whose multiple skeletal parts were scanned. This sample group consists of three individuals buried within the crypt of Church of Espírito Santo, Évora (IESE) (SKRC, SKLC, SKL1) and six individuals from the Collection of identified Skeletons of Évora (CEIE) (SKP1, SKP2, SKP3, SKNP1, SKNP2, SKNP3). The mean concentration obtained for various long bones (femur, tibia, and humerus) and cranial bone were taken together to represent an overall mean elemental concentration for each individual. The standard deviation and mean concentration calculated for these individuals are presented in figure 30. Notably, a higher deviation was recorded for iron and manganese concentrations, indicating variability in the mean values measured across different bones within an individual.

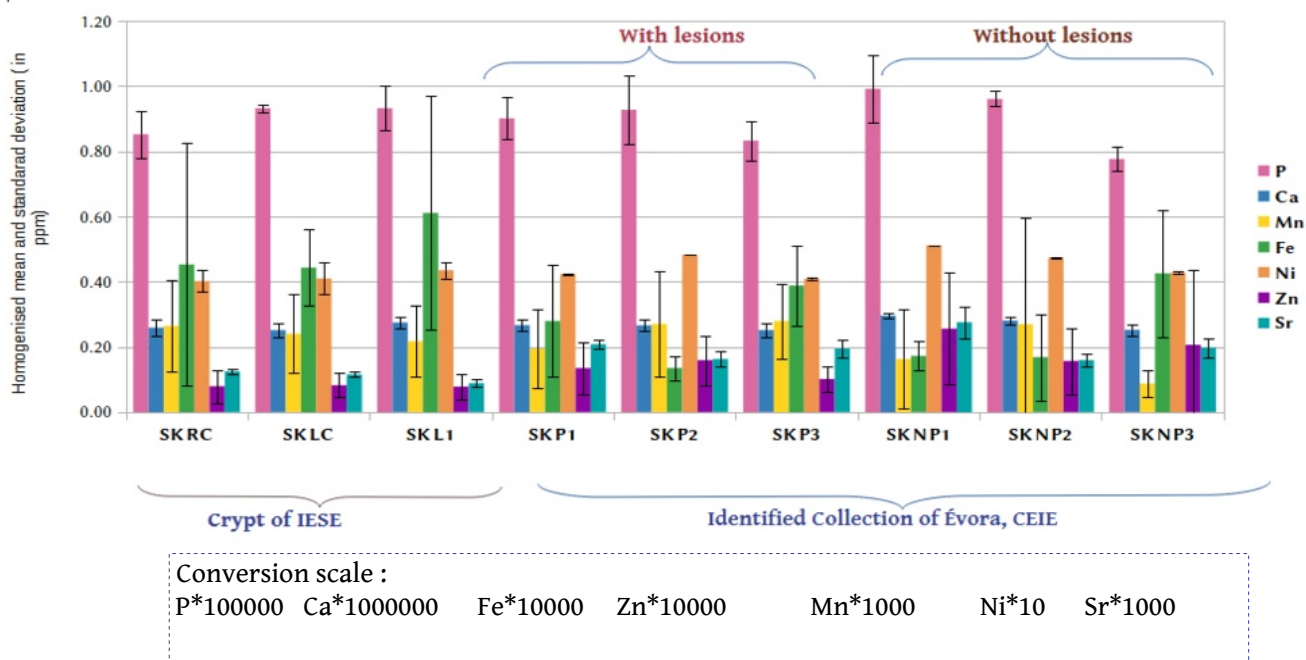


Figure 32: Intra-skeletal homogenised mean and SD of element concentration in individuals from the Church of Espírito Santo and collection of identified skeletons of Évora (in ppm)

A one-way ANOVA test was conducted using JASP software to analyse the significant intra-skeletal variability at the individual level, and the obtained results are shown in Table 12. A significant difference in mean concentration ($p < 0.05$) was visible for Ni, Sr, Mn, Zn, and Fe (see table 12). A uniform distribution of Ca and P concentrations was observed across different

bones within same skeleton for all individuals. Among the analysed individuals SKLC and SKL1 did not exhibit any significant intra-skeletal variability. Additionally, SKP1 was the only individual showing heterogeneous Ni concentration across its skeleton, with a higher Ni content observed in the humerus. Furthermore, non-uniform concentrations of Sr was observed for SKP3 and SKNP3, indicating differences in Sr content within their analysed bones. A notable intra-skeletal variation in Mn and Fe concentrations among the studied individuals may be influenced by the differential rate of diagenesis underwent by various bones of the same individual.

Table 12: ANOVA results for intra-skeletal variability. ** highlighted columns show individuals with significant intra-skeletal variability for elements with (i.e. p -value < 0.05)

Context	Individual	P		Ca		Ni		Sr		Mn		Fe		Zn	
		F value	P value	F value	P value	value F	value P	F value	P value	value F	P value	value F	P value	value F	P value
CEIE- Individual with Pathology	SKP1	0.58	0.64	3.05	0.06	16.81	<0.001	3.09	0.06	9.43	<0.001	3.41	0.04	6.87	0.003
	SKP2	1.68	0.21	0.64	0.6	0.34	0.797	3.16	0.05	2.66	0.08	2.007	0.15	3.36	0.04
	SKP3	0.75	0.54	1.88	0.17	2.34	0.112	5.52	0.01	2.05	0.15	4.54	0.02	6.22	0.005
CEIE- individual with no pathology	SKNP1	2.36	0.11	0.68	0.58	0.49	0.692	6.44	0.005	5.98	0.006	1.44	0.27	2.69	0.08
	SKNP2	0.09	0.97	0.57	0.65	0.44	0.727	2.421	0.1	20.04	<0.001	20.5	<0.001	6.07	0.006
	SKNP3	1.55	0.92	0.67	0.58	1.4	0.22	4.105	0.02	2.08	0.14	5.09	0.01	1.16	0.35
IESE- crpypt	SKRC	1.3	0.3	2.06	0.17	1.45	2.68	0.464	0.64	2.95	0.09	4.864	0.02	4.08	0.04
	SKLC	1.61	0.24	1.99	0.16	5.05	0.15	0.649	0.59	0.99	0.43	0.687	0.58	2.34	0.12
	SKL1	0.31	0.82	0.31	0.82	0.32	0.81	0.811	0.51	1.51	0.25	1.57	0.24	1.13	0.37

5.6 Inter -individual variability within the individuals from Porto

Four cranial bones unearthed from the necropolis at Porto represent the population that inhabited the city during the 18th century AD. Inter-individual variability among these four individuals was evaluated based on the elemental concentrations of their cranial bones (see Table 13). Individual PC1 exhibits higher concentration of Ca (30 ± 2 wt%), P (11 ± 2 wt%), Ni (5 ± 1 ppm), and Sr (234 ± 12 ppm) compared to the other three cranial bones examined from Porto. The concentrations of Fe (5899 ± 2158 ppm) in PC3 and Mn (111 ± 56 ppm) in PC2 were higher among the four. The concentrations of Ca and P in PC4 were lower in comparison to the other cranial bones from Porto (Table 14).

Table 13: Mean Concentrations and standard deviations for cranial bones from Porto

Elements / Cranium	P (wt%)	Ca (wt %)	Mn (ppm)	Fe (ppm)	Zn (ppm)	Ni (ppm)	Sr (ppm)
PC1	11 ± 2	30 ± 3	20 ± 10	2771 ± 1090	289 ± 46	4.9 ± 0.6	234 ± 12
PC2	9 ± 1	25 ± 3	111 ± 56	3290 ± 2357	506 ± 154	4 ± 0.5	168 ± 12
PC3	8 ± 1	24 ± 3	51 ± 41	5899 ± 2158	3199 ± 2129	4.1 ± 0.7	167 ± 34
PC4	2 ± 1	8 ± 4	28 ± 14	1030 ± 1626	2129 ± 4040	2 ± 1.8	64 ± 69

To determine significant difference in elemental concentration among the four individuals, one-way ANOVA and Post -Hoc tTukey tests were applied to the obtained values (see Appendix Table A.3). All elements except Zn showed a significant difference in the mean concentrations with $p > 0.05$. Zn value were higher in PC3 (3199 ± 1852 ppm) and in PC4 ($2,129 \pm 4,040$ ppm), which themselves were higher than reported values for other archaeological contexts (see Table 14). Similarly, the values for Zn noted in individuals PC1 (289 ± 46 ppm) and PC2 (506 ± 154 ppm) were comparatively lower than the values noted for cranial bones PC3 and PC4 from Porto. Zinc, which can be associated primarily with a meat or marine diet may indicate dietary difference (Allmae et al., 2016). But, Zn concentrations in mammalian bones of herbivores, carnivores, and omnivores, are also relatively lower than values obtained for the cranial bones from Porto (Janos et al., 2011). Therefore, Zn found within the archaeological bone via metal absorption can also be considered. The geological location and soil chemistry of the site

indicate that clayey soil constitute the burial ground (Inácio et al., 2008). The natural clayey soils exhibit higher adsorption of zinc, and may have contributed to metal sorption in bones (Behroozi et al., 2021; Choulet et al., 2016). However, such observations require further investigation through burial soil analysis.

5.7 Inter -individual variability within the individuals from Évora

Individuals from Évora include two groups, spanning the 15th to 19th century AD, from the excavated contexts of the church of Espírito Santo, Évora (IESE) and from the Collection of Identified Skeletons of Évora (CEIE). The state of preservation of these human remains varied among groups. Hence, we can assume that the diagenetic accumulation of elements may be influenced by exposure duration, and burial location (Miculescu et al., 2011). Additionally, individuals from CEIE include human remains with visible pathological lesions. Therefore, the mean elemental concentrations for these groups were calculated based on three aspects such as bone types, archaeological context (ossuary, crypt, pathological group, and non-pathology group), and pathological conditions. The mean values and standard deviations are listed in Tables 15 and 16.

Based on the measurements of all the bones types (humerus, femur, tibia, and cranium), higher Fe values (5502 ± 825 ppm) were noted for individuals retrieved from the crypt compared to the rest of the individuals from the identified collection of Évora and those unearthed from ossuary of the church (see Table 15 and 16). Similarly, individuals from the crypt also present a higher Fe concentration than the values mentioned in other archaeological contexts (less than 2121 ± 2264 ppm) (see table 14). A moderate variation in Fe content was observed among the individuals with and without pathological lesions, with a notable difference in the mean concentrations of tibia and cranium (see Table 16).

The estimated concentrations of Zn and Mn in cranial bones from the ossuary were lower than individuals buried in the crypt (Tables 14 and 15). Macroscopic observation also shows intact cranial bone preservation in the context of ossuary than that of crypt. As noted from the excavation, two of the skeletons (SKL1 and SKL2) were partially and completely covered by lime. Lime was traditionally used to accelerate the disintegration of human remains in

medieval burial chambers (Gutiérrez et al., 2013). This can alter the pH of the soil within the context and thereby influence the availability of elements such as Mn, Zn, and Fe, which bind to the organic fractions of soil. Changes in pH can enhance the mobility of these elements, leading to their incorporation into or leaching from the bones. This results in the dissolution of bone minerals and the introduction of new minerals to the bones (Shuman 1986; Mamatha et al., 2019). Hence, the evaluation of burial soil will also help to understand the influence of local soil as well as role of lime in diagenesis of bones.

The overall mean concentration of Zn was higher in the bones of the individuals from the identified collection, compared to those excavated from the Church of Espírito Santos, Évora. Contrastingly, the Zn values obtained from all individuals in Évora ($315 \pm 193 - 3722 \pm 2581$ ppm) indicate a higher concentration than the values reported in archaeological studies (less than 270.3 ± 126.8 ppm; refer Table 14) and in modern human bones (> 200 ppm) (Janos et al., 2011; Moroni et al., 2017; Zapata et al., 2006). Though zinc was considered an element less prone to diagenesis, the possibility of metal sorption from the burial soil cannot be excluded (Lopes-Costas et al., 2016).

Strontium concentrations of cranial and long bones from all individuals from the Church of Espírito Santos range between 117 ± 20 to 192 ± 5 ppm. Concentration taken together for the identified collection was higher ($178 \pm 36 - 238 \pm 106$ ppm) in comparison to the individuals from the Church of Espírito Santo, Évora. Sr content obtained from overall evaluation of individuals from Évora was slightly lower than archaeologically reported values and the value noted for modern humans (>200 ppm)(refer Table 14).

The bones from the individuals buried in the crypt and in the ossuary exhibit lower levels of phosphorous compared to those from the identified collection, indicating a depletion of P content in the former. When compared to modern human phosphorous levels, which are typically around 18%, the values obtained for all the individuals from Évora were lower than 10% (Zapata et al., 2006). Additionally, calcium concentration varies slightly between the individuals from the identified collection, but higher than the values found in the individuals from the crypt and ossuary. The calcium values from both contexts align with findings from

Table 14: Concentration of various elements reported in archaeological and modern human bones

	Type of Bone	Ca %	P %	Mn (ppm)	Fe (ppm)	Ni (ppm)	Zn (ppm)	Sr (ppm)
Janos et al., 2006	Vertebrae	24.4 ± 2.6	10.4 ± 14	115 ± 96.6	1506 ± 788	-	89.2 ± 21.6	488 ± 206
Carvalho et al., 2000	Not specified	-	-	55 ± 35.3	269 ± 167.5	-	90 ± 63.3	152.5 ± 38.9
Velasco-Vásquez et al., 1997	Not specified	21.7 ± 3.4	-	51.46 ± 43.41	-	-	25.1 ± 34	1515.6 ± 506.6
Moroni et al., 2017 (late medieval)	Femur	37.4 ± 2.7	-	14 ± 9.68	171.9 ± 163.6	5.2 ± 3.6	93.50 ± 26.8	631.28 ± 252.1
	Humerus	38.9 ± 1.9	-	19.7 ± 19	157.6 ± 183.7	3.9 ± 1	139.2 ± 46.5	580.33 ± 281.6
Moroni et al., 2017 (Copper Age)	Femur	37 ± 2.05	-	39 ± 39.2	183 ± 213.1	2.77 ± 0.7	144.5 ± 79	282.8 ± 7.6
	Humerus	38.9 ± 3.5	-	227 ± 138	174.4 ± 84.4	14.6 ± 11.6	224.3 ± 97	305.5 ± 24.7
Lopez-Costas et al., 2016	Cranial	22.8 ± 0.4	13.4 ± 3	77 ± 13	0.8 ± 0.1	-	130 ± 10	823 ± 35
	Long bone	22.8 ± 0.3	13.3 ± 4	90 ± 20	0.7 ± 0.1	-	159 ± 15	820 ± 35
Zapata et al., 2006	Long bone	27.9 ± 4.9	12.1 ± 1.3	26 ± 25	208 ± 198	-	205 ± 81	1120 ± 170
	Modern human bone	38	18	<10	<200	--	<200	<200
Bergmann, 2018	Modern Bone	6683 ± 65.8 (ppm)	-----	-	409.6 ± 16	---	----	874.6 ± 20.5
Allmae et al., 2016	Powdered Tibial bone	27.6 ± 3.4	-----	226.8 ± 141	----	-----	108.8 ± 29.9	115.6 ± 27.2
Perrone et al., 2014	Humerus	25.9 ± 19.7	42.6 ± 13.7	320.62 ± 99	2120.8 ± 2264	79.6 ± 13.5	239.2 ± 94.8	-
	Femur	24.3 ± 6.05	33.5 ± 16.9	361.1 ± 233	1919 ± 3248	78.4 ± 26.1	270.3 ± 126.8	-
	Tibia	25.2 ± 2.5	38.6 ± 17.9	325.7 ± 162	1013 ± 863	81 ± 13.6	162.3 ± 52.9	-

other archaeological sites (Moroni et al., 2017; Lopes-Costas et al., 2016; Allamae et al., 2012; Yoshinga et al., 1995). Ni concentrations showed less variation among the individuals from the Church of Espírito Santos and identified collections of Évora. Though, individuals from identified collection had higher nickel content in the bones, than those from the church context. In particular, mean concentration obtained for nickel was much lower in femoral bones of individuals excavated from crypt.

Table 15: Mean concentration and SD for various bones from ossuary and crypt of Church of Espírito Santo, Évora

Element	Cranium/ ossuary COS(n=5)		Cranium/ CRYPT (n=4)		Femur (n=5)/ CRYPT		Humerus (n=4)/ CRYPT		Tibia (n=4)/ CRYPT		Ribs (n=3)/CRYP T	
	Mean	SD	Mean	SD	Mean	SD	Mean	SD	Mean	SD	Mean	SD
Mn (ppm)	152	83	378	364	230	108	202	167	255	114	154	41
Fe (ppm)	1906	680	4120	1661	5926	1938	5393	3119	6200	4099	5871	3296
Ni (ppm)	4	0.5	4	0.4	4	0.6	4	0.3	4	0.5	4	0.8
Zn (ppm)	315	193	371	119	1075	141	778	331	707	549	1257	945
Sr (ppm)	130	38	113	28	124	22	117	20	131	50	125	11
Ca (wt%)	29	3	22	12	25	1	26	3	27	2	27	1
P (wt%)	9	3	8	3	9	0.4	8	1	9	1	10	2

Table 16: Mean concentration and SD for various bones from collection of identified skeletons of Évora (CEIE)

Element	Individuals with pathology								Individuals with no pathology							
	Cranium		Femur		Humerus		Tibia		Cranium		Femur		Humerus		Tibia	
	Mean	SD	Mean	SD	Mean	SD	Mean	SD	Mean	SD	Mean	SD	Mean	SD	Mean	SD

Mn (ppm)	171	165	226	37	262	94	331	179	109	33	98	27	288	404	197	172
Fe (ppm)	2878	1186	2459	2332	2972	1047	2382	1730	1776	785	2199	1681	2836	1227	3397	3177
Ni (ppm)	4	0.6	4	0.3	5	0.9	4	0.5	5	0.5	5	0.4	4	0.7	5	0.3
Zn (ppm)	962	425	1124	409	1990	977	1180	330	953	399	1254	630	2311	850	3722	2581
Sr (ppm)	200	42	183	130	178	36	192	5	201	53	203	33	200	51	238	106
Ca (wt%)	26	1	27	2	27	3	26	1	27	3	28	2	27	4	28	1
P (wt%)	9	1	9	1	9	1	8	1	9	2	9	1	9	2	9	1

(a) Analysis of cranial bones from ossuary and crypt of the church of Espírito Santo, Évora

An independent student's t-test was conducted to assess the variation in mean elemental concentration within the cranial bones from the ossuary and crypt (Appendix Table A.6). Since the individuals from the church context included both isolated cranial bones and complete skeletal remains, a common ground for statistical analysis was established by selecting only cranial bones from both sets. The mean concentration of each of the five cranial bones from the ossuary was considered as one group, while the four cranial bones from fully preserved individuals in the crypt were taken as the second group. The normality of the elemental concentrations in both groups was verified using the Shapiro-Wilk test as the first step for analysis (see Appendix Tables A.4 and A.5). A statistically significant difference was noted between the two groups for the mean concentration of Fe ($p=0.03$).

Similarly, Pearson's correlation analysis was performed for the entire cranium from the crypt and ossuary to examine the inter-elemental relationships. The correlation matrix is given below (Table 17). A strong positive correlation between Ca and P ($r= 0.789$) indicates the association of these elements as the primary chemical components in bone apatite (Jankuhn

and Butz, 2000). Besides, a significant positive correlation was identified among Fe and Mn ($r=0.629$), suggesting that Fe(II), Fe(III), and Mn(II) ions exhibit parallel mobility to osseous tissues due to their similar ionic radii. Mn and Fe ions incorporated into the bone apatite via ionic substitution or exchange with Ca ions can exhibit a strong negative correlation, indicating diagenesis (Butalag et al., 2007; Jankuhn and Butz, 2000; Janos et al., 2011). In contrast, a moderate negative non-significant correlations between Ca and Fe ($r= -0.330$) and Ca and Mn ($r= -0.185$) were noted in for these cranial bones. Therefore, a non-significant moderate positive correlation between Sr and Ca ($r=0.309$) limits the interpretation regarding diet or diagenesis.

Table 17: Correlation matrix for cranial bones from Church of Espírito Santo, Évora

Variable		P	Ca	Mn	Fe	Ni	Zn	Sr
1. P	Pearson's r	—						
	p-value	—						
2. Ca	Pearson's r	0.789	—					
	p-value	0.011	—					
3. Mn	Pearson's r	-0.136	-0.185	—				
	p-value	0.727	0.633	—				
4. Fe	Pearson's r	0.003	-0.330	0.629	—			
	p-value	0.994	0.386	0.070	—			
5. Ni	Pearson's r	0.450	0.628	0.319	0.165	—		
	p-value	0.224	0.070	0.402	0.670	—		
6. Zn	Pearson's r	-0.169	0.029	0.221	0.312	0.543	—	
	p-value	0.664	0.941	0.568	0.413	0.131	—	
7. Sr	Pearson's r	-0.151	0.309	0.091	-0.259	0.351	0.068	—
	p-value	0.698	0.419	0.816	0.500	0.354	0.862	—

(b) Comparison between individuals from crypt of the church of Évora and identified collection of Évora

The two groups of individuals (IESE and CEIE) from Évora vary in terms of their chronology and the burial location. In addition, the lesions observed in the bones of three individuals from CEIE

can influence bone composition. The mean and standard deviation of the three groups (individuals from the crypt (SKC), individuals with pathological lesions (SKP), and individuals with no pathological lesions (SKNP)) are given in Table 18. Descriptive statistics suggest a hierarchy among the element concentrations of these groups. High values were observed for Sr, Ca, P, and Ni concentrations within individuals of control group, with no lesions (SKNP). Similarly, mean value of Mn was high for the individuals with pathological lesions (SKP) and Fe was high in individuals from IESE (SKC). The variation may be associated with the influence of diagenesis and pathology, which likely affected the osteological tissues of these groups of individuals.

Table 18: Mean and standard Deviation between individual from IESE and CEIE (SKC- Individual from IESE; SKNP- individual with no pathological lesions (control Group); SKP- Pathological Group)

Groups	P (wt %)	Ca (wt %)	Mn (ppm)	Fe (ppm)	Ni (ppm)	Zn (ppm)	Sr (ppm)
SKC- (n=3)	9 ± 0.4	26 ± 1	240 ± 23	5017 ± 940	4 ± 0.2	797 ± 22	109 ± 19
SKNP (n=3)	9 ± 1	27 ± 2	173 ± 92	2525 ± 1494	5 ± 0.4	2060 ± 495	210 ± 59
SKP (n=3)	9 ± 0.5	26 ± 1	248 ± 47	2673 ± 1269	4 ± 0.4	1314 ± 289	188 ± 23

The variation among the three groups was assessed by one-way ANOVA and Post Hoc analyses. The mean concentration obtained for individuals from IESE- SKC (SKRC, SKLC, SKL1), individuals with pathological conditions- SKP (SKP1, SKP2, SKP3), and control group or individuals with no pathology- SKNP (SKNP1, SKNP2, SKNP3) as three different groups. ANOVA test results indicate a statistical significance in the mean concentration of Zn ($p= 0.01$) and Sr ($p= 0.039$). This suggests that there exists a significant difference within the observed mean concentrations of Sr and Zn among these individuals. Post-Hoc analysis shows that the individuals buried within the crypt yield lower Zn concentration than the remaining two groups. Similarly, difference in strontium was higher in group of individuals with no pathological lesions than the other two groups examined (see Appendix Table A.7).

The significant inter-individual variation within the individuals from Évora observed from the analyses was mainly associated with Fe, Zn, and Sr. Fe, was linked to the primary sources of burial contamination in archaeological bones (Shafer et al., 2017). The comparison of Fe concentrations in different bone types (long bones, cranium, and vertebrae) from archaeological sites to those individuals excavated from crypts also shows a difference, where the latter have high concentration (Moroni et al., 2017; Zapata et al., 2016). Zn concentration mentioned in various archaeological and pathological studies vary between 270 – 125 ppm (Magalhães et al., 2021; Janos et al., 2011; Lopes-Costas et al., 2016). In comparison to this range of values, the present study indicates higher concentration of Zn among various groups of individuals from Évora.

Strontium (Sr), an alkaline metal that can replace Ca due to similarity in ionic sizes, is often manifested as a chemical element absorbed on bone surfaces from burial contexts, typically within 0.5 mm of the cortical layer (Rasmussen et al., 2019). Sr is also associated with palaeodietary studies. The values of Sr, obtained for individuals from Évora align with reported values from literature, as in Table 14. In this study, normalizing the ratios of Zn and Sr to that of Ca values to delineate the dietary pattern was challenged by the possibility of diagenesis (Moroni et al., 2017).

5.8 Variation between individuals from Évora and Porto

As presented in Table 19, variability was noted for the mean concentration and standard deviation calculated for cranial bones from Porto and Évora. Elevated concentrations of Fe, Zn, and Sr were noted in the cranial bones of individuals from Porto. The remaining elements such as Ca, P, and Mn were comparatively higher in the cranial bone from Évora. The nickel content found in the cranial bones of individuals from both regions was relatively similar.

Table 19: Mean and SD from the cranial bones Measurements from Porto and Évora

Site	P	Ca	Mn	Fe	Ni	Zn	Sr
Évora (n=15)	9 ± 2	28 ± 3	211 ± 208	2,664 ± 1463	4 ± 0.5	590 ± 388	153 ± 52
Porto (n=4)	8 ± 4	22 ± 10	53 ± 41	3,248 ± 2014	4 ± 1	1,531 ± 1383	158 ± 70

To examine the significant variations within the descriptive values, one-way ANOVA and post hoc analyses were conducted on elemental values measured from cranial bones from Porto and Évora (Appendix A.8). A statistically significant difference was observed in the mean concentrations of Zn ($p=0.02$) and Ca ($p=0.04$) between the cranial bones from Porto and Évora, with higher concentrations of Zn and Ca in the cranial bones from Evora as noted in the post-hoc analysis.

5.9 Ca, P, and Ca/ P

Ca and P are the two major elements of hydroxyapatite ($Ca_{10}(PO_4)_6(OH)_2$) in bones. Hydroxyapatite undergoes chemical alterations like ionic exchange and ionic substitutions during the burial period (Bergmann, 2019). As a result, ions from the buried environment can substitute the innate ions constituting the bones. The Ca/P ratio has been used as a measure to assess the preservation of osteological remains from an archaeological contexts (Shafer et al., 2008). The Ca/P ratio can be indicative of secondary Ca carbonates accumulated in archaeological bones during the *post-mortem* period, which will result in a higher concentration of Ca than the normal level.

Relatively, the Ca/P ratio is used in palaeopathological studies as a biomarker for bone health. Calcium is released from the skeletal component when calcium homeostasis undergoes disturbance. If such conditions persist over the short-term, the bone replenishes without leaving any traces of it at the corporal level. However, the long duration of such a scenario can affect bone quality. On the other hand, phosphorus is present in the bone based on its bioavailability. Interaction between intestinal absorption, renal reabsorption and excretion, and redistribution between the extracellular phosphate, intracellular spaces, and the bone

phosphate storage pool facilitate maintaining a mean serum level of phosphate (Zdral et al., 2021). Table 20 shows Ca/P ratios for modern and archaeological human bones.

Table 20: Ca/P Ratio reported in literature

Reference	Type Technique	Type of Bone	Ca: P ratio
Zdral et al., (2021)	p-XRF	Dry bone with pathology vs normal	Femoral neck: 2.05 ± 0.18 vs. 2.19 ± 0.23 ; Femoral mid shaft: 1.89 ± 0.14 vs. 1.96 ± 0.13
Nganvongpanit et al., (2016)	p-XRF	Archaeological bone	2-3
Fabig and Herrmann, (2002); Zwanziger (1989).	AAS	Fresh bone	1.6 -2.3
Kilburn et al., (2021)	p-XRF	Archaeological bone	2.92
Zapata et al., (2006)	ED-XRF	Archaeological bone	2.30 - 2.50
Bergmann (2020)	p-XRF	Archaeological bone	1.6 -2.3
Gomes et al., (2021)	p-XRF	Dry bone with pathology vs normal	2.02 ± 0.14 (<i>Cribrra cranii</i>)- vs 2.05 ± 0.21 2.09 ± 0.18 (<i>Anaemia</i>) vs 2.01 ± 0.19

Table 21: Mean and SD of Ca and P and Ca/P

Label	Calcium (in wt%)	Phosphorous (n wt%)	Ca/P	Label	Calcium (in wt%)	Phosphorous (n wt%)	Ca/P
	Mean	Mean	Mean		Mean	Mean	Mean
PC1	30 ± 3	11 ± 2	2.8 ± 0.2	COS1	29 ± 4	7 ± 2	4.8 ± 1.2
PC2	25 ± 3	9 ± 1	2.8 ± 0.1	COS2	25 ± 7	6 ± 3	4.9 ± 2.3
PC3	24 ± 3	8 ± 1	2.9 ± 0.1	COS3	29 ± 2.4	10 ± 1	2.9 ± 0.1
PC4	8 ± 4	2 ± 1	3.9 ± 0.7	COS4	33 ± 2	14 ± 1	3 ± 0.8
SKP1-C	25 ± 3	9 ± 2	2.9 ± 0.2	COS5	31 ± 10	9.5 ± 1	3.2 ± 0.3
SKP1-F	28 ± 3	10 ± 2	2.9 ± 0.2	SKRC-C	30 ± 3	9 ± 2	3.2 ± 0.5
SKP1-H	29 ± 2	10 ± 1	3.1 ± 0.3	SKRC-F	23 ± 5	8 ± 1	2.8 ± 0.7

SKP1-T	26 ± 3	8 ± 2	3.2 ± 0.3	SKRC-H	24 ± 3	7 ± 2	3.3 ± 0.5
SKP2-C	27 ± 4	10 ± 2	2.7 ± 0.1	SKRC-T	27 ± 4	9 ± 1	3 ± 0.1
SKP2-F	24 ± 9	8 ± 3	3.2 ± 0.4	SKRC-R	26 ± 0.4	8 ± 0.6	3.3 ± 0.2
SKP2-H	28 ± 1	10 ± 4	2.8 ± 0.07	SKLC-C	24 ± 4	7 ± 2	3.7 ± 1.7
SKP2-T	27 ± 1	9 ± 4	3 ± 0.06	SKLC-F	26 ± 4	9 ± 1	2.7 ± 0.1
SKP3-C	25 ± 4	9 ± 2	2.9 ± 0.3	SKLC-H	28 ± 3	9 ± 1	3.04 ± 0.1
SKP3-F	28 ± 2	9 ± 1	3.2 ± 0.1	SKLC-T	23 ± 1	9 ± 1	2.4 ± 0.2
SKP3-H	23 ± 2	8 ± 7	2.9 ± 0.04	SKLC-R	27 ± 3	9 ± 1	3.06 ± 0.1
SKP3-T	24 ± 5	8 ± 2	3.2 ± 0.3	SKL1-C	28 ± 1	10 ± 3	2.8 ± 0.2
SKNP1-C	30 ± 4	11 ± 2	2.8 ± 0.2	SKL1-F	26 ± 4	9 ± 2	3 ± 0.3
SKNP1-F	29 ± 5	9 ± 2	3.2 ± 0.4	SKL1-H	29 ± 4	10 ± 2	2.9 ± 0.1
SKNP1-H	30 ± 5	11 ± 4	2.8 ± 0.1	SKL1-T	27 ± 6	9 ± 3	3.3 ± 1.03
SKNP1-T	29 ± 2	9 ± 1	3.3 ± 0.4	SKL2-F	25 ± 3	8 ± 1	3.03 ± 0.2
SKNP2-C	28 ± 3.5	10 ± 2	3 ± 0.3	SKL2-H	25 ± 5	9 ± 2	2.8 ± 0.2
SKNP2-F	29 ± 4	10 ± 2	3.02 ± 0.2	SKL2-T	29 ± 1	6 ± 2	4.7 ± 1.4
SKNP2-H	26 ± 5	9 ± 2	2.9 ± 0.2	SKL2-R	28 ± 2	11 ± 1	2.5 ± 0.05
SKNP2-T	28 ± 3	10 ± 1	3 ± 0.1	SKC-C	27 ± 2	9 ± 2	2.9 ± 0.2
SKNP3-C	24 ± 5	8 ± 2	3.2 ± 0.1	SKC-F	25 ± 3	9 ± 3	2.8 ± 0.1
SKNP3-F	26 ± 2	8 ± 6	3.3 ± 0.3				
SKNP3-H	23 ± 6	7 ± 2	3.2 ± 0.3				
SKNP3-T	27 ± 4	8 ± 3	3.8 ± 1.3				

As shown in Table 21, the calcium and phosphorus concentrations of the analysed bone vary within the range of 23 - 33 (in wt%) and 6 - 11 (in wt%). In comparison to phosphorous content in archaeological bones and modern human bones(18%), the concentration of P in the studied bones from Évora and Porto was lower (< 11 wt%)(refer to Table 14). The overall Ca concentration obtained from this study was similar to the values mentioned for archaeological bones in the literature (Table 14).

The current analysis resulted in Ca/P ratio varying between 2.3 and 5. Examined cranial bones from Porto (PC1, PC2, and PC3) range around 2.8 to 3.9. On the other hand, cranium PC4 shows high variability and lower mean values for Ca and P. Macroscopically, PC4 has a poorly preserved cortical surface, which has influenced the measurements, leading to higher intra-bone variability. The analysis of the Ca/P in different bones from the Church of Espírito Santo falls within the range of 2.4 to 4.9. An extremely higher ratio was observed for cranial bones COS1(4.8 ± 1.2) and COS2 (4.9 ± 2.3) from ossuary and tibia of individual SKL2 (4.7 ± 1.4). The Ca/P in normal human bones was recorded as 1.6 to 2.3 and in archaeological bones that underwent diagenesis as 2.30 – 2.92 (Fabig and Hermann, 2002; Zwanziger 1989; Zapata et al., 2006; Janos et al., 2011). In comparison to these values, most of the analysed bones from the context of church (both ossuary and crypt) show an elevated Ca/P, which suggests an active loss of bone mineral quality, potential diagenesis, and the differential degree of bones disintegration within the same site.

The average Ca/P calculated for the individuals from the identified collection varies from 2.8 to 3.8. The mean value obtained in this study for the individuals with lesions (3 ± 0.1) was similar to the individuals with no pathological lesions (3 ± 0.2). In contrast to the previous palaeopathological studies (as shown in Table 20), Ca/P values derived in this study are high. Hence, poor bone mineral density can be observed among these individuals, which was possibly associated with the pathological condition or age (Ensrud et al., 1995). Additionally, muddy soil of the burial ground extends a high occurrence of diagenesis. Therefore, the lesions created on the surface may have facilitated ionic exchange, leading to a high Ca/P ratio. Thus, the overall elemental content within these bones could be the combined result of diagenesis, physiological conditions, and pathology.

5.10 Pathological evaluation of individuals

The three individuals from the identified collection were associated with pathologies such as anemia and neoplasm. Anemia is characterised by reduced haemoglobin levels and can be acute or chronic in nature. The occurrence of lesions like *cribra orbitalia* has been central to diagnosing anemia in ancient skeletal remains and was visible in the skeletons of individuals SKP1, SKP2, and SKP3 (Brickley, 2024; Stuart Macadam, 2008). Additionally, individual SKP3 is

associated with neoplasia, characterized by abnormal cell growth, which can be either benign or malignant (Markret, 1968). Anemia is often found associated with other chronic conditions such as neoplasm, kidney failure and it can have an effect on over all element concentration (Cavill et al., 2006).

Table 22: Elemental concentration reported from palaeopathological studies

	Pathological Condition	*Ca (g/kg)	*P (g/kg)	Mn (ppm)	*Fe (g/kg)	Zn (ppm)	Sr (ppm)
Gomes et al., 2021 (Cranium)	Anemia	257.5 ± 7.7	124.01 ± 12.6	169.9 ± 102.5	1.08 ± 1.04	475.2 ± 343.6	103.7 ± 41.1
	CC	262.4 ± 6.5	130.6 ± 10.32	263.05 ± 145.7	2.4 ± 1.2	324.80 ± 133.66	113.8 ± 29.8
	Control Group	263.3 ± 7.3	132.4 ± 12.8	190.6 ± 141.5	1.3 ± 1.01	414.65 ± 347.71	110.2 ± 23.4
Magalhase et al., 2021 (cranium)		263.3 ± 2.7	132.6 ± 8.7	259.2 ± 149.3		298.5 ± 96.7	
Zdral et al., 2021	Osteoporosis		130.5 ± 877.4	257.12 ± 103.8	2.2 ± 2.7	1675.7 ± 1641.3	102.6 ± 33.7
	Control Group		138 ± 123.9	260.7 ± 849.9	3.3 ± 5.1	1910.4 ± 1520.4	105.3 ± 25.9

Bone concentration obtained via p-XRF was taken into account to evaluate possible asymmetries that can result from pathological conditions. Table 23 presents mean concentrations of Ca, P, Ni, Mn, Zn, Fe, and Sr measured in individuals with pathological lesions and in the control group (with no lesions). Based on the data, higher concentrations of Ca, P, Ni, Sr, and Zn were found within the control group. On the other hand, iron concentration is higher for individuals exhibiting visible lesions.

The concentration of Ca and P in both groups falls within the range of (~ 26- 28 wt%) and (8.9- 9 wt %), and are similar to the values noted for palaeopathological studies on human remains (see Table 22). On the other hand, the Ca/P ratio was found to be higher for both groups in comparison to literary mentions. Five of the six individuals in this analysis belonged to an age group over 70 years old. Therefore, increased Ca/P ratio can be indicative of loss of bone mineral as a result of physiological conditions. The youngest female individual (59 years) from the control group (with no pathological lesions) showed a Ca/P ratio 3.35 ± 0.3 , which was also higher than the values noted in previous conducted palaeopathological researches. Sexual dimorphic influence in the concentration of elements indicates a higher concentration of Ca and P in males than females. However, contrary to data observed from this analysis, studies on bones suggest higher Ca, and P levels in elderly females (Boyd et al., 1998).

The iron concentration observed in the studied pathological (2673 ± 1269 ppm) and non-pathological categories (2552 ± 1471 ppm) was higher than the value for anaemic subjects (1080 ± 1040 ppm) and the normal category (650 ± 1500 ppm) given in the literature (Gomes et al., 2024). Similarly, the high iron content estimated for the pathological group in this study contradicts the narrative of the deficiency in iron content among individuals who suffered from anemia and exhibited *porotic hyperostosis* (see table 23). Previous studies focused on anaemic individuals were found to have higher ferrous content in their bones (Maya 2019). Therefore, elevated content of Fe in the pathological group can be associated with multiple possibilities. Fe ions can percolate into the voids and cracks in the bone matrix rather than substituting Ca ions pointing to diagenesis (Lambert et al., 1985). Similarly, Fe deposition through the pathway of aeration of anoxic water can also raise iron content in the archaeological bones (Rasmussen et al., 2019). Absorption of non-heme Fe found in plants can also accumulate in the bones via the consumption of alcoholic beverages such as wine and beer due to the iron-sugar combination within these beverages (Sandford 1993). Alcoholic beverage consumption within the lower strata of the society of 19th century Portugal reinforces this possibility (Hens et al., 2019; Gomes et al., 2021).

Mn concentrations obtained for the group with bone pathological lesions (247.6 ± 47 ppm) and without lesions (173 ± 92 ppm) were analogous to values reported in the literature. However, the detected amount of Mn exceeds the value reported for normal human bones, which is < 10

ppm. Sr concentrations derived for individuals from CEIE are identical to the values reported from palaeopathological contexts (see table 22 and 23). Among the studied individuals, SKP1 has a comparatively lower concentration of Sr in comparison to the rest of the individuals.

Table 23: Mean concentration calculated for individual with pathological lesions and with no pathological lesions and female and male Individuals

Elements	Individuals with Pathology(n=3)	Control Group-(n=3)	Male (n=2)	Female (n=4)
Ca * (wt %)	26 ± 1	28 ± 0.2	27 ± 3.1	26.6 ±1
P* (wt %)	8.9 ± 0.5	9 ±1	9 ± 1 0.1	8.9± 01
Mn (ppm)	248 ± 47	173 ± 92	220 ± 82	205 ± 75
Fe (ppm)	2673 ± 1269	2552 ±1471	2800 ± 1525	2519 ± 1133
Ni (ppm)	4 ± 0.4	4.7 ± 0.4	4.6 ± 0.7	4.5 ± 0.3
Zn (ppm)	1314 ± 289	2060 ± 495	1783 ±1092	1639 ± 260
Sr (ppm)	188 ± 23	210 ± 59	234 ±57	182 ± 21
Ca/P	3 ± 0.07	3 ± 0.2	3 ± 0.01	3 ± 0.2

In addition, a t-test conducted using JASP software showed non-significant differences in the mean concentrations among the two groups ($p > 0.001$). Further, a correlation analysis was performed on these values from the six individuals to analyse the association of health and element concentrations (Table 24). A significant correlation between Ca and P ($p = 0.05$) was resulted from analysis, as these elements constitute the basic composition of bones. Additionally, positive correlations ($r = 0.828$ and $r = 0.853$) were also noticed between Ca-Ni and P-Ni. Ni is known to have both positive and negative influences on human health. Nickel toxicity, stemming from environmental pollution driven by natural and anthropogenic sources poses adverse effects on human health (Genchi et al., 2020). Its exposure has also been found to disrupt bone health by altering the remodelling process (Rodriguez and Mandalunis, 2018). The amount of Ni found in both groups of individuals from identified collection resembles to the values stated in archaeological bones from late medieval samples ($3 \pm 0.9 - 5 \pm 3.6$ ppm) and was lower than values of individuals from anthropological reference collection ($78 \pm 26 - 81 \pm 13$

ppm) (Moroni et al., 2017, Perrone et al., 2014) (see Table 21). So far, no studies have explicitly examined Ca, P, and Ni relationships in archaeological bones. In-vivo studies mention Ni deficiency in rats reduces calcium and phosphorus content in bones and alters the Ca: P ratio (Knuuttila et al., 1982). In contrast, Ni also plays a role in activating calcium receptors on osteoclasts triggering intracellular calcium signals that can inhibit bone resorption (Shankar et al., 1993).

Table 24: Correlation matrix for measurement of Elements in Individual from collection of identified skeletons (CEIE)

		P	Ca	Ni	Sr	Mn	Fe	Zn
P	Pearson's r	—						
	p-value	—						
Ca	Pearson's r	0.941						
	p-value	0.005						
Ni	Pearson's r	0.828	0.853					
	p-value	0.042	0.031	—				
Sr	Pearson's r	0.236	0.384	0.291	-----			
	p-value	0.653	0.452	0.576				
Mn	Pearson's r	0.369	0.086	0.053	-0.528	—		
	p-value	0.472	0.871	0.921	0.281	—		
Fe	Pearson's r	-0.932	-0.825	-0.861	0.013	-0.423	—	
	p-value	0.007	0.043	0.028	0.981	0.404	—	
Zn	Pearson's r	0.310	0.543	0.684	0.646	-0.675	-0.269	—
	p-value	0.550	0.266	0.134	0.166	0.141	0.607	---

According to the correlation matrix, significant negative correlations were visible among Fe-Ca (-0.932) and Fe-P (-0.825). Both iron overload and deficiencies have a negative impact on bone and body metabolism. An overload of iron affects bone remodelling by suppressing bone formation and aggravating bone resorption. These scenarios potentially affect the functioning

of osteoclasts and osteoblasts (Brackel and Oheim, 2024). Similarly, consumption of calcium-rich food like dairy products can decrease bioavailability, since calcium can bind with iron to form insoluble complexes. This makes iron less insoluble limiting its absorption (Lynch, 2007). Analysed cranial bones from the current study indicate a high value of Fe for the pathological group (2878 ± 185 ppm) and control group (1776 ± 785 ppm) in comparison to the values reported for individuals from similar spatio-temporal contexts and pathological conditions such as CC (2450 ± 1220 ppm), anaemia (1080 ± 1040 ppm), and control groups (650 ± 150 to 1280 ± 1010 ppm) (Gomes et al., 2024). Besides, the interpretation of Fe in archaeological bones should also address the possibility of contamination due to the high deviation observed within the samples measured. Fe and Ca negative correlation can be indicative of diagenesis, where Fe²⁺ and Fe³⁺ iron can fill the bone matrix when bone is exposed to burial soil. This lithogenic influence can be affirmed by analysing Fe content in soil and bone (Janos et al, 2011).

Further, an insignificant positive correlation for Zn-Ca ($r= 0.543$), Zn-Ni ($r= 0.684$), and Zn- Sr ($r= 0.646$) and a negative non-significant relationship among Mn-Sr ($r= 0.528$) and Zn- Mn ($r= 0.675$) were visible from the analysis. Elements such as Zn and Mn contribute to the study of metabolic conditions, diet, and diagenesis. Zinc is essential for the growth and mineralization of bone tissues, which is less affected by diagenesis and has a strong correlation with bone mineral density (Zdral et al., 2021; Moroni et al., 2017). The individuals with lesion from the study had a Zn mean concentration of 953 ± 399 ppm, from the cranial bones, while the non-pathological individuals indicate 965 ± 425 ppm. The amount of Zn noted from these individuals was comparatively higher than the values reported in palaeopathological studies (see Table 22).

5.11 Diet and diagenesis from the analysis

Analysis with p-XRF detected seven elements from two sets of individuals representing two different localities. Among these elements, Zn and Sr are often associated with dietary patterns followed by an individual or a population in an archaeological context (Shafer et al., 2017). Concentration of Sr in bone is representative of a plant-based diet. Similarly, Zn in archaeological bone has been linked to meat and marine food consumption. Janos et al. (2011) give typical ranges of Zn and Sr concentrations in mammalian bones denoting their food consumption patterns: (i) herbivores- Sr: 400-500 $\mu\text{g/g}$; Zn: 90-150 $\mu\text{g/g}$ (ii) omnivores-Sr: 150-400 $\mu\text{g/g}$; Zn: 120-200 $\mu\text{g/g}$ (iii) Carnivores -Sr: 100-300 $\mu\text{g/g}$; Zn: 175-250 $\mu\text{g/g}$. Beck (1985)

proposes some guidelines to establish a non-erroneous interpretation for dietary studies in terms of elements: (i) a direct relationship established between dietary levels and bone levels (ii) element concentration should not be affected by any pathological condition, since these can interfere with the measurement and concentration (iii) exclusion of diagenetic phenomena. However, interpretations based on the mentioned scale can be challenging due to the possibility of contamination.

In order to establish the dietary relationship based on the concentration of Zn and Sr, a correction with Ca needs to be established. A loss or enrichment of calcium in archaeological bones involves a corresponding loss or enrichment of other elements, which in turn affect the element-calcium ratio (Moroni et al., 2017). As per this, calcium concentration in the bones must be devoid of contamination. Elevated Ca/P ratio and higher deviation in element concentration s detected for Fe and Mn within analysed bones suggest the possibility of diagenesis. In addition, the macroscopic observation of some of the bone elements also exhibits a disintegrated surface. This can facilitate elemental alteration within the bones via different pathways such as: (i) incorporation of micro grains from the burial soil to the micro voids of the bone matrix and (ii) diffusion of elements from soil solution into the bone via ionic substitution or adsorption (Shafer et al., 2017). The CEIE collection included individuals with pathological conditions and varying Ca/P values. As noted, the Ca/P ratio from these individuals align with values that were established for diagenetically altered archaeological and palaeopathological bones. Previous studies on elemental mapping of archaeological bones insist on soil analysis as a beneficial tool to account for diagenetic changes (Gomes et al., 2024). Based on aforementioned aspects, the dietary pattern of the population is inconclusive.

Iron, manganese, and zinc concentrations in different bone elements from individuals of both regions have a high relative standard deviation, indicating the possibility of diagenesis induced by the burial environment. All these elements can percolate into the bones via metal sorption or ionic exchange. Besides, a significant difference in zinc concentrations in individuals from Porto and Evora can also be attributed to varying geographical locations.

CHAPTER -6

CONCLUSION

Portable X-ray fluorescence, as an analytical technique, is beneficial for examining the composition of archaeological human remains. It can be used as a qualitative and quantitative analytical method to derive chemical element concentrations in archaeological bones. As an emerging technique, associated features portability and rapid information retrieval can help in using it on-site and in the lab. The current study applied the technique to analyse human bones tissues collected from following archaeological sites: (i) necropolis associated with the Hospital of Third Order of Our Lady of Carmo, Porto (ii) Church of Espírito Santo, Évora, along with individuals chosen from Collection of Identified Skeletons of Évora (CEIE).

Seven elements, calcium (Ca), phosphorous (P), manganese (Mn), zinc (Zn), iron (Fe), nickel (Ni), and strontium (Sr) were detected and quantified with this technique. An appropriate sampling strategy formulated based on previous studies, focused on sampling flat surfaces of bones. Therefore, the analysis concentrated on cranial bones and long bones mainly the femur, humerus, and tibia. Randomly chosen portions for p-XRF scanning included spots on parietal, temporal, and occipital portions of cranial bones and diaphysis and metaphysis portions in long bones.

As per statistical analysis and calculated relative standard deviation (in %), a significant intra-bone variability in terms of elemental concentration was observed. The element concentrations of nickel and strontium showed less variation within the bones. Among the various bone types analysed, the cranium depicts the least intra-bone variation. Intra-bone variability asserts the impact of diagenetic alterations, and differential turnover ratio across bone tissues (trabecular vs cortical tissues). Intra-skeletal variability examined for nine individuals indicates a significant difference in mean concentration of various elements across different bone types. This variation was mainly visible for the concentration of manganese and iron. Elements such as calcium and phosphorous did not implied any significant variation, suggesting a uniform distribution Ca and P across the skeletons of studied individuals.

The inter-individual variation was analysed at three levels. The first of these include comparison of elemental concentrations obtained from four cranial bones of individuals from Porto. The results indicates differences in the estimated means of all elements except Zn. Similarly, the individuals from the Church of Espírito Santo, Évora indicate significant difference in their iron concentrations. Comparative analysis involving completely preserved skeletal remains of individuals from the Church of Espírito Santos, Évora and Collection of identified skeletal remains of Évora, resulted a significant variation in the elemental levels of Zn and Sr. Assessing the groups of individuals from all the sites, higher heterogeneity in elemental values within the individuals from Evora was visible. On evaluating the mean elemental values of cranial bones of individuals from Porto and Évora resulted a significant difference in their Ca and Zn concentrations.

The estimated mean concentrations slightly differed between individuals with pathological lesions and individuals with no pathological lesions. Higher values of Mn, and Zn were found for the individuals with no pathological lesions. Additionally, a positive correlation was found between calcium-phosphorus, calcium-nickel, and phosphorous-nickel concentrations measured from the bones of these individuals. These correlations were primarily associated to the role of these major elements (Ca and P) in bone composition and role of nickel in general bone metabolism.

The higher Ca/P ratio obtained from the study indicating the possibility of diagenesis in the bones of the individuals from Porto and from the Church of Espírito Santo, Évora,. The elevated Ca/P ratio observed for individuals from the identified collection (CEIE) due to loss of bone mineral integrity irrespective of pathological conditions. This can be associated with physiological conditions linked to older age and diagenetic influences. In addition, higher deviation and RSD% noted for iron, manganese, and zinc concentration per bone were indicate the higher possibility of diagenesis.

Besides, being a non-invasive analytical technique, p-XRF poses limitations when applied to human remains, primarily in terms of its sensitivity. Compared to the other sensitive techniques, the range of elements that can be analysed from human remains are limited in number. However, the accuracy and precision were found to be considerable enough to detect

major and some minor elements such as Ca, P, Fe, Ni, Sr, and Zn in human bones. The inaccurate quantification for many other major and minor elements constituting human remains limits interpretations of diagenetic and pathological conditions. Hence utilization of p-XRF in conjunction with other methods can provide in-depth information about archaeological human remains. Unable to analyse soil from the respective archaeological sites associated with the human remains poses difficulty in assigning the exact role of elements such as iron and manganese, since both can be significant in interpreting the bone chemistry diagenetically as well as metabolically. Hence future analysis including the remains from the same sites along with the analysis of soil samples can enhance our understanding of these aspects.

6.1 Practical suggestions for non-invasive p-XRF analysis of human bone tissues:

Obtaining optimal results from quantitative analysis of human bone tissues using p-XRF depends on multiple factors such as the selection of bone types, setting up of machines, selecting instrumental parameters, and calibration using matrix-matched standards. Regardless of the machines or methods used, the most necessary factor that needs to be addressed is safety precautions. Understanding the machine parts, its switches, associated symbols, and the working of the machine is relevant for conducting the study in safely. Therefore, referring the p-XRF safety and working manual is strongly recommended.

The initial step in this analysis involves selecting bones with flat surfaces (e.g., femur, humerus, tibia, cranium), to yield accurate results and reduced air attenuation. Besides, scanning should focus on clean bone surfaces without soil, clay encrustations, or labeling, as these can provide values that are less representative of bone composition, and the incident X-rays cover only a few millimetres of bone matrix. Although abrasive sampling surface preparation for more representative results was mentioned in the literature, this study followed a gentle cleaning method using distilled water. Keeping the bones dry at room temperature will reduce the influence of moisture while scanning.

Determining appropriate measurement parameters such as voltage, current, and duration, is crucial in the application of the p-XRF machine. In addition, the machine can be used filter and non-filter modes for analysis as seen in previous works. A strategy combining the appropriate

mode of scanning and instrumental parameters should be confirmed prior to the analysis by measuring a standard reference material or materials of similar composition. The use of matrix-matched standards such as NIST 1400 Bone Ash is suggested for pre-test and routine measurements. This approach helps in assessing the machine conditions and precision of the analysis. For an accurate quantification, measurements obtained for reference material and archaeological bone tissues can be considered (mean and relative standard deviation%), which will particularly help to identify extreme values which can either be the result of instrument conditions or due to diagenesis as observed in the study. Additionally, movement of both machine, and bones during analysis can lead to erroneous measurements. Though the machine is designed to operate by holding it in hand, long time measurement can be tedious. Hence stable positioning of the machine using a tripod stand will offer an easy and mobile way of measuring bones.

REFERENCES

- Allmae, R., J. Limbo-Simovart, L. Heapost, and E. Vers. (2012). The Content of Chemical Elements in Archaeological Human Bones as a Source of Nutrition Research. *Papers on Anthropology* 21, 27-49. <https://doi.org/10.12697/POA.2012.21.03>
- Almeida, M. A. (2021). As epidemias de cólera em Portugal 1833-1975. Em Jorge Couto (Eds.), *Atlas de história de Portugal: uma perspectiva geopolítica* (pp.232-233). Sociedade Francisco Manuel dos Santos. <http://hdl.handle.net/10071/26110>
- Argüello Menéndez, J. J., & da Silva Teixeira, S. A. (2008). *Catálogo do espólio fúnebre e funerário do Cemitério da Ordem do Carmo (1801-1869)*, Porto.
- Bamford, S. A., Wegrzynek, D., Chinea-Cano, E., & Markowicz, A. (2004). Application of X-ray fluorescence techniques for the determination of hazardous and essential trace elements in environmental and biological materials. *Nukleonika*, 49(3), 87-95.
- Barago, N.; Pavoni, E.; Floreani, F.; Crosera, M.; Adami, G.; Lenaz, D.; Larese Filon, F.; Covelli, S. (2022) Portable X-ray Fluorescence (pXRF) as a Tool for Environmental Characterisation and Management of Mining Wastes: Benefits and Limits. *Appl. Sci.*, 12, 12189. <https://doi.org/10.3390/app122312189>
- Bartl, R., & Bartl, C (2017). Structure and architecture of bone. In: *Bone Disorder: Biology, Diagnosis, Prevention, Therapy*. Springer, Cham. https://doi.org/10.1007/978-3-319-29182-6_2
- Bergmann, C. L. (2018). *Elemental analyses of archaeological bone using PXRF, ICP-MS, and a newly developed calibration to assess Andean Paleodiets* (Graduate thesis). Iowa State University.
- Behroozi, A., Arora, M., Fletcher, T. D., & Western, A. W. (2021). Understanding the impact of soil clay mineralogy on the adsorption behaviour of zinc. *International Journal of Environmental Research*, 15, 559-569. <https://doi.org/10.1007/s41742-021-00334-0>
- Bianchi, N., Moroni, A., Bonucci, S., Capecchi, G., Ancora, S., Ricci, S., & Leonzio, C. (2017). Trace Elements in Eneolithic and Late Medieval Human Bones from Two Archaeological Sites in Tuscany: Evaluation of Diagenetic Processes, Diet and Exposure to Heavy Metals. *Journal of Anthropology and Archaeology*, 5(2). <https://doi.org/10.15640/jaa.v5n2a3>

- Bloch, L. (2015). Use of Handheld XRF Bruker Tracer III-SD. Research Laboratories of Archaeology, The University of North Carolina at Chapel Hill.
- Bosch, P., Moreno-Castilla, C., Zapata-Benabithé, Z., Alemán, I., Lara, V. H., Mansilla, J., Pijoan, C., & Botella, M. (2014). On porosity of archeological bones I — Textural characterization of pathological Spanish medieval human bones. *Palaeogeography Palaeoclimatology Palaeoecology*, 414, 486–492. <https://doi.org/10.1016/j.palaeo.2014.09.018>
- Brouwer, P. (2003). *Theory of XRF: Getting Acquainted with the Principles*. PAN ANALYTICAL.
- Brynes, J. F., and P. J. Bush. (2016). Practical Considerations in Trace Element Analysis of Bone By Portable X-ray Fluorescence. *Journal of Forensic Science* 61(4):1041-1045.
- Burton, J. H., Price, T. D., & Middleton, W. D. (1999). Correlation of Bone Ba/Ca and Sr/Ca due to Biological Purification of Calcium. *Journal of Archaeological Science*, 26(6), 609–616. <https://doi.org/10.1006/jasc.1998.0378>
- Butalag, K., Quarta, G., Calcagnile, L., Arthur, P., Maruccio, L., D'Elia, M., & Caramia, A. (2007). PIXE analysis of trace elements in Middle age human and animal bones. *Proceedings of the XI International Conference on PIXE and its Analytical Applications, Puebla, Mexico*.
- Capobianco, G., Pelosi, C., Agresti, G., Bonifazi, G., Santamaria, U., & Serranti, S. (2017). X-ray fluorescence investigation on yellow pigments based on lead, tin and antimony through the comparison between laboratory and portable instruments. *Journal of Cultural Heritage*, 29, 19–29. <https://doi.org/10.1016/j.culher.2017.09.002>
- Caruso, V., Marinoni, N., Diella, V., Berna, F., Cantaluppi, M., Mancini, L., Trombino, L., Cattaneo, C., Pastero, L., & Pavese, A. (2020). Bone diagenesis in archaeological and contemporary human remains: an investigation of bone 3D microstructure and mineralo-chemical assessment. *Archaeological and Anthropological Sciences*, 12(8). <https://doi.org/10.1007/s12520-020-01090-6>
- Cascão, Rui (1993), „Demografia e sociedade”, in José Mattoso (ed.) – História de Portugal, vol. 5ª (Lisboa, Círculo de Leitores): 425-439.
- Çirak MT (2016) Anthropological assessment of element levels in anemic individuals. *Turk Stud* 12:169–178. <http://dx.doi.org/10.7827/TurkishStudies.12709>
- Clinton, C. K., Duncan, C. M., Shaw, R. K., Jackson, L., & Jackson, F. L. C. (2019). Identification of trace metals and potential anthropogenic influences on the historic New York African Burial Ground population: A pXRF technology approach. *Scientific Reports*, 9(1). <https://doi.org/10.1038/s41598-019-55125-7>
- Conrey, Richard & Goodman Elgar, Melissa & Bettencourt, N. & Seyfarth, Alexander & Steiner, Ashley & Wolff, J. (2014). Portable X-ray fluorescence spectrometer calibration for archaeological samples using influence coefficients. *Geochemistry: Exploration*,

Environment, Analysis.14.291-301.10.1144/geochem2013-198.
<https://doi.org/10.1144/geochem2013-198>

Craig, N., Speakman, R. J., Popelka-Filcoff, R. S., Glascock, M. D., Robertson, J. D., Shackley, M. S., & Aldenderfer, M. S. (2007). Comparison of XRF and PXRF for analysis of archaeological obsidian from southern Perú. *Journal of Archaeological Science*, 34(12), 2012-2024.
<https://doi.org/10.1016/j.jas.2007.01.015>

Curto, A., & Lopez, C. (2022). *Relatório de campo referente às intervenções antropológicas realizadas na Capela de São José da Igreja do Espírito Santo de Évora*.

Davis, I. (2023). Cholera comes to Portugal: Myth and science during the 1833-1834 epidemic and beyond. Cambridge Open Engage. <https://doi:10.33774/coe-2023-nlfvx>

Ensrud, K. E., Palermo, L., Black, D. M., Cauley, J. A., Jergas, M. D., Orwoll, E. S., Nevitt, M. C., Fox, K. M., & Cummings, S. R. (1995). Hip and calcaneal bone loss increase with advancing age: Longitudinal results from the study of osteoporotic fractures. *Journal of Bone and Mineral Research*, 10, 1778-178.
<https://doi.org/10.1002/jbmr.5650101122>

Fabig, Alexander & Herrmann, Bernd. (2002). Trace elements in buried human bones: Intra-population variability of Sr/Ca and Ba/Ca ratios- Diet or diagenesis?. *Die Naturwissenschaften*. 89. 115-9. <https://doi.org/10.1007/s00114-001-0294-7>

Ferrand et.al., 2014. ON THE ORIGIN OF THE GREEN COLOUR OF ARCHAEOLOGICAL BONE ARTEFACTS OF THE GALLO-ROMAN PERIOD, *Archaeometry* 56, 6 (2014) 1024-1040.
<http://dx.doi.org/10.1111/arcm.12042>

Finlayson, Janet E., Eric J. Bartelink, Alexandra Perrone, and Kevin Dalton 2017 Multimethod Resolution of a Small-Scale Case of Commingling. *Journal of Forensic Sciences* 62(2), 493-497. <https://doi.org/10.1111/1556-4029.13265>

Florencio-Silva, R., Sasso, G. R., Sasso-Cerri, E., Simões, M. J., & Cerri, P. S. (2015). Biology of Bone Tissue: Structure, Function, and Factors That Influence Bone Cells. *BioMed research international*, 2015, 421746. <https://doi.org/10.1155/2015/421746>

Frahm, E., & Doonan, R. C. (2012). The technological versus methodological revolution of portable XRF in archaeology. *Journal of Archaeological Science*, 40(2), 1425-1434.
<https://doi.org/10.1016/j.jas.2012.10.013>

Gancz, Abigail S. 2019 Evaluating the Utility of Portable X-Ray Fluorescence to the Discrimination of Human Remains from Commingled Contexts. Senior Honors Thesis. Department of Anthropology, University of North Carolina at Chapel Hill. Chapel Hill.

- Gauss, R., Bátorá, J., Nowaczinski, E., & Rassmann, K. (2013). A multimethodological approach for the investigation of archaeological ditches – Exemplified by the Early Bronze Age settlement of Fidvár near Vrábľe (Slovakia). *Archaeological Prospection*, 19(4).
<https://doi.org/10.1016/j.jas.2011.10.029>
- Gilbertson, Theresa Jane. (2015). A Comparative Analysis of Portable X-ray Fluorescence Spectrometry and Stable Isotopes in Assessing Ancient Coastal Peruvian Diets. Graduate Theses and Dissertations. <https://scholarcommons.usf.edu/etd/5951>
- Gomes, R.A.M.P., Catarino, L., Santos, A. L.,(2021). Anemia, cribra cranii and elemental composition using portable X-ray fluorescence: A study in individuals from the Coimbra Identified Osteological Collections. *J. Archaeol. Sci.* 136.
<https://doi.org/10.1016/j.jas.2021.105514>
- Gonzalez-Rodriguez, J., & Fowler, G. (2013). A study on the discrimination of human skeletons using X-ray fluorescence and chemometric tools in chemical anthropology. *Forensic Science International*, 231(1–3), 407. e1-6. <https://doi.org/10.1016/j.forsciint.2013.04.035>
- Goodale, N., Bailey, D. G., Jones, G. T., Prescott, C., Scholz, E., Stagliano, N., & Lewis, C. (2011). pXRF: a study of inter-instrument performance. *Journal of Archaeological Science*, 39(4), 875–883. <https://doi.org/10.1016/j.jas.2011.10.014>
- Goodale, Nathan, Madeleine Bassett, David G. Bailey, Ryan Lash, and Ian Kuijt. (2018). Early Medieval Seascapes in Western Ireland and the Geochemistry of Ecclesiastical Cross Stones. *Journal of Archaeological Science* 19, 894–902.
<https://doi.org/10.1016/j.jasrep.2017.06.015>
- Granite, G.E., 2012. Portable X-Ray fluorescence spectroscopy and its research applications to northern European bog bodies (Doctoral dissertation). State University of New York, New York.
- Grave, P., Attenbrow, V., Sutherland, L., Pogson, R., & Forster, N. (2012). Non-destructive pXRF of mafic stone tools. *Journal of Archaeological Science*, 39(6), 1674-1686.
<https://doi.org/10.1016/j.jas.2011.11.011>
- Greenlee, D.M. (1996). An electron microprobe evaluation of diagenetic alteration in archaeological bone. <https://doi.org/10.1021/bk-1996-0625.ch024>
- Gutiérrez, A., Nociarová, D., Malgosa, A., Fernández-Jalvo, Y., & Armentano, N. (2023). What does lime tell us about cadaveric remains?. *Historical Biology*, 1–10.
<https://doi.org/10.1080/08912963.2023.2297911>
- Hall, G. & Bonham-Carter, Graeme & Buchar, Angelina. (2014). Evaluation of portable X-ray fluorescence (pXRF) in exploration and mining: Phase 1, control reference materials.

- Geochemistry: Exploration, Environment, Analysis. 14. 99-123. 10.1144/geochem 2013-241.
- Hens, S. M., Godde, K., & Macak, K. M. (2019). Iron deficiency anemia, population health and frailty in a modern Portuguese skeletal sample. *PloS one*, 14(3). <https://doi.org/10.1371/journal.pone.0213369>
- Herrmann, B., Grupe, G., Hummel, S., Piepenbrink, H., & Schutkowski, H. (1990). *Prähistorische Anthropologie: Leitfaden der Feld- und Labormethoden*. Springer.
- Hughes, R. E. (1998). On Reliability, Validity, and Scale in Obsidian Sourcing Research. In *Unit Issues in Archaeology: Measuring Time, Space, and Material*, edited by A.F. Ramenofsky and A. Steffen, pp. 103-114. The University of Utah Press, Salt Lake City.
- Inácio, M., Pereira, V., & Pinto, M. (2008). The Soil Geochemical Atlas of Portugal: Overview and applications. *Journal of Geochemical Exploration*, 98(1-2), 22-33. <https://doi.org/10.1016/j.gexplo.2007.10.004>
- Inoue, S., Otsuka, H., Takito, J., & Nakamura, M. (2017). Decisive differences in the bone repair processes of the metaphysis and diaphysis in young mice. *Bone Reports*. <https://doi.org/10.1016/j.bonr.2017.11.003>
- János, I., Szathmáry, L., Nádas, E., Béni, Á., Dinya, Z., & Máthé, E. (2011). Evaluation of elemental status of ancient human bone samples from Northeastern Hungary dated to the 10th century AD by XRF. *Nuclear Instruments and Methods in Physics Research Section B: Beam Interactions with Materials and Atoms*, 269(20), 2593-2599.
- Johnson K, Quinn CP, Goodale N, Conrey R. (2024) Best Practices for Publishing pXRF Analyses. *Advances in Archaeological Practice*, 12(2), 156-162. <https://doi.org/10.1017/aap.2024.6>
- Johnson, K., Quinn, C. P., Goodale, N., & Conrey, R. (2024). Best Practices for publishing PXRF analyses. *Advances in Archaeological Practice*, 1-7. <https://doi.org/10.1017/aap.2024.6>
- Jomova, K., Makova, M., Alomar, S. Y., Alwasel, S. H., Nepovimova, E., Kuca, K., Rhodes, C. J., & Valko, M. (2022). Essential metals in health and disease. *Chemico-Biological Interactions*, 367, 110173. <https://doi.org/10.1016/j.cbi.2022.110173>.
- Kaiser, B., & Wright, A. (2008). *Draft Bruker XRF Spectroscopy User Guide: Spectral Interpretation and Sources of Interference*. Retrieved October 1, 2015, from http://www.trs-environmental.com/Specs-Manuals/BAXS_S1_TURBO_SDR_Manual.
- Kawalkar, A. C. (2014). A comprehensive review on osteoporosis. *Journal of Trauma & Orthopaedics*, 9(4), 3- 12. <https://doi.org/10.1016/j.jto.2014.09.003>

- Kilburn, N., Gowland, R. L., Halldórsdóttir, H., Williams, R., & Thompson, T. (2021). Assessing pathological conditions in archaeological bone using portable X-ray fluorescence (pXRF). *Journal of Archaeological Science. Reports*, 37, Article 102980. <https://doi.org/10.1016/j.jasrep.2021.102980>
- Kimmerle, E. H., & Baraybar, J. P. (2008). *Skeletal Trauma: Identification of Injuries Resulting from Human Rights Abuse and Armed Conflict* (1st ed.). CRC Press. <https://doi.org/10.1201/9781420009118>
- Kobylarz, D., Michalska, A., & Jurowski, K. (2023). Field portable X-ray fluorescence (FP-XRF) as powerful, rapid, non-destructive and 'white analytical tool' for forensic sciences - State of the art. *TrAC Trends in Analytical Chemistry*, 169, 117355. <https://doi.org/10.1016/j.trac.2023.117355>
- Krzysztof Szostek, Henryk Głąb, Aleksandra Pudło. (2009). The use of strontium and barium analyses for the reconstruction of the diet of the early medieval coastal population of Gdańsk (Poland): A preliminary study, *HOMO*, Volume 60, Issue 4, Pages 359-372.
- Kučera, L., Lundová, M., Šín, L., Dehnerová, H., Pechancová, R., Kurka, O. & Bednář, P. (2023). Evaluation of chemical composition of *cribra orbitalia* from post-medieval children graves (Olomouc, Czech Republic). *Praehistorische Zeitschrift*, 98(1), 389-398. <https://doi.org/10.1515/pz-2022-2045>
- Kumar, Vinay, Ebenezer, Supriya, & Thor, Andreas. (2021). Bone Augmentation Procedures in Implantology. In K. Bonanthaya, E. Panneerselvam, S. MaNuel, V. V. Kumar, & A. Rai(Eds.), *Oral and Maxillofacial Surgery for the Clinician* (pp. 407- 426). Springer Singapore. DOI: 10.1007/978-981-15-1346-6_19
- Lebon, M., Reiche, I., Bahain, J. J., Chadeaux, C., Moigne, A. M., Fröhlich, F., Sémah, F., & Falguères, C. (2010). New insights on diagenetic alterations of bones from the site of Payre (Middle Palaeolithic, Ardèche, France) using a multi-analytical approach. *Journal of Archaeological Science* 37(9), 1991-2000 37(9).
- Lemière, B. A review of pXRF (field portable X-ray fluorescence) applications for applied geochemistry. *Journal of Geochemical Exploration*. 188, 350-63 (2018). <https://doi.org/10.1016/j.gexplo.2018.02.006>
- Longoni, A., Fiorini, C., Leutenegger, P., Sciuti, S., Fronterotta, G., Strüder, L., & Lechner, P. (1998). A portable XRF spectrometer for non-destructive analyses in archaeometry. *Nuclear Instruments and Methods in Physics Research Section A: Accelerators, Spectrometers,*

Detectors and Associated Equipment, 409(1-3), 407-409. [https://doi.org/10.1016/S0168-9002\(98\)001132](https://doi.org/10.1016/S0168-9002(98)001132).

- Lopes, C., & Fernandes, T. (2022). The Identified Skeleton Collection of Évora: importance for forensic science and bioarchaeology in the southern inland of Portugal. *International journal of legal medicine*, 136(3), 955–962. <https://doi.org/10.1007/s00414-021-02725-6>
- López-Costas, O., Lantes-Suárez, Ó., & Martínez Cortizas, A. (2016). Chemical compositional changes in archaeological human bones due to diagenesis: Type of bone vs soil environment. *Journal of Archaeological Science*, 67, 43-51. <https://doi.org/10.1016/j.jas.2016.02.001>
- Loy, C., Brock, F., & Dyer, C. (2023). Investigating diagenesis of archaeological bones from Etton Causewayed enclosure, UK. *Quaternary International*. <https://doi.org/10.1016/j.quaint.2022.12.012>
- Magalhaes, B.M., Catarino, L., Carreiro, I., Gomes, R.A.M.P., Gaspar, R.R., Matos, V.M.J., Santos, A.L., (2021). Differential diagnosis of a diffuse sclerosis in an identified male skull (early 20th century Coimbra, Portugal): A multi methodological approach for the identification of osteosclerotic dysplasias in skeletonized individuals. *Int. J. Paleopathol.* 34. <https://doi.org/10.1016/j.ijpp.2021.06.002>
- Mamatha, D., Gowda, R. C., & Shivakumara, M. N. (2019). Effect of basic slag and lime on chemical properties of acid soil. *Emergent Life Sciences Research*, 5(2), 8-11. <https://doi.org/10.31783/elsr.2019.520811>
- Mamede, A. P., Gonçalves, D., Marques, M. P. M., & De Carvalho, L. a. E. B. (2017). Burned bones tell their own stories: A review of methodological approaches to assess heat-induced diagenesis. *Applied Spectroscopy Reviews*, 53(8), 603–635. <http://dx.doi.org/10.1080/05704928.2017.140044>
- Marín Arroyo, A. B., Landete Ruiz, M. D., Vidal Bernabeu, G., Seva Román, R., González Morales, M. R., & Straus, L. G. (2008). Archaeological implications of human-derived manganese coatings: A study of blackened bones in El Mirón Cave, Cantabrian Spain. *Journal of Archaeological Science*, 35(3), 801-813. <https://doi.org/10.1016/j.jas.2007.06.007>
- Loy, C., Brock, F., & Dyer, C. (2023). Investigating diagenesis of archaeological bones from Etton Causewayed enclosure, UK. *Quaternary International*, 660, 21-30. <https://doi.org/10.1016/j.quaint.2022.12.012>
- Maya, E. (2020). Testing the Iron Deficiency Anemia Hypothesis using p-XRF. Retrieved from <https://digscholarship.unco.edu/mcnair/1>

- McCormack, J., Szpak, P., Bourgon, N., Richards, M., Hyland, C., Méjean, P., Hublin, J.-J., & Jaouen, K. (2021). (2021). Zinc isotopes from archaeological bones provide reliable trophic level information for marine mammals. *Commun Biol* 4 (683). <https://rdcu.be/dY7rX>
- McGarry, A., Floyd, B., Littleton, J. (2021). Using portable X-ray fluorescence (pXRF) spectrometry to discriminate burned skeletal fragments. *Archaeol. Anthropol. Sci.* 13, 1–13. <https://doi.org/10.1007/s12520-021-01368-3>
- Miculescu, F., Ciocan, L. T., Miculescu, M., Ernuteanu, A., & Antoniac, I. (2011). The influence of the thermal treatment on the bone diagenesis phenomena. *Digest Journal of Nanomaterials and Biostructures*, 6(1), 225-233.
- Müller, K., Chadefaux, C., Thomas, N., and Reiche, I., (2011), Microbial attack of archaeological bones versus high concentrations of heavy metals in the burial environment: a case study of animal bones from a mediaeval copper workshop in Paris, *Palaeogeography, Palaeoclimatology, Palaeoecology*, 310, 39–51.
- Panchbhai, Arati S. (2015). Wilhelm Conrad Röntgen and the discovery of X-rays: Revisited after centennial. *Journal of Indian Academy of Oral Medicine and Radiology* 27(1),90-95. DOI: 10.4103/0972-1363.167119
- Pankowska, A., Monik, M., & Nechvátal, M. (2018). Reading the silhouettes of burnt dead: Using elemental analysis (pXRF) to identify Late Bronze and Early Iron Age urn cenotaphs. *Anthropologie (Brno)*, 56(1), 39-52. <http://dx.doi.org/10.26720/anthro.17.08.28.1>
- Pate F. Donald Noble Andrew H. (2000) Geographic distribution of C3 and C4 grasses recorded from stable carbon isotope values of bone collagen of South Australian herbivores. *Australian Journal of Botany* 48, 203-207. <http://dx.doi.org/10.1071/BT98024>
- Pemmer, B., Roschger, A., Wastl, A., Hofstaetter, J. G., Wobrauschek, P., Simon, R., Thaler, H. W., Roschger, P., Klaushofer, K., & Strelci, C. (2013). Spatial distribution of the trace elements zinc, strontium and lead in human bone tissue. *Bone*, 57(1), 184-193. <https://doi.org/10.1016/j.bone.2013.07.038>
- Perrone, A., Finlayson, J. E., Bartelink, E. J., & Dalton, K. D. (2014). Application of portable X-ray fluorescence (XRF) for sorting commingled human remains. In *Commingled Human Remains* (pp. 145-165). Academic Press.
- Pinto, Alexandre. (2018). Portable X-Ray Fluorescence Spectrometry: Principles and Applications for Analysis of Mineralogical and Environmental Materials. *Aspects in Mining & Mineral Science*. <http://dx.doi.org/10.31031/AMMS.2018.01.000506>

- Piorek, S. (1997). Field-portable X-ray fluorescence spectrometry: Past, present, and future. *Field Anal Chem. Technol* 1. [https://doi.org/10.1002/\(SICI\)1520-6521\(199712\)1:6%3C317](https://doi.org/10.1002/(SICI)1520-6521(199712)1:6%3C317)
- Portable Spectral Services. (2024, August 13). *Portable Spectral Services | Portable Analysers | Hire and sale*. <https://www.portaspecs.com/>
- Potts, P. J. (2008). *Portable X-ray fluorescence spectrometry : capabilities for in situ analysis*. Rsc Publishing, Cop. <https://doi.org/10.1039/9781847558640>
- Potts, Philip & Sargent, Mike. (2022). In situ measurements using hand-held XRF spectrometers: a tutorial review. *Journal of Analytical Atomic Spectrometry* 37. <http://dx.doi.org/10.1039/D2JA00171C>
- Radiology Star. (2022). *Production of X-rays*. Retrieved October 22, 2024, from <https://www.radiologystar.com/production-of-x-ray/>
- Rasmussen, K. L., Milner, G., Skytte, L., Lynnerup, N., Thomsen, J. L., & Boldsen, J. L. (2019). Mapping diagenesis in archaeological human bones. *Heritage Science*, 7(41). <https://doi.org/10.1186/s40494-019-0285-7>
- Rebocho, J. P., Carvalho, M. L., Marques, A. F., Ferreira, F. E., & Chettle, D.R. (2006). Lead post-mortem intake in human bones of ancient populations by (109)Cd-based X-ray fluorescence and EDXRF. *Talanta*, 70(5), 957-61. <https://doi.org/10.1016/j.talanta.2006.05.062>
- Ribeiro, B. T., Silva, S. H. G., Silva, E. A., & Guilherme, L. R. G. (2017). Portable X-ray fluorescence (pXRF) applications in tropical Soil Science. *Ciência e Agrotecnologia*, 41(3), 245-254.
- Richards, J. D., and C. R. Jones 2015 Using PXRF Technology to Aid in the Recovery and Analysis of Human Remains. Paper presented at the 80th Annual Meeting of the Society for American Archaeology, San Francisco, CA.
- Rodríguez, J., & Mandalunis, P. M. (2018). A Review of Metal Exposure and Its Effects on Bone Health. *Journal of toxicology*, 2018, 4854152. <https://doi.org/10.1155/2018/4854152>
- Sandford, M. K., Van Gerven, D. P., & Meglen, R. R. (1983). Elemental hair analysis: new evidence on the etiology of cribra orbitalia in Sudanese Nubia. *Human biology*, 55(4), 831-844.
- Ščesnaitė-Jerdiakova, A., Pliss, L., Gerhards, G., Gordina, E.P., Gustiņa, A., Pole, I., Zole, E., Kimsis, J., Jansone, I., & Ranka, R. (2015). Morphological Characterisation And Molecular Sex Determination Of Human Remains From The 15th-17th Centuries

In Latvia. *Proceedings of the Latvian Academy of Sciences. Section B. Natural, Exact, and Applied Sciences*, 69, 13 - 8. <https://dx.doi.org/10.2478/prolas-2014-0013>

Schattmann, A., Bertrand, B., Vatteoni, S., & Brickley, M. (2016). Approaches to co-occurrence: Scurvy and rickets in infants and young children of 16–18th century Douai, France. *International Journal of Paleopathology*, 12, 63–75. <https://doi.org/10.1016/j.ijpp.2015.12.002>

Schwartz, T. C. (2021). Determining dietary niche in primates using portable X-ray fluorescence. *Ursidae: The Undergraduate Research Journal at the University of Northern Colorado*, 10(1), Article 6. https://digscholarship.unco.edu/ug_pres_2020/29

Setiawati, Rosy & Rahardjo, Paulus. (2018). Bone Development and Growth. *Osteogenesis and bone regeneration* (pp. 5). Intechopen. DOI: 10.5772/intechopen. 82452.

Shackley, M. (2010). Is there reliability and validity in portable X-ray fluorescence spectrometry (PXRF)?. *SAA Archaeological Record*, 10(2), 17-18.

Shafer, M. M., Siker, M., Overdier, J. T., Ramsel, P. C., Teschler-Nicola, M., & Farrell, P. M. (2008). Enhanced methods for assessment of the trace element composition of Iron Age bone. *Journal of Archaeological Science*, 35(6), 1421-1434.

Sheppard, Peter & Irwin, Geoff & Lin, Sam & Mccaffrey, Cameron. (2011). Characterization of New Zealand obsidian using PXRF. *Journal of Archaeological Science*, 38(1), 45–56. <https://doi.org/10.1016/j.jas.2010.08.007>

Shuman, L. M. (1986). Effect of liming on the distribution of manganese, copper, iron, and zinc among soil fractions. *Soil Science Society of America Journal*, 50(5), 1236-1240. <https://doi.org/10.2136/sssaj1986.03615995005000050030x>

Simpson, R., Cooper, D. M.L., Swanston, T., & et al., (2021). Historical overview and new directions in bioarchaeological trace element analysis: A review. *Archaeological and Anthropological Sciences*, 13 (24). <https://doi.org/10.1007/s12520-020-01262-4>

Simpson, R., Varney, T. L., Coulthard, I., Swanston, T., Grimes, V., Munkittrick, T. J. A., Jankauskas, R., & Cooper, D. M. (2021). Insights into biogenic and diagenetic lead exposure in experimentally altered modern and archaeological bone: Synchrotron radiation X-ray fluorescence imaging. *The Science of the Total Environment*, 790, 148144. <https://doi.org/10.1016/j.scitotenv.2021.148144>

Smith, Rachel R. 2021. The Use of Portable X-ray Fluorescence to Resolve Commingled Assemblages of Human Remains. Masters Thesis. Department of Anthropology. Indiana University of Pennsylvania.

- Skytte, L., & Rasmussen, K.L. (2013). Sampling strategy and analysis of trace element concentrations by inductively coupled plasma mass spectrometry on medieval human bones- the concept of chemical life history. *Rapid communications in mass spectrometry: RCM*, 27 14, 1591-9. <https://doi.org/10.1002/rcm.6607>
- Snoeck, C., Lee-Thorp, J. A., Schulting, R. J., de Jong, J., Debouge, W., & Mattielli, N. (2014). Investigating the influence of cremation on the isotopic composition of bone: A case study from Stonehenge. *Journal of Archaeological Science*, 42, 72-82.
- Specht, A. J., Parish, C. N., Wallens, E. K., Watson, R. T., Nie, L. H., & Weisskopf, M. G. (2018). Feasibility of a portable X-ray fluorescence device for bone lead measurements of condor bones. *Science of the Total Environment*, 615, 398-403. <https://doi.org/10.1016/j.scitotenv.2017.09.295>
- St. Jankuhn, J., & Vogt, T. Butz. (2000). Investigation of ancient human bone by means of ionoluminescence and μ PIXE. *Nucl. Instrum. Meth. B*, vol. 161-163, pp. 894.
- Szostek, K., Głęb, H., & Pudło, A. (2009). The use of strontium and barium analyses for the reconstruction of the diet of the early medieval coastal population of Gdańsk (Poland): A preliminary study. *HOMO*, 60(4), 359-372. <https://doi.org/10.1016/j.jchb.2009.01.001>
- Thompson, R., et al. (2009). Sampling errors and their impact on data collection. *Journal of Statistical Science*, 24(3), 215-230.
- Walker, J (2020). Skeletal system 1: the anatomy and physiology of bones. *Nursing Times* [online]; 116: 2, 38-42
- Wilburn, A., Monahan, K., & Kimmerle, E. H. (2017). Commingling and the analysis of mixed skeletal remains. In E. H. Kimmerle & J. E. Baraybar (Eds.), *A companion to forensic anthropology*(pp. 123-145). Wiley-Blackwell.
- Winburn, Allysha & Rubin, Katie & Legarde, Carrie & Finlayson, Janet. (2017). Use of Qualitative and Quantitative Techniques in the Resolution of a Small-scale Medicolegal Case of Commingled Human Remains. *Florida Scientist*, 80, 24-37.
- Zaichick, S., Zaichick, V., Karandashev, V., & Nosenko, S. (2011). Accumulation of rare earth elements in human bone within the lifespan. *Metallomics: integrated biometal science*, 3(2), 186-194. <https://doi.org/10.1039/c0mt00069h>
- Zapata, J., P'erez-Sirvent, C., Martínez-S'anchez, M. J., Tovar, P. (2006). Diagenesis, not biogenesis: Two late Roman skeletal examples. *Science of the Total Environment* 369, 357-368. <https://doi.org/10.1016/J.SCITOTENV.2006.05.021>

- Zdral, S., Monge Calleja, A.M., Catarino, L., Curate, F., Santos, A. L. (2021). Elemental composition in female dry femora using portable X-Ray fluorescence (pXRF): Association with age and osteoporosis. *Calcif. Tissue Int.* 109, 231–240. <https://doi.org/10.1007/s00223-021-00840-5>
- Zimmerman, H. A., Meizel-Lambert, C. J., Schultz, J. J., & Sigman, M. E. (2015). Chemical Differentiation of Osseous, Dental, and Non-skeletal Materials in Forensic Anthropology using Elemental Analysis. *Science & Justice*, 55(2), 131–138. <https://doi.org/10.1016/j.scijus.2014.11.003>
- Zuckerman, M. K. (2010). *Sex, society, and syphilis: a social, ecological, and evolutionary history of syphilis in late medieval and early modern England (c. 1494-1865)* (Doctoral dissertation) Emory University.
- Zwanziger H. (1989). The multielemental analysis of bone. A review. *Biological trace element research*,19(3), 195– 232. <https://doi.org/10.1007/bf02924296>

APPENDIX

Table A.1: List of analysed individuals and bone types from all archaeological contexts

Provenance/ Context	Individual label	Type of Bone	Bone Analysed	Graphical Label	Provenance /Context	Individual label	Type of Bone	Bone Analysed	Graphical Label
Necropolis at Hospital of Church of Our Lady of Carmo, Porto(UE)	UE6394	Cranium	C	PC1(Porto Cranium 1)	Crypt and Ossuary at Church of Espiritos Santos, Evora (IESE)	IEESE/21-5	Femur	F	SKL2-F (Skeleton in Lime 2 -FEMUR)
	UE6138	Cranium	C	PC2(Porto Cranium 2)			Humerus	H	SKL1-F (Skeleton in Lime1 -Humerus)
	UE6094	Cranium	C	PC3(Porto Cranium 3)			Tibia	T	SKL1-T (Skeleton in Lime1 -Tibia)
	UE6117	Cranium	C	PC4(Porto Cranium 4)			Ribs	R	SKL1-R (Skeleton in Lime1 -Ribs)
Crypt and Ossuary at Church of Espiritos Santos, Evora (IESE)	IEESE-1	Cranium	C	COS1(Cranium from Ossuary No1)	Collection of Identified Skeletons From Evora	CEIE-123	Cranium	C	SKP1-C(Skeleton with Pathology1-Cranium)
	IEESE-2	Cranium	C	COS2(Cranium from Ossuary No2)			Femur	F	SKP1-F(Skeleton with Pathology1-Femur)
	IEESE-5	Cranium	C	COS3(Cranium from Ossuary No)			Humerus	H	SKP1-H(Skeleton with Pathology1-Humerus)
	IEESE-Cranio Ossario 1	Cranium	C	COS4(Cranium from Ossuary No4)			Tibia	T	SKP1-T(Skeleton with Pathology1-Tibia)
	IEESE-4	Cranium	C	COS5(Cranium from Ossuary No5)		CEIE-141	Cranium	C	SKP2-C(Skeleton with Pathology2-Cranium_
	IEESE/21-1	Cranium	C	SKC-C(Skeleton in Coiffing-Cranium)			Femur	F	SKP2-F(Skeleton with Pathology2-Femur
		Femur	F	SKC-F(Skeleton in Coffin-Femur			Humerus	H	SKP2-H(Skeleton with Pathology2-Humerus)
Crypt and Ossuary at Church of	IEESE/21-2	Cranium	C	SKC-RC(Skeleton right of Coffin-Cranium)			Tibia	T	SKP2-T(Skeleton with Pathology2-Tibia)
		Femur	F	SKC-RC(Skeleton right of Coffin-Femur)			CEIE-94	Cranium	C

Espiritos Santos, Evora (IESE)		Humerus	H	SKC-RC(Skeleton right of Coffin-Humerus)			Femur	F	SKP3-F(Skeleton with Pathology3-Femur)
		Tibia	T	SKC-RC(Skeleton right of Coffin-Tibia)			Humerus	H	SKP3-H(Skeleton with Pathology-Humerus)
	IESE /21-3	Cranium	C	SKC- C (Skeleton in Left of Coffin-Cranium)		CEIE-40	Tibia	T	SKP1-T(Skeleton with Pathology-Tibia)
		Femur	F	SKC- F (Skeleton in Left of Coffin-Femur)			Cranium	C	SKNP1-C(Skeleton with NoPathology1-Cranium)
		Humerus	H	SKC- H (Skeleton in Left of Coffin-Humerus)			Femur	F	SKNP1-F(Skeleton with No Pathology1-Femur)
		Tibia	T	SKC- T (Skeleton in Left of Coffin-Tibia)			Humerus	H	SKNP1-C(Skeleton with NoPathology1-Humerus)
		Ribs	R	SKC- C (Skeleton in Left of Coffin-Ribs)			Tibia	T	SKNP1-C(Skeleton with No Pathology 1-Tibia)
	IESE/21-4	Cranium	C	SKL1- C (Skeleton in Lime1 -Cranium)		CEIE-43	Cranium	C	SKNP2-C(Skeleton with No Pathology 2-Cranium)
		Femur	F	SKL1-F (Skeleton in Lime1 -FEMUR)			Femur	F	SKNP2-F(Skeleton with No Pathology2-Femur)
		Humerus	H	SKL1-H (Skeleton in Lime1 -Humerus)			Humerus	H	SKNP2-H(Skeleton with No Pathology2-Humerus)
		Tibia	T	SKL1-T (Skeleton in Lime1 -Tibia)			Tibia	T	SKNP2-T(Skeleton with No Pathology2-Tibia)
		Ribs	R	SKL1-R (Skeleton in Lime1 -Ribs)		CEIE--29	Cranium	C	SKNP3-C(Skeleton with No Pathology-Cranium)
					Femur		F	SKNP3-F(Skeleton with No Pathology 3-Femur)	
					Humerus		H	SKNP3-H(Skeleton with No Pathology-Humerus)	
				Tibia	T		SKNP1-T(Skeleton with No Pathology-Tibia)		

Table A.2: ANOVA results for intra-bone variation

Sample	Ca		P		Sr		Mn		Ni		Zn		Fe	
PC1	54.89	0.001	15.44	P<0.001	2624.33	P<0.001	45.699	P<0.001	1052.26 2	P<0.001	32558.094	P<0.001	525240.279	P<0.001
PC2	2.086	0.22	3.209	0.116	0.554	0.706	1392.379	P<0.001	1.625	0.301	16.065	0.05	84.467	P<0.001
COS1	220.734	P<0.001	143.698	P<0.001	39.466	P<0.001	359.915	P<0.001	73.854	P<0.001	3705.06	P<0.001	3587.35	P<0.001
COS2	40.644	0.002	5.66	0.064	2.955	0.161	1.252	0.402	152.790	P<0.001	1.434	0.357	0.691	0.601
COS3	180.058	P<0.001	44.802	P<0.001	7.68	0.023	121.405	P<0.001	435.61	P<0.001	14.67	0.006	84.14	P<0.001
COS4	174.670	P<0.001	1353.95	P<0.001	1127.886	P<0.001	5.84	0.04	7.06	0.03	12.981	0.008	5.66	0.042
COS5	90.224	P<0.001	53.08	P<0.001	50.23	P<0.001	56.305	P<0.001	91.957	P<0.001	149.45	P<0.001	387.562	P<0.001
SKC-C	1811.794	P<0.001	1534.156	P<0.001	309.11	0.003	10082.042	P<0.001	26905	P<0.001	451.27	P<0.001	4937.747	P<0.001
SKC-F	449.603	P<0.001	155.837	P<0.001	331.983	P<0.001	22925.9	P<0.001	693.134	P<0.001	284370.7	P<0.001	580.927	P<0.001
SKRC-C	28.67	P<0.001	65.03	P<0.001	30.456	0.001	52.413	P<0.001	14.63	0.06	34.22	P<0.001	11.7	0.009
SKRC-F	1131.632	P<0.001	189.738	P<0.001	2209.45	P<0.001	8266.854	P<0.001	938.502	P<0.001	2267.73	P<0.001	147487.110	P<0.001
SKRC-H	8738.5	P<0.001	171.577	P<0.001	192.54	P<0.001	131.082	P<0.001	43.876	0.02	269.207	P<0.001	3322.5	P<0.001
SKLC-C	1.302	0.382	3.384	0.107	0.931	0.514	13.055	0.007	1.282	0.388	184.211	P<0.001	241.68	P<0.001
SKLC-F	341.905	P<0.001	678.726	P<0.001	????	P<0.001	29636.79	P<0.001	12306	0.017	2625.378	P<0.001	1962.103	P<0.001
SKLC-T	76.267	P<0.001	155.28	P<0.001	49.780	P<0.001	13301.753	P<0.001	2.748	0.152	3094.215	P<0.001	202.049	P<0.001
SKLC-H	2524.804	P<0.001	552.721	P<0.001	170.544	P<0.001	7171.681	P<0.001	5.661	0.064	86.425	P<0.001	250.501	P<0.001
SKL1-C	123.380	P<0.001	126.04	P<0.001	12.163	0.009	3.874	0.085	169.529	P<0.001	1.255	0.396	2.010	0.231
SKL1-T	39214.95	P<0.001	26469.81	P<0.001	32.301	P<0.001	9492.358	P<0.001	225.704	P<0.001	652.879	P<0.001	248971.764	39214.946
SKL1-F	5182.611	P<0.001	2028.200	P<0.001	277.191	P<0.001	11780.81	P<0.001	860.345	P<0.001	118647.213	P<0.001	33633.847	P<0.001
SKLI-H	20072.133	P<0.001	3409.214	P<0.001	23.28	0.005	3088	P<0.001	2246.85	P<0.001	19720.05	P<0.001	146062.02	P<0.001
SKL2-F	105338.77	P<0.001	2318.6	P<0.001	310.516	P<0.001	1992.600	P<0.001	726.36	P<0.001	3438.844	P<0.001	139676.28	P<0.001

SKL2-T	150.320	P<0.001	10.748	0.043	505.089	P<0.001	133.24	0.01	73.85	0.03	0.59	0.009	5262.751	P<0.001
SKL2-H	59586.05	P<0.001	6205.29	P<0.001	627.717	P<0.001	1647.9	P<0.001	3030.62	P<0.001	3593.43	P<0.001	193428.08	P<0.001
SKP1-C	2034	P<0.001	2868.8	P<0.001	66.82	P<0.001	11.56	P<0.001	451.967	P<0.001	2164.13	P<0.001	4977.954	P<0.001
SKP1-F	60.024	P<0.001	82.35	P<0.001	92.028	P<0.001	944.78	P<0.001	88.12	P<0.001	3351.508	P<0.001	5285.46	P<0.001
SKP1-H	131.132	P<0.001	49.42	P<0.001	41.093	P<0.001	2242.34	P<0.001	45.53	P<0.001	14.447	P<0.001	850.331	P<0.001
SKP1-T	53214.267	P<0.001	13050.067	P<0.001	60.185	P<0.001	782.638	P<0.001	1013.37 3	P<0.001	21257.210	P<0.001	142141.175	P<0.001
SKP2-C	5.247	0.015	13.839	P<0.001	3.357	0.55	904.657	P<0.001	2.239	0.137	14117.68	P<0.001	240.69	P<0.001
SKP2-F	37.712	P<0.001	15.354	P<0.001	150.220	P<0.001	2.078	0.166	32.098	P<0.001	4.275	0.033	2.185	0.152
SKP2-H	1357.994	P<0.001	637.112	P<0.001	52.941	P<0.001	5196.194	P<0.001	460.984	P<0.001	3578.403	P<0.001	82222.976	P<0.001
SKP2-T	218.328	P<0.001	72.527	P<0.001	83.642	P<0.001	867.517	P<0.001	144.587	P<0.001	971.485	P<0.001	2512.307	P<0.001
SKP3-C	2190.969	P<0.001	1031.541	P<0.001	219.073	P<0.001	27413.312	P<0.001	914.218	P<0.001	4371.800	P<0.001	13316.736	P<0.001
SKP3-F	1713.389	P<0.001	552.068	P<0.001	104.787	P<0.001	823.207	P<0.001	588.603	P<0.001	781.668	P<0.001	430.644	P<0.001
SKP2-H	50.920	P<0.001	15.717	P<0.001	117.838	P<0.001	2.925	0.083	59.693	P<0.001	43.897	P<0.001	70.690	P<0.001
SKP2-U	1755.186	P<0.001	1704.786	P<0.001	211.530	P<0.001	14555.088	P<0.001	1021.59 3	P<0.001	3475.971	P<0.001	37826.820	P<0.001
SKNP1-C	152.101	P<0.001	101.823	P<0.001	9.039	0.003	86.521	P<0.001	177.625	P<0.001	4.430	0.030	8.392	0.004
SKNP1-F	5275.169	P<0.001	7870.992	P<0.001	64.506	P<0.001	781.941	P<0.001	609.762	P<0.001	4499.593	P<0.001	858.582	P<0.001
SKNP1-H	0.441	0.776	1.855	0.203	6.200	0.011	83.951	P<0.001	0.541	0.710	31.929	P<0.001	34.592	P<0.001
SKPNP1-T	229.857	P<0.001	75.254	P<0.001	24.721	P<0.001	15.505	P<0.001	64.904	P<0.001	28.590	P<0.001	19.024	P<0.001
SKNP2-C	10751.37	P<0.001	17737.96	P<0.001	114.137	P<0.001	950.549	P<0.001	1070.91 1	P<0.001	4037.182	P<0.001	3272.878	P<0.001
SKNP2-F	8020.368	P<0.001	2591.209	P<0.001	273.532	P<0.001	2001.716	P<0.001	2318.44 1	P<0.001	2547.277	P<0.001	4555.697	P<0.001
SKNP2-H	5275.169	P<0.001	7870.992	P<0.001	64.506	P<0.001	781.941	P<0.001	609.762	P<0.001	4499.59	P<0.001	858.582	P<0.001
SKNP2-T	11739.86	P<0.001	3490.578	P<0.001	174.88	P<0.001	529.768	P<0.001	898.294	P<0.001	1259.142	P<0.001	21843.318	P<0.001

SKNP3-C	27966.195	P<0.001	1265.250	P<0.001	373.753	P<0.001	2531.158	P<0.001	1139.340	P<0.001	6253.979	P<0.001	43175.311	P<0.001
SKNP3-F	98.964	P<0.001	54.386	P<0.001	3936.21	P<0.001	86.022	P<0.001	65.291	P<0.001	11.531	P<0.001	76.670	P<0.001
SKNP3-H	56352.266	P<0.001	13189.007	P<0.001	1119.619	P<0.001	50.938	P<0.001	3486.373	P<0.001	3578.058	P<0.001	5379.96	P<0.001
SKNP3-T	88.407	P<0.001	402.934	P<0.001	4.834	0.04	130.121	P<0.001	5.823	0.026	89224.177	P<0.001	279.178	P<0.001

Table A.3 ANOVA and post-hoc analysis results from cranial bone of necropolis at Hospital of Third Order of Our Lady of Carmo, Porto

P		Ca		Mn		Fe		Ni		Zn		Sr	
F value	P value	F value	P value	F value	P value	F value	P value	F value	P value	F value	P value	F value	P value
27.273	P<0.001	32.683	P<0.001	6.161	0.006	5.200	0.012	7.313	0.003	2.253	0.124	16.242	p<.001

P		Post Hoc Comparisons - _col1	Mean Difference	SE	t	Ptukey			Post Hoc Comparisons - _col1	Mean Difference	SE	t	Ptukey
P	PC1	PC2	17940.368	9573.688	1.874	0.280	Fe	PC1	PC2	0.943	0.605	1.559	0.430
		PC3	27815.899	9573.688	2.905	0.048			PC3	0.892	0.605	1.475	0.476
		PC4	88102.602	10154.430	8.676	<.001			PC4	2.948	0.641	4.597	0.002
	PC2	PC3	9875.531	9573.688	1.032	0.734		PC2	PC3	-0.051	0.605	-0.084	1.000
		PC4	70162.234	10154.430	6.910	<.001			PC4	2.005	0.641	3.127	0.031
		PC3	60286.703	10154.430	5.937	<.001			PC3	2.056	0.641	3.206	0.027
Ca	PC1	PC2	47454.319	21952.989	2.162	0.179	Ni	PC1	PC2	-217.613	1293.996	-0.168	0.998
		PC3	62886.834	21952.989	2.865	0.052			PC3	-2910.771	1293.996	-2.249	0.155
		PC4	221191.640	23284.661	9.499	<.001			PC4	-1840.564	1372.490	-1.341	0.553
	PC2	PC3	15432.515	21952.989	0.703	0.894		PC2	PC3	-2693.158	1293.996	-2.081	0.204
		PC4	173737.321	23284.661	7.461	<.001			PC4	-1622.951	1372.490	-1.182	0.647
		PC3	158304.807	23284.661	6.799	<.001			PC3	1070.207	1372.490	0.780	0.862

Mn	PC1	PC2	-91.246	23.253	-3.924	0.007	Zn	PC1	PC2	65.500	23.054	2.841	0.054
		PC3	-30.718	23.253	-1.321	0.564			PC3	66.735	23.054	2.895	0.049
		PC4	-7.695	24.664	-0.312	0.989			PC4	170.121	24.452	6.957	<.001
	PC2	PC3	60.528	23.253	2.603	0.084		PC2	PC3	1.236	23.054	0.054	1.000
		PC4	83.552	24.664	3.388	0.019			PC4	104.621	24.452	4.279	0.430
	PC3	PC4	23.024	24.664	0.934	0.788		PC3	PC4	103.386	24.452	4.228	0.004

Table A.4 Cranium from Ossuary of the church of Espírito Santo, Évora-Normality Check

	P	Ca	Mn	Fe	Ni	Zn	Sr
Missing	0	0	0	0	0	0	0
Shapiro-Wilk	0.946	0.997	0.958	0.776	0.871	0.862	0.783
P-value of Shapiro-Wilk	0.711	0.997	0.791	0.051	0.272	0.234	0.059

Table A.5 Shapiro -Wilk test result for cranial bones from the church of Espírito Santo, Évora(IESE)

	P	Ca	Mn	Fe	Ni	Zn	Sr
Valid	4	4	4	4	4	4	4
Shapiro-Wilk	0.784	0.977	0.791	0.961	0.747	0.882	0.796
P-value of Shapiro-Wilk	0.077	0.882	0.088	0.784	0.036	0.349	0.096

Table A.6: T -test result for cranial bones from the church of Espírito Santo, Évora

Independent	Elements	df	Independent	Independent	Elements	df	

Samples T-Test			t Samples T-Test	Samples T-Test			
Student	p	7	0.801	Student	Ni	7	0.615
Mann-Whitney		7	0.905	Mann-Whitney		7	0.730
Student	Ca	7	0.240	Student	Zn	7	0.632
Mann-Whitney		7	0.190	Mann-Whitney		7	0.413
Student	Mn	7	0.213	Student	Sr	7	0.470
Mann-Whitney		7	0.286	Mann-Whitney		7	0.905
Student	Fe	7	0.029				
Mann-Whitney		7	0.063				

Table A.7: Result of ANOVA and post- hoc analysis on measurements of individuals from the church of Espírito Santo (IESE) and Collection of identified Skeletons of Évora

P		Ca		Mn		Ni		Fe		Zn		Sr	
F value	P value	F value	P value	F value	P value	F value	P value	F value	P value	F value	P value	F value	P value
0.078	0.926	0.968	0.432	1.370	0.324	1.919	0.227	3.722	0.089	11.019	0.010	5.816	0.039

		Post Hoc Comparison s - _col1	Mean Difference	SE	t	tTukey			Post Hoc Comparisons - _col1	Mean Difference	SE	t	tTukey
P	SKC	SKNP	-1990.485	6244.833	-0.319	0.946	Ni	SKC	SKNP	-0.548	0.281	-1.946	0.206
		SKP	257.132	6244.833	0.041	0.999			SKP	-0.224	0.281		0.720
		SKNP	2247.617	6244.833	0.360	0.932		SKNP	SKP	0.324	0.281	1.152	0.520
Ca	SKC	SKNP	13691.294	10843.544	-1.263	0.464	Fe	SKC	SKNP	2492.380	1024.954	2.432	0.111

		SKP	-1354.091	10843.544	-0.125	0.991			SKP	2344.460	1024.954	2.287	0.134
	SKNP	SKP	12337.202	10843.544	1.138	0.946		SKNP	SKP	-147.920	1024.954	-0.144	0.989
	SKNP	SKP	12337.202	10843.544	1.138	0.528	Zn	SKC	SKNP	-1263.112	270.528	-4.669	0.008
Mn	SKC	SKNP	67.311	49.705	1.354	0.420			SKP	-517.495	270.528	-1.913	0.215
		SKP	-7.310	49.705	-0.147	0.988		SKNP	SKP	745.617	270.528	2.756	0.074
	SKNP	SKP	-74.621	49.705	-1.501	0.355	Sr	SKC	SKNP	-101.222	31.199	-3.244	0.040
									SKP	-79.031	31.199	-2.533	0.098
								SKNP	SKP	22.191	31.199	0.711	0.766

Table A.8: ANOVA and post-hoc analysis results on individuals from Porto and Évora

P		Ca		Mn		Fe		Ni		Zn		Sr	
F value	P value	F value	P value	F value	P value	F value	P value	F value	P value	F value	P value	F value	P value
1.222	0.284	4.877	0.040	2.197	0.156	0.442	0.514	1.289	0.271	60.376	0.021	0.027	0.872
Element				Mean Difference		SE		t		Ptukey			
P		EC-PC		13947.147		12617.979		1.105		0.284			
Ca		EC-PC		56762.921		25704.419		2.208		0.040			
Mn		EC-PC		158.108		106.668		1.482		0.156			
Fe		EC-PC		-583.347		876.956		-0.665		0.514			
Ni		EC-PC		0.421		0.371		1.135		0.271			
Zn		EC-PC		-940.576		372.499		-2.525		0.021			
Sr		EC-PC		-5.062		30.861		-0.164		0.872			

Measurements from analysis of human remains

Measurement From Cranial Bones, Necropolis at Hospital of Third order of Our Lady of Carmo, Porto

PC1-UE6394										
Element	Spot1		Spot2		Spot3		Spot4		Spot5	
	mean	SD	Mean	SD	Mean	SD	Mean	SD	Mean	SD
Al	17,207,845.44	9,183,638.14	9,131,460.24	922,836.35	17,363,897.70	346,849.28	13,586,031.77	1,191,027.95	19,524,176.91	465,196.31
P	131,227.84	57,417.20	124,262.74	26.28	88,459.98	1,940.59	106,175.59	1,342.93	99,048.23	33.20
K	4,024,140.91	5,689,856.32	764.45	12.88	126,561.18	48,482.89	791.25	1.45	8,843,719.90	1,450,172.53
Ca	331,781.88	69,399.68	328,904.38	33.47	257,075.35	1,980.02	307,994.80	244.97	283,847.12	131.28
V	0.52	0.74	0.00	0.00	0.00	0.00	1.21	0.15	1.17	0.15
Mn	25.42	10.49	7.96	6.76	34.58	0.68	15.83	0.64	17.67	5.30
Fe	3,206.23	3,584.08	1,504.60	6.36	4,064.93	6.03	1,771.08	125.70	3,309.71	11.55
Co	0.24	0.07	0.23	0.01	0.24	0.02	0.19	0.03	0.24	0.03
Ni	5.61	0.67	5.30	0.03	4.20	0.00	5.23	0.00	4.64	0.03
Cu	20.72	9.99	15.55	0.47	23.17	2.60	18.05	0.94	18.02	1.58
Zn	355.72	312.33	263.09	7.82	283.22	3.03	233.97	1.29	307.39	5.35
As	0.00	0.00	0.00	0.00	0.00	0.00	0.00	0.00	0.00	0.00
Se	0.61	0.03	0.62	0.25	0.55	0.36	0.70	0.08	0.38	0.29
Sr	242.16	15.43	219.87	4.19	222.35	4.58	240.28	4.77	244.03	5.56
Sn	0.27	0.27	0.06	0.05	0.07	0.07	0.13	0.06	0.13	0.09
Sn	0.20	0.06	0.24	0.02	0.14	0.00	0.19	0.00	0.17	0.00
Ba	462.72	65.78	446.22	628.10	476.38	351.38	427.33	61.70	1,541.06	587.34
Ba	166.43	218.11	11.94	0.61	11.04	0.04	12.01	1.55	4,576.10	6,456.08
Ce	0.29	0.41	0.33	0.10	0.48	0.23	0.24	0.00	0.23	0.17
Ce	2,118.31	743.43	2,330.14	364.87	1,295.28	366.76	10,449.03	108.30	9,694.31	265.56
Nd	0.16	0.01	0.15	0.00	0.49				0.19	0.07
Pb	109.07		57.50	2.37	43.79	5.95	71.63	6.25	88.25	2.82

Pb 0.00 0.00 0.00 0.00 0.00 0.00 0.001 0.00 0.00 0.00

PC2-6138

Element	Spot1		Spot2		Spot3		Spot4		Spot5	
	Mean	SD	Mean	SD	Mean	SD	Mean	SD	Mean	SD
Al	8,567,583.48	406,465.30	10,420,613.49	399,533.88	16,381,278.16	8,723,024.65	9,588,307.75	284,835.49	19,097,341.77	424,396.89
P	96,374.62	294.17	110,296.08	744.61	68,220.51	26,904.01	89,794.03	240.64	94,787.30	388.05
K	35,956.17	4,570.21	18,992.94	1,069.68	9,214,552.82	460,785.07	1,616,439.71	1,867,547.38	1,727,761.87	274,384.21
Ca	274,762.14	69.75	286,258.21	83.57	204,887.25	68,813.97	247,499.53	239.58	258,924.80	1,278.82
V	0.00	0.00	0.81	0.31	0.18	0.25	0.52	0.74	0.01	0.01
Mn	64.31	0.43	125.93	2.23	186.60	1.15	48.79	1.20	132.07	3.80
Fe	1,323.52	2.45	1,832.35	1.07	2,927.15	723.32	3,070.81	17.25	7,297.35	366.42
Co	0.14	0.01	0.17	0.00	0.16	0.08	0.19	0.00	0.31	0.03
Ni	4.26	0.05	4.72	0.05	3.31	1.30	3.83	0.01	4.13	0.04
Cu	17.00	0.63	23.27	1.21	25.01	6.70	17.90	2.87	18.71	1.51
Zn	352.11	3.66	719.76	5.93	359.08	119.87	553.55	0.70	546.96	15.03
As	0.00	0.00	0.00	0.00	0.00	0.00	0.00	0.00	0.00	0.00
Se	0.46	0.04	0.39	0.15	0.47	0.13	0.46	0.06	0.41	0.11
Sr	164.99	5.40	188.34	2.11	161.04	51.20	158.72	1.93	168.10	4.24
Sn	0.04	0.04	0.06	0.06	0.07	0.07	0.07	0.01	0.08	0.04
Sb	0.17	0.00	0.17	0.00	0.11	0.03	0.14	0.00	0.14	0.00
Ba	392.05	503.77	631.85	360.03	941.96	166.94	934.96	540.75	1,138.66	59.02
Ba	11.88	0.47	10.86	0.01	11.20	0.13	13.43	4.17	11.76	0.02
Ce	0.13	0.11	0.27	0.19	0.34	0.05	0.32	0.02	0.28	0.21
Ce	10,077.34	343.14	10,879.37	326.63	7,960.77	1,598.68	9,448.44	660.12	9,223.89	148.25
Nd	0.19	0.06	0.38	0.41	0.44	0.28	0.55	0.47	0.11	0.02
Pb	61.48	3.86	54.22	4.74	77.05	37.64	56.89	0.66	136.23	2.32
Pb	0.00	0.00	0.00	0.00	0.00	0.00	0.00	0.00	0.00	0.00

PC3-UE6095

Element	Spot1		Spot2		Spot3		Spot4		Spot5	
	Mean	SD	Mean	SD	Mean	SD	Mean	SD	MEAN	SD
Al	13,248,459.91	2,566,687.32	13,893,708.36	118,506.47	26,297,616.16	2,079,434.39	4,663,944.13	312,028.78	20,827,123.70	511,423.17

P	86,983.79	1,895.48	101,188.58	705.29	62,243.29	8,266.39	82,399.21	1,280.50	77,280.01	924.30
				2,415,180.						
K	19,491,089.25	11,127,801.10	1,854,009.09	88	50,327,180.04	15,783,329.36	831,838.30	40,448.66	18,251,249.74	296,448.79
Ca	246,048.37	4,453.03	285,372.91	223.16	187,162.03	14,951.17	231,058.61	1,651.07	245,527.44	732.92
V	0.14	0.19	1.01	0.25	0.07	0.06	0.00	0.00	1.43	0.08
Mn	37.61	1.69	29.02	8.07	118.13	1.29	10.70	3.28	59.59	0.10
Fe	7,144.53	1,215.15	3,102.76	9.15	8,555.41	117.62	4,453.62	6.69	6,237.65	13.55
Co	0.16	0.03	0.11	0.00	0.29	0.03	0.15	0.02	0.26	0.03
Ni	4.27	0.00	4.77	0.01	3.34	0.20	3.40	0.02	4.73	0.02
Cu	5,773.60	476.27	2,302.17	4.15	3,093.36	113.76	630.82	0.90	12,430.68	25.64
Zn	4,401.32	218.95	3,361.79	4.75	5,446.60	355.63	813.69	3.31	1,973.85	12.70
As	0.06	0.08	0.33	0.46	0.90	0.16	0.00	0.00	3.53	0.08
Se	0.18	0.02	0.26	0.08	0.14	0.07	0.59	0.11	0.17	0.23
Sr	175.76	2.57	166.55	1.03	155.26	4.11	122.01	2.99	215.41	0.83
Sn	0.13	0.05	0.10	0.03	0.09	0.09	0.12	0.05	0.10	0.00
Sn	0.16	0.01	0.17	0.00	0.12	0.01	0.14	0.00	0.14	0.00
Ba	788.10	512.06	1,584.58	533.67	317.79	1.81	437.36	614.76	813.15	1,144.90
Ba	12.42	1.13	16.30	6.48	11.45	0.24	10.85	0.14	15.58	4.76
Ce	0.15	0.22	0.12	0.06	0.48	0.25	0.19	0.14	0.03	0.05
Ce	10,319.07	832.23	10,419.43	120.76	8,260.10	53.27	9,602.50	81.03	10,418.38	441.38
Nd	0.03	0.01	0.13	0.12	0.28	0.20	0.38	0.22	0.21	0.24
Pb	57.62	0.31	77.34	7.97	126.78	7.48	65.96	1.76	85.58	5.88
Pb	0.00	0.00	0.00	0.00	0.00	0.00	0.00	0.00	0.00	0.00

PC4-UE6117

Element	Spot1		Spot2		Spot3		Spot4	
	Mean	SD	MEAN	SD	Mean	SD	Mean	SD
Al	1,475,313.07	1,102,891.02	561,803.07	276,978.75	1,082,401.23	379,587.85	3,589,588.95	61,826.02
P	32,629.72	8,849.89	4,854.63	46.37	21,157.99	916.42	28,286.76	231.57
K	517,723.59	615,413.34	685.29	3.42	610,588.37	110,639.11	24,031,059.87	1,340,383.24
Ca	101,396.81	15,586.63	23,342.33	125.59	79,834.93	2,515.47	118,342.19	437.02
V	0.06	0.07	0.30	0.27	0.00	0.00	1.09	0.58
Mn	43.40	3.82	13.12	2.56	20.27	3.27	35.15	1.16

Fe	280.10	4.78	87.16	2.37	290.34	3.17	3,465.51	1.30
Co	0.05	0.01	0.03	0.00	0.04	0.01	0.23	0.01
Ni	1.45	0.14	0.77	0.01	1.31	0.04	4.66	0.05
Cu	275.45	79.89	79.84	1.41	105.50	1.82	35,356.82	229.55
Zn	145.37	30.79	80.03	1.10	101.95	1.42	8,189.62	55.31
As	0.50	0.18	0.00	0.00	0.43	0.20	22.90	1.08
Se	0.22	0.13	0.12	0.06	0.28	0.03	0.11	0.15
Sr	44.44	1.10	12.73	0.07	32.17	0.41	165.12	3.62
Sn	0.07	0.01	0.02	0.00	0.01	0.01	0.04	0.02
Sn	0.06	0.01	0.01	0.00	0.05	0.00	0.05	0.01
Ba	75.27	#DIV/0!	383.80	130.26	483.62	163.35	648.13	74.52
Ba	1,748.09	#DIV/0!	429.61	584.79	26.39	2.88	5,932.44	8,370.33
Ce	0.00	0.00	0.00	#DIV/0!	0.00	0.00	0.45	0.24
Ce	5,056.70	515.52	1,725.52	130.22	4,226.84	343.87	9,185.57	357.92
Nd	1.39	0.12	0.64	0.09	1.01	0.18	0.09	#DIV/0!
Pb	20.08	2.52	8.34	0.32	18.07	1.71	397.96	7.03
Pb	0.00	0.00	0.00	0.00	0.00	0.00	0.00	0.00

Overall Mean and SD of each Cranium

Element	PC1-UE6394			PC2-UE6138			PC3-UE-6095			PC4-UE6117			
	Mean	SD	SD%	Mean	SD	SD%	Mean	SD	SD%	MEAN	SD	SD%	
Al	15,362,682.41	4,083,875.09		26.58	12,811,024.93	4,646,806.85	36.27	15,786,170.45	8,210,161.49	52.01	1,677,276.58	644.13	79.21
P	109,834.88	17,694.99		16.11	91,894.51	15,263.74	16.61	82,018.98	14,193.34	17.30	21,732.27	.19	56.16
K	2,599,195.54	3,893,649.43		149.80	2,522,740.70	3,830,358.09	151.83	18,151,073.28	20,016,603.89	110.28	6,290,014.28	1	188.08
Ca	301,920.71	31,600.88		10.47	254,466.39	31,421.10	12.35	239,033.87	35,330.47	14.78	80,729.06	.08	51.25
V	0.58	0.59		102.03	0.30	0.35	116.08	0.53	0.65	121.92	0.36	0.50	138.73
Mn	20.29	10.11		49.84	111.54	55.75	49.98	51.01	41.44	81.23	27.99	13.78	49.23
Fe	2,771.31	1,090.59		39.35	3,290.24	2,357.45	71.65	5,898.79	2,158.16	36.59	1,030.78	1,625.	157.73

	84											
Co	0.23	0.02	9.62	0.20	0.07	33.41	0.19	0.08	40.58	0.08	0.10	113.60
Ni	4.99	0.57	11.33	4.05	0.52	12.91	4.10	0.70	17.00	2.05	1.77	86.43
										17,601		
Cu	19.10	2.92	15.28	20.38	3.54	17.38	4,846.13	4,628.67	95.51	8,954.40	.83	196.57
										4,040.		
Zn	288.68	46.16	15.99	506.29	154.03	30.42	3,199.45	1,851.65	57.87	2,129.24	34	189.75
As	0.00	0.00	20.33	0.00	0.00	20.33	0.96	1.48	153.79	5.96	11.30	189.63
Se	0.57	0.12	20.70	0.44	0.03	7.68	0.27	0.19	70.37	0.18	0.08	45.57
Sr	233.74	11.64	4.98	168.24	11.80	7.01	167.00	33.85	20.27	63.62	68.92	108.34
Sn	0.13	0.09	65.20	0.07	0.01	22.59	0.11	0.02	18.35	0.04	0.03	75.12
Sn	0.19	0.04	19.62	0.15	0.02	16.54	0.15	0.02	12.17	0.04	0.02	54.50
Ba	670.74	486.87	72.59	807.90	294.72	36.48	788.20	494.78	62.77	397.71	241.01	60.60
										2,700.		
Ba	955.50	2,025.08	211.94	11.83	0.99	8.36	13.32	2.47	18.54	2,034.13	88	132.78
Ce	0.31	0.10	32.29	0.27	0.08	30.80	0.20	0.17	86.13	0.11	0.22	197.65
										3,100.		
Ce	5,177.42	4,492.45	86.77	9,517.96	1,081.95	11.37	9,803.90	928.14	9.47	5,048.66	15	61.41
Nd	0.20	0.17	86.85	0.33	0.18	53.97	0.21	0.13	64.98	0.78	0.55	70.64
Pb	74.05	25.61	34.58	77.17	34.18	44.28	82.66	26.88	32.52	111.11	191.30	172.17
Pb	0.00	0.00	0.00	0.00	0.00	0.00	0.00	0.00	0.00	0.00	0.00	66.67

Measurements for cranial bones from the Church of Espírito Santos, Évora

COS1- CRANIUM FROM OSSUARY NO:1

Element	Spot1		Spot2		Spot3		Spot4		Spot5	
	Mean	SD	Mean	SD	Mean	SD	Mean	SD	Mean	SD
Al	7,298,194.07	984,568.90	5,296,393.00	28,927.19	6,113,292.43	425,511.50	4,611,258.90	731,226.23	4,298,675.16	551,202.16
P	109,092.58	5,630.96	60,259.75	878.17	56,489.84	975.77	84,378.00	2,035.87	55,105.70	690.37
K	801.84	1.28	800.10	0.03	17,506.84	23,641.31	771.92	0.19	780.02	0.86
Ca	337,513.92	8,087.67	331,111.42	622.21	270,086.60	1,679.91	247,061.91	1,109.90	282,669.98	264.91

V	1.08	0.98	1.04	0.63	2.95	1.29	0.54	0.24	0.70	0.04
Mn	112.68	4.17	332.44	2.96	388.51	16.98	187.48	4.57	270.16	1.96
Fe	753.86	64.14	3,388.85	27.92	5,200.97	37.95	1,660.50	38.30	2,259.97	20.24
Co	0.12	0.00	0.23	0.00	0.25	0.02	0.16	0.01	0.17	0.00
Ni	5.14	0.18	4.63	0.04	4.21	0.01	3.87	0.03	3.96	0.06
Cu	25.21	0.10	26.74	3.13	28.41	3.10	20.98	0.23	19.50	2.13
Zn	222.17	0.10	553.14	3.24	1,091.88	19.10	997.73	1.71	321.24	6.11
As	4.87	0.23	4.25	0.44	4.13	0.30	3.40	1.23	3.85	1.63
Se	0.87	0.02	0.87	0.10	0.63	0.03	0.82	0.03	0.55	0.22
Sr	139.31	5.23	160.35	7.47	152.47	2.35	159.67	3.73	111.45	1.69
Sn	0.24	0.02	0.10	0.07	0.20	0.06	0.09	0.03	0.05	0.02
Sn	0.21	0.01	0.21	0.00	0.16	0.00	0.15	0.00	0.17	0.00
Ba	433.51	311.44	611.37	192.96	1,864.48	254.96	1,519.29	226.10	751.01	355.30
Ba	13.79	2.78	16.08	6.18	12,091.92	16,551.77	10.62	0.36	9,980.21	2,415.54
Ce	0.24	0.22	0.39	0.08	0.17	0.16	0.46	0.07	0.06	0.09
Ce	12,078.78	478.72	11,418.91	14.66	9,817.02	396.78	10,202.22	393.46	9,946.27	183.57
Nd	0.09	0.11	0.00							
Pb	81.45	2.34	124.78	1.90	111.76	8.91	152.66	3.63	143.73	5.43
Pb	0.00	0.00	0.00	0.00	0.00	0.00	0.00	0.00	0.00	0.00

COS2-CRANIUM FROM OSSUARY NO:2

Element	Spot1		Spot2		Spot3		Spot4	
	Mean	SD	MEAN	SD	MEAN	SD	Mean	SD
Al	5668630.87	246942.06	4470877.88	86326.33	1836877.75	296723.92	4847419.77	980827.02
P	77770.09	1115.57	71231.05	233.72	17548.79	49.63	72965.21	22501.47
K	778.18	1.39	771.1	0.63	49003.29	68261.64	779.83	2.89
Ca	286185.77	2714.69	268445.82	492.58	146360.01	1294.5	283675.67	3694.53
V	0.14	0.2	0.57	0.23	0	0	0.91	0.66
Mn	180.14	4.23	135.17	0.7	198.07	0.22	299.99	193.73
Fe	1128.76	5.75	949.94	11.19	1681.5	20.83	1723.15	1259.91
Co	0.16	0.03	0.16	0.02	0.11	0.01	0.17	0.04

Ni	4.05	0.07	3.77	0.05	1.84	0.01	4.22	0
Cu	19.87	1.29	19.13	0.69	17.54	0.65	21.72	1.66
Zn	147.62	8.84	138.64	4.95	116.47	0.48	192.11	35.55
As	1.86	0.93	2.34	0.09	2.13	1.63	0	0
Se	0.86	0.12	0.49	0.1	0.54	0.13	0.59	0.17
Sr	123.09	4.14	113.09	0.56	62.88	4.53	125.48	8.82
Sn	0.11	0.1	0.16	0.03	0.08	0.01	0.14	0.03
Sn	0.18	0	0.16	0	0.09	0	0.18	0.01
Ba	1295.97	534.56	950.66	205	203.53	30.39	861.93	411.82
Ba	515.71	711.51	10.42	1.33	13.97	1.76	21.34	10.31
Ce	0.47	0.04	0.49	0.03	0	0	0.44	0.26
Ce	10545.19	52.26	10001.26	260.2	6653.64	268.18	10444.38	946.82
Nd	0		0		0.39	0.22	0	
Pb	110.41	3.37	140.14	1.87	95.67	6.11	179.48	15.59
Pb	0	0	0	0	0	0	0	0

COS3-CRANIUM FROM OSSUARY NO:3

Element	Spot1		Spot2		Spot3		Spot4		Spot5	
	Mean	SD	Mean	SD	Mean	SD	Mean	SD	Mean	SD
Al	2928028.42	370613.77	5248561.97	987043.43	3528672.01	873323.48	4101489.38	48715.4	4280828.83	37837.04
P	84700.51	93.81	100159.94	16.17	109328.2	2831.75	97832.67	587.05	97824.17	2984.83
K	763.07	1.65	770.92	0.87	783.83	0.4	776.96	2.03	769.03	1.98
Ca	255682.65	196.31	266012.4	375.9	318838.13	3822.2	282019.16	629.74	269323.96	4259.06
V	0	0	0	0	0.03	0.04	0.01	0.01	0	0
Mn	59.2	0.08	54.81	5.44	43.87	2.13	48.71	2.96	210.7	19.01
Fe	1551.95	1.83	1638.67	3.25	1603.3	23.08	1318.45	3.85	1701.52	43.34
Co	0.16	0	0.16	0.02	0.17	0.01	0.17	0	0.14	0.02
Ni	3.09	0.02	3.41	0.03	4.37	0.02	3.93	0	3.38	0.06
Cu	12.18	2.9	13.78	0.63	14.37	0.3	15.67	0.2	13.85	0.85
Zn	257.87	5.88	217.25	3.24	275.32	3.81	256.44	13.49	322.3	27.32
As	0	0	0	0	0	0	0	0	0	0
Se	0.57	0.09	0.51	0.06	0.56	0.35	0.66	0.03	0.5	0.08

Sr	93.46	1.05	101.85	2.9	115.54	8.59	110.03	0.85	103.75	2.66
Sn	0.05	0	0.13	0.05	0.08 #DIV/0!		0.08	0.09	0.1	0.03
Sn	0.16	0	0.16	0	0.21	0	0.17	0	0.17	0
Ba	676.25	322.92	1275.62	115.32	668.49	116.08	918.87	15.65	915.45	746.01
Ba	11.49	0.04	11.95	0.03	11.85	0.21	122.17	83.11	11.37	0.14
Ce	0.55	0.11	0.29	0.01	0.24	0.03	0.51	0.11	0.45	0.08
Ce	2017.54	278.64	2132.97	198.07	1924.45	571.16	2290.19	485.78	1955.57	687.56
Nd	0.3	0.22	0.32	0.1	0.25	0.03	0.07 #DIV/0!		0.52 #DIV/0!	
Pb	343.77	1.59	210.92	2.04	292.82	2.35	343.92	7.92	246.11	7.18
Pb	0	0	0	0	0	0	0	0	0	0

COS4 Cranium from Ossuary No:4											
Element	Spot1		Spot2		Spot3		Spot4		Spot5		
	Mean	SD	Mean	SD	Mean	SD	Mean	SD	Mean	SD	
Al	350268.39	132034.86	2384703.12	64651.02	7282228.37	526611.2	8056909.9	140419.28	8372081.76	2091377.41	
P	7600.67	15	45352.72	593.56	138410.29	1002.14	141827.12	440.46	129120.07	5169.47	
K	693.68	0.19	7118947.74	684279.75	797.11	0.86	795.5	1.43	614.5	262.79	
Ca	32555.09	122.58	156876.24	1126.53	341958.53	1174.21	347721.32	494.96	304479.69	32947.24	
V	0.14	0.19	0	0	0.72	1.01	0.73	0.35	1.76	2.49	
Mn	6.64	1.04	22.32	5.22	47.05	8.09	47.23	5.75	46.73	21.65	
Fe	119.97	3.82	2622.05	8.58	1361.8	7.8	869.06	7.92	4093.24	2081.83	
Co	0.04	0.01	0.14	0	0.15	0.01	0.16	0.01	0.93	0.96	
Ni	0.78	0.01	2	0.01	4.76	0	4.78	0	3.03	2.08	
Cu	11.24	0.59	13.25	0.57	13.6	0.65	14.51	2	26.69	16.17	
Zn	35.34	5.45	216.66	1.07	276.16	3.69	188.96	9.95	145.23	78.23	
As	0.13	0.18	0	0	0	0	0	0	0	0	
Se	0.19	0.06	0.36	0.07	0.74	0.14	0.8	0.19	0.73	0.31	
Sr	9.9	0.39	58.93	0.5	96.23	0.75	103.4	3.04	109.59	2.28	
Sn	0.02	0.02	0.08	0.01	0.07	0.08	0.09	0.11	0.11	0.05	
Sn	0.02	0	0.09	0	0.22	0	0.22	0	1.68	2.08	
Ba	265	75.33	362.49	282.35	1645.49	164.24	493.98	162.39	963.05	686.07	
Ba	6315.83	3711.1	14.05	3.83	15.02		11.75	0.15	23.87	15.23	

Ce	0	0	0.03	0.05	0		0.27	0.06	0.32	0.46
Ce	1.95	0.02	2.01	0.03	2.08	0	2.03	0.05	2.06	0
Nd	0.75	0.05	0.35	0.07	0	0			0	0
Pb	14.14	1.76	92.08	0.2	220.71	3.22	97.62	5.47	150.87	61.1
Pb	0	0	0	0	0	0	0	0	0	0

COS5

Cranium from ossuary No:5

Element	Spot1		Spot2		Spot3		Spot4		Spot5	
	Mean	SD	Mean	SD	Mean	SD	Mean	SD	Mean	SD
Al	5694371.21	524725.53	3972836.07	187354.41	5091102.37	275973.49	5569360.23	214451.43	5759741.67	500290.3
P	104885.72	929.72	95946.14	219.44	91898.21	3272.61	85342.11	97.38	99019.83	365.43
K	790.41	1.17	783.6	0.73	773.55	17.31	798.64	0.48	792.86	0.25
Ca	308100.67	2327.88	293582.32	520.7	302122.29	2125.9	319518.88	372.5	310465.52	24.7
V	1.28	0.08	0.31	0.43	0.07	0.1	1.49	1.15	0	0
Mn	95.87	2.39	173.16	0.96	157.25	18.11	219.96	4.98	140.28	0.46
Fe	693.85	7.3	879.39	20.64	1192.28	86.35	1776.01	7.48	2009.16	10.04
Co	0.17	0	0.13	0.01	0.16	0.02	0.15	0	0.16	0
Ni	4.65	0.04	4.26	0.04	4.37	0.04	4.88	0.04	4.55	0.01
Cu	23.73	1.59	24.39	0.45	30.6	2.83	27.66	1.64	26.27	1.02
Zn	228.76	3.14	534.33	13.06	293.66	7.88	216.11	8.86	392.45	6.42
As	0.54	0.01	1.62	0.55	0.82	0.22	0.91	0.35	0.45	0.63
Se	0.79	0.21	0.8	0.07	0.96	0.26	0.99	0.39	0.68	0.27
Sr	179.6	8.04	164.83	0.43	189.3	3.33	220.82	0.34	199.25	4.2
Sn	0.13	0.05	0.19	0.12	0.09	0.06	0.16	0.06	0.08	0.02
Sn	0.19	0.01	0.19	0	0.21	0.03	0.2	0	0.2	0
Ba	1328.63	129.32	346.13	91.38	119.53	163.8	681.47	596.08	438.32	614.35
Ba	11.91	0.3	12.99	2.41	12.43	1.35	2707.96	3809.15	12.84	0.28
Ce	0.29	0.07	0.44	0.01	0.29	0.09	0.41	0.26	0.42	0.02
Ce	12050.28	581.61	11001.31	298.46	11674.34	661.34	11247.03	15	12051.36	212.41
Nd			0.19		0.01				0.01	

Pb	91.19	1.07	173.74	5.07	91.07	1.72	108.06	5.1	144.75	3.79
Pb	0	0	0	0	0	0	0	0	0	0

COS1- CRANIUM FROM OSSUARY NO:1

Element	Mean	SD
Al	5,523,562.71	1,212,574.89
P	73,065.17	23,383.85
K	4,132.14	7,476.69
Ca	293,688.77	39,286.25
V	1.26	0.97
Mn	258.25	110.47
Fe	2,652.83	1,716.09
Co	0.19	0.05
Ni	4.36	0.53
Cu	24.17	3.80
Zn	637.23	392.39
As	4.10	0.54
Se	0.75	0.15
Sr	144.65	20.40
Sn	0.14	0.08
Sn	0.18	0.03
Ba	1,035.93	621.38
Ba	4,422.52	6,083.30
Ce	0.26	0.16
Ce	10,692.64	1,001.64
Nd	0.03	0.05
Pb	122.88	28.13
Pb	0.00	0.00

COS2-CRANIUM FROM OSSUARY NO:2

Element	Mean	SD
Al	4,205,951.57	1,656,664.21
P	59,878.79	28,355.22
K	12,833.10	24,113.46
Ca	246,166.82	66,997.97
V	0.41	0.41
Mn	203.34	69.65
Fe	1,370.84	390.04
Co	0.15	0.03
Ni	3.47	1.10
Cu	19.57	1.73
Zn	148.71	31.76
As	1.58	1.07
Se	0.62	0.17
Sr	106.14	29.33
Sn	0.12	0.04
Sn	0.15	0.04
Ba	828.02	456.49
Ba	140.36	250.27
Ce	0.35	0.23
Ce	9,411.12	1,853.44
Nd	0.10	0.20
Pb	131.43	36.99
Pb	0.00	0.00

COS3-CRANIUM FROM OSSUARY NO:3

Element	Mean	SD	SD%
Al	4,017,516.12	868,592.39	21.62
P	97,969.10	8,802.33	8.98
K	772.76	7.93	1.03
Ca	278,375.26	24,496.14	8.80
V	0.01	0.01	162.98
Mn	83.46	71.37	85.52
Fe	1,562.78	147.02	9.41
Co	0.16	0.01	7.65
Ni	3.64	0.51	14.02
Cu	13.97	1.26	8.99
Zn	265.84	38.05	14.31
As	0.00	0.00	#DIV/0!
Se	0.56	0.06	11.36
Sr	104.93	8.38	7.99
Sn	0.09	0.03	33.52
Sn	0.17	0.02	11.92
Ba	890.94	247.45	27.77
Ba	33.77	49.42	146.36
Ce	0.41	0.14	33.44
Ce	2,064.14	149.42	7.24
Nd	0.29	0.16	55.19
Pb	287.51	59.07	20.54
Pb	0.00	0.00	#DIV/0!

Element	COS4 Cranium from Ossuary No:4		
	Mean	sd%	SD%
Al	7,998,210.11	495,370.88	6.19

COS5 Cranium from ossuary No:5		
Mean	SD	SD%
5,217,482.31	743,371.12	14.25

P	137,649.18	5,878.45	4.27	95,418.40	7,362.10	7.72
K	751.79	91.55	12.18	787.81	9.63	1.22
Ca	334,501.80	20,157.97	6.03	306,757.94	9,662.77	3.15
V	0.85	0.66	78.55	0.63	0.70	111.54
Mn	56.01	18.01	32.16	157.30	45.39	28.86
Fe	2,635.41	1,767.34	67.06	1,310.14	566.77	43.26
Co	0.36	0.38	104.62	0.15	0.02	9.85
Ni	4.29	0.84	19.68	4.54	0.24	5.34
Cu	17.35	6.25	36.01	26.53	2.75	10.38
Zn	191.73	59.26	30.91	333.06	132.42	39.76
As	0.00	0.00	#DIV/0!	0.87	0.46	53.17
Se	0.76	0.03	4.12	0.84	0.13	15.28
Sr	103.89	5.70	5.48	190.76	21.06	11.04
Sn	0.09	0.02	19.52	0.13	0.05	35.67
Sn	0.59	0.73	124.79	0.20	0.01	4.23
Ba	891.48	552.25	61.95	582.82	463.01	79.44
Ba	489.28	944.81	193.10	551.63	1,205.43	218.52
Ce	0.17	0.15	88.43	0.37	0.07	19.95
Ce	2.06	0.02	1.00	11,604.86	473.00	4.08
Nd	0.04	0.07	173.21	0.07	0.10	148.46
Pb	182.61	72.72	39.82	121.76	36.38	29.88
Pb	0.00	0.00		0.00	0.00	#DIV/0!

Measurements of fully preserved individuals excavated from the crypt of the church of Espírito Santos, Évora

IESES/21-2

SKRC Element	Tibia		Humerus		Femur		Sternum		Cranium	
	MEAN	SD	Mean	SD	Mean	SD	Mean	SD	Mean	SD
Al	3,364,432.65	1,229,439.65	5,246,724.36	1,230,789.85	4,389,329.19	1,136,107.09	1,422,205.18	1,115,143.26	3,665,982.89	1,639,120.62
P	90,519.17	11,677.65	75,568.35	18,622.17	83,954.30	12,470.29	78,564.36	6,654.70	80,059.64	3,739.52

K	780.18	13.97	76,178.86	142,899.89	46,391.97	91,257.37	685.43	78.92	38,566.34	31,453.76
Ca	272,643.31	38,897.25	240,744.44	32,141.74	231,799.16	47,611.16	259,329.05	4,713.38	245,750.41	12,013.96
V	0.59	0.37	0.50	0.59	0.84	0.83	0.33	0.33	0.56	0.21
Mn	116.03	79.29	444.20	330.31	206.29	173.59	114.89	10.98	246.43	139.89
Fe	2,469.85	1,392.59	10,011.42	7,920.51	3,643.08	3,819.53	1,529.99	3.69	4,899.52	3,619.39
Co	0.17	0.03	0.34	0.16	0.20	0.07	0.08	0.04	0.20	0.10
Ni	3.99	0.66	4.18	0.82	3.57	0.58	3.16	0.36	3.66	0.42
Cu	19.87	3.99	39.13	27.17	28.19	15.47	31.45	1.00	32.10	4.87
Zn	1,230.00	756.58	439.98	129.93	1,216.63	1,135.09	297.30	103.50	687.47	410.40
As	0.18	0.31	0.00	0.00	0.16	0.18	0.08	0.08	0.09	0.06
Se	0.67	0.13	0.49	0.08	0.41	0.15	0.83	0.01	0.58	0.18
Sr	115.35	14.07	125.70	31.06	123.76	35.46	119.60	3.02	122.54	2.72
Sn	0.12	0.02	0.15	0.07	0.12	0.04			0.13	0.02
Sn	0.17	0.03	0.15	0.02	0.14	0.03	0.64	0.48	0.30	0.24
Ba	1,054.41	435.17	248.18	216.19	710.60	148.09	274.39	12.78	451.27	226.82
Ba	918.98	1,814.33	7,532.97	6,101.32	367.03	688.63	10.56	1.95	2,529.49	3,471.78
Ce	0.35	0.28	0.27	0.28	0.46	0.22	0.40	0.00	0.38	0.08
Ce	11,126.73	898.34	10,119.42	1,121.13	9,739.74	1,178.30	9,307.04	378.39	9,809.86	375.47
Nd	0.52	#DIV/0!	0.00	0.00	0.13	0.19	0.27	0.22	0.16	0.12

SKLC

IESE/21-3

Element	Tibia		Humerus		Femur		Ribs		Cranium	
	Mean	sd	Mean	sd	Mean	sd	Mean	sd	Mean	SD
Al	5,325,475.15	726,697.84	4,900,016.16	1,091,895.41	5,541,467.49	663,787.57	5,130,176.15	1,727,544.00	5,224,283.74	273,770.55
P	94,210.95	8,998.31	92,070.65	12,280.04	94,034.27	14,347.43	88,761.41	8,491.59	92,269.32	2,531.79
K	769.73	6.12	782.35	11.41	779.13	10.14	783.11	15.44	778.58	6.15
Ca	226,090.92	9,869.81	279,393.01	32,650.93	256,475.10	38,754.70	271,419.51	27,697.17	258,344.63	23,507.33
V	0.30	0.44	0.02	0.04	0.13	0.25	0.35	0.37	0.20	0.15
Mn	212.16	155.83	145.17	49.98	416.53	459.57	123.06	76.35	224.23	133.68
Fe	3,463.21	953.85	3,444.72	1,399.17	5,774.38	1,293.12	5,520.75	4,765.16	4,550.76	1,270.73
Co	0.18	0.01	0.18	0.01	0.22	0.02	0.22	0.09	0.20	0.02
Ni	3.85	0.35	4.08	0.48	4.80	0.14	4.92	0.58	4.41	0.53
Cu	27.94	4.78	22.71	3.29	26.49	5.17	39.47	18.74	29.15	7.22

Zn	1,112.69	552.15	993.23	187.24	897.71	892.28	1,332.25	1,697.80	1,083.97	187.43
As	0.00	0.00	0.02	0.03	0.00	0.00	0.00	0.00	0.01	0.01
Se	0.69	0.05	0.72	0.04	0.68	0.14	0.64	0.27	0.68	0.03
Rb	1.24	0.70	1.72	0.77						
Sr	111.88	18.04	115.56	26.76	107.19	6.07	128.26	11.33	1.48	0.34
Sn	0.11	0.05	0.11	0.03	0.17	0.03	0.07	0.04	115.72	9.03
Sn	0.14	0.01	0.18	0.02	0.16	0.03	0.17	0.02	0.11	0.04
Ba	1,008.74	367.12	827.79	599.53	959.98	182.91	397.34	236.56	0.16	0.02
Ba	10.61	0.39	14.52	5.68	30.22	31.41	420.03	818.09	798.46	278.13
Ce	0.51	0.13	0.50	0.12	0.50	0.24	0.37	0.14	118.84	200.97
Ce	2.06	0.02	2.14	0.04	2.10	0.06	2.12	0.07	0.47	0.07
Nd	0.07	0.06	0.07	0.09	0.11	0.11	0.26	0.03	2.10	0.03
Gd	0.11	0.02	0.09	0.03	0.20	0.07	0.16	0.09	0.13	0.09
Pb	164.61	46.06	152.19	14.72	203.05	61.41	206.41	59.09	0.14	0.05
Pb	0.00	0.00	0.00	0.00	0.00	0.00	0.00	0.00		

IESE/21-4

SKL1 Element	Mean	Tibia SD%	Humerus Mean	sd	Femur Mean	SD	Ribs Mean	SD	Cranium Mean	SD
Al	15,938,207.43	15,460,436.89	6,632,390.16	1,168,649.74	9,606,890.66	3,872,260.93	13,198,551.41	9,845,622.89	6,152,746.66	1,841,406.06
P	87,796.53	32,579.73	101,825.27	15,976.69	87,405.95	23,625.00	109,640.41	17,462.66	95,674.02	27,536.22
K	11,473,645.06	25,617,619.59	781.67	18.73	4,883.96	9,178.96			284,749.31	634,968.08
Ca	266,618.32	63,735.64	290,475.24	39,479.63	255,847.60	40,865.95	287,521.89	38,128.52	266,619.11	67,308.39
V	2.31	4.49	0.02	0.03	3.24	7.23	1.96	3.29	0.01	0.01
Mn	372.20	274.83	160.03	127.76	212.05	201.37	193.52	266.72	123.51	133.96
Fe	11,445.66	11,096.46	4,559.36	4,316.75	4,678.39	2,911.52	9,360.45	4,794.15	3,721.02	2,520.54
Co	0.34	0.16	0.23	0.10	0.20	0.08	0.35	0.11	0.20	0.07
Ni	4.34	0.80	4.67	0.89	4.05	0.67	4.63	0.84	4.36	1.29
Cu	25.26	12.69	24.58	10.11	31.73	27.22	28.26	19.86	23.31	11.32
Zn	376.39	123.69	1,121.50	999.91	1,092.79	1,099.56	873.39	506.22	526.33	565.47
As	0.00	0.00	0.00	0.00	0.00	0.00	0.00	0.00	0.01	0.01
Se	0.56	0.32	0.69	0.26	0.59	0.16	0.53	0.09	0.59	0.19
Sr	92.93	7.79	89.47	14.41	98.24	48.73	113.46	75.16	71.85	20.72

Sn	0.10	0.05	0.12	0.03	0.09	0.04	0.11	0.01	0.09	0.02
Sn	0.16	0.05	0.19	0.03	0.16	0.03	0.17	0.03	0.17	0.05
Ba	721.40	265.24	719.68	303.75	837.93	242.13	602.87	401.43	434.38	199.32
Ba	11,139.20	24,882.15	23.95	22.11	11.74	0.61	42.95	63.16	10.72	1.66
Ce	0.37	0.13	0.21	0.19	0.22	0.07	0.34	0.27	0.26	0.14
Ce	2.20	0.09	2.15	0.06	2.14	0.05	2.13	0.07	1.99	0.32
Nd	0.25	0.14	0.35	0.24	0.29	0.16	0.25	0.10	0.25	0.25
Gd	0.29	0.27	0.14	0.09	0.11	0.05	0.20	0.10	0.13	0.08
Pb	88.88	25.60	110.39	21.29	82.36	29.52	100.02	37.26	89.57	35.88
Pb	0.00	0.00	0.00	0.00	0.00	0.00	0.00	0.00	0.00	0.00

IESE/21-5

SKL2

Element	Tibia		Humerus		Femur		Ribs	
	Mean	SD	Mean	SD	Mean	SD	Mean	SD
Al	10,379,230.20	1,286,575.55	6,812,568.57	4,477,922.82	7,801,561.22	2,578,515.92	9,012,476.60	4,040,640.94
P	65,128.68	18,741.90	90,814.97	21,694.75	82,405.23	7,529.21	108,586.01	6,274.24
K	1,313,887.41	1,668,426.79	12,600.20	17,604.25	335,052.03	509,695.58	65,524.45	112,152.87
Ca	287,114.93	8,190.97	253,267.98	54,827.21	249,766.04	26,757.06	275,584.48	18,689.19
V	1.73	1.47	0.63	0.95	1.88	2.22	2.35	2.26
Mn	321.45	184.93	59.63	57.04	140.71	76.38	183.77	213.47
Fe	7,419.46	4,399.76	3,556.56	3,327.87	6,917.17	3,719.02	7,072.00	6,184.88
Co	0.28	0.09	0.20	0.12	0.25	0.07	0.26	0.14
Ni	4.99	0.21	4.00	1.11	4.18	0.54	4.13	0.48
Cu	31.61	10.03	25.55	9.75	23.54	4.31	78.45	98.66
Zn	109.65	15.40	556.06	322.42	966.60	484.97	2,524.67	3,189.41
As	0.00	0.00	0.00	0.00	0.00	0.00	0.04	0.08
Se	0.70	0.08	0.67	0.18	0.48	0.15	0.47	0.14
Sr	204.21	39.46	136.96	37.84	154.45	22.25	138.83	25.88
Sn	0.12	0.06	0.06	0.07	0.16	0.08	0.06	0.03
Sn	0.17	0.00	0.15	0.04	0.17	0.04	0.17	0.01
Ba	832.13	81.82	802.78	372.69	796.78	385.16	512.55	334.92
Ba	20,478.94	26,127.87	14.61	8.25	11.80	0.59	1,315.52	2,259.72
Ce	0.48	0.14	0.18	0.13	0.35	0.18	0.25	0.05

Ce	2.25	0.07	2.11	0.09	2.17	0.04	2.08	0.06
Nd	0.25	0.03	0.00	0.00	0.20	0.15	0.17	0.28
Gd	0.20	0.12	0.08	0.03	0.19	0.11	0.12	0.08
Pb	61.86	12.05	58.93	14.30	138.77	61.71	83.34	56.27
Pb	0.00	0.00	0.00	0.00	0.00	0.00	0.00	0.00

SKC

IESES/21-1

Elements	Femur		Cranium	
	Mean	SD	Mean	SD
Al	5,892,273.07	2,415,476.48	4,682,528.98	592,148.53
P	86,257.55	11,282.93	94,823.67	15,749.09
K	468,658.83	577,559.87	779.99	8.30
Ca	246,516.00	27,644.86	273,307.78	24,412.58
V	0.17	0.29	0.15	0.18
Mn	173.47	165.95	915.10	553.13
Fe	8,619.22	2,643.48	5,762.66	2,352.29
Co	0.25	0.06	0.26	0.07
Ni	3.28	0.52	4.46	0.37
Cu	620.00	1,007.19	35.22	9.01
Zn	1,203.48	1,362.58	402.71	156.31
As	0.16	0.28	0.00	0.00
Se	0.42	0.18	0.68	0.20
Rb	1.12	0.27		
Sr	134.09	31.78	120.22	13.53
Sn	0.12	0.04	0.07	0.02
Sn	0.14	0.02	0.17	0.02
Ba	882.64	313.91	1,072.75	540.87
Ba	70.19	101.05	846.63	961.52
Ce	0.31	0.13	0.24	0.21
Ce	1,708.08	408.98	2.12	0.02
Nd	235.27	128.26	0.00	0.00
Pb	0.00	0.00	169.51	73.47
Al				

Measurements obtained for Collection of identified Skeletons of Évora

SKP1-CEIE-123

Element	CRANIUM			FEMUR			
	Mean	SD	%SD	Mean	SD	SD%	
Al	3,270,925.78	634,351.83		19.39	2,531,722.97	465,632.67	18.39
P	86,623.45	15,049.79		17.37	96,072.99	15,057.81	15.67
K	42,299.03	68,495.74		161.93	781.59	9.59	1.23
Ca	245,865.73	27,269.66		11.09	275,941.91	28,606.76	10.37
V	0.17	0.17		103.33	0.07	0.10	135.01
Mn	58.20	7.09		12.19	268.38	212.03	79.00
Fe	4,973.04	2,492.42		50.12	1,374.84	1,090.91	79.35
Co	0.17	0.05		28.10	0.13	0.01	9.77
Ni	3.41	0.47		13.88	4.01	0.50	12.53
Cu	41.67	29.59		71.01	20.10	1.84	9.18
Zn	1,391.52	340.55		24.47	681.69	307.76	45.15
As	0.00	0.00		16.11	0.06	0.09	145.20
Se	0.60	0.14		23.06	0.69	0.08	11.27
Rb	1.63	0.38		23.18	1.05	0.36	33.79
Sr	221.64	20.83		9.40	199.71	23.95	11.99
Sn	0.07	0.04		48.87	0.11	0.04	37.94
Sn	0.14	0.02		12.05	0.17	0.02	12.24
Ba	713.83	307.91		43.14	752.40	324.21	43.09
Ba	74.88	140.19		187.22	74.03	135.99	183.71
Ce	0.42	0.17		41.49	0.33	0.11	34.11
Ce	2.13	0.04		1.66	2.14	0.02	0.92
Nd	0.05	0.06		104.17	0.16	0.12	76.85
Gd	0.14	0.06		38.46	0.05	0.02	37.78
Pb	268.04	47.33		17.66	400.51	97.42	24.32
Pb	0.00	0.00		0.00	0.00	0.00	0.00

Element	HUMERUS			TIBIA			
	Mean	SD	SD%	Mean	SD	SD%	
Al	2,868,306.01	988,118.37		34.45	1,882,241.78	355,652.28	18.90
P	94,766.33	12,539.77		13.23	82,855.89	16,091.40	19.42
K	4,633.78	5,830.96		125.84	773.24	14.76	1.91
Ca	286,646.00	11,465.99		4.00	257,994.57	28,422.50	11.02
V	0.15	0.15		99.85	0.13	0.13	103.62
Mn	319.57	172.84		54.08	130.27	48.21	37.01
Fe	3,367.12	960.56		28.53	1,453.31	1,756.91	120.89
Co	0.18	0.02		13.04	0.13	0.05	36.58
Ni	5.10	0.24		4.74	4.40	0.55	12.46
Cu	56.75	45.01		79.32	28.84	8.55	29.66
Zn	2,438.88	713.46		29.25	872.75	718.93	82.38
As	0.00	0.00		15.21	0.26	0.29	110.79
Se	0.64	0.16		25.04	0.61	0.12	19.88
Rb	1.43	0.53		37.08	1.32	0.40	30.03
Sr	219.34	15.90		7.25	190.99	18.26	9.56
Sn	0.12	0.03		25.65	0.09	0.04	47.59
Sn	0.18	0.01		5.70	0.16	0.02	10.68
Ba	634.58	251.29		39.60	540.49	161.71	29.92
Ba	20.26	13.08		64.59	749.02	1,648.15	220.04
Ce	0.46	0.19		41.89	0.40	0.17	42.51
Ce	2.16	0.01		0.63	2.13	0.03	1.29
Nd	0.22	0.06		27.70	0.42	0.19	45.64
Gd	0.17	0.06		37.84	0.09	0.04	41.59
Pb	393.66	96.98		24.63	439.65	154.03	35.03
Pb	0.00	0.00		0.00	0.00	0.00	0.00

SKP2-CEIE141

Element	CRANIUM			FEMUR			
	Mean	SD	SD%	Mean	SD	SD%	
Al	3,833,018.83	684,054.14		17.85	3,639,508.01	1,377,169.39	37.84
P	98,376.97	15,042.44		15.29	78,202.44	31,975.31	40.89
K	745.16	89.60		12.02	2,607.70	4,110.87	157.64

Ca	268,140.13	37,999.25	14.17	241,072.16	87,098.72	36.13
V	0.01	0.02	172.57	0.04	0.04	91.96
Mn	95.12	78.65	82.68	198.81	247.24	124.36
Fe	1,425.45	697.56	48.94	866.07	372.82	43.05
Co	0.13	0.02	18.26	0.12	0.03	25.04
Ni	4.68	0.79	16.98	4.58	1.52	33.29
Cu	48.41	47.27	97.64	18.44	2.58	13.99
Zn	955.16	616.76	64.57	1,200.88	1,328.53	110.63
As	0.05	0.08	185.86	0.06	0.14	219.96
Se	0.73	0.17	23.45	0.68	0.21	31.08
Rb	1.78	0.33	18.38	1.90	0.72	37.69
Sr	151.98	26.06	17.15	147.78	44.17	29.89
Sn	0.08	0.05	62.74	0.09	0.03	29.61
Sn	0.16	0.02	14.96	0.14	0.06	39.13
Ba	625.79	306.56	48.99	508.23	163.45	32.16
Ba	10.56	1.43	13.51	223.84	474.14	211.82
Ce	0.29	0.04	15.49	0.27	0.12	45.07
Ce	2.01	0.24	12.10	2.12	0.04	2.02
Nd	0.26	0.16	64.18	0.23	0.17	73.46
Gd	0.09	0.03	35.95	0.14	0.09	67.43
Pb	93.60	26.17	27.96	71.65	56.28	78.54
Pb	0.00	0.00	11.77	0.00	0.00	0.00

Element	HUMERUS			TIBIA		
	Mean	SD	SD%	Mean	SD	%SD
Al	4,055,518.87	428,602.77	10.57	3,642,493.95	265,637.78	7.29
P	101,725.23	4,465.05	4.39	92,590.07	3,786.67	4.09
K	785.10	7.74	0.99	782.20	3.75	0.48
Ca	280,179.48	10,150.48	3.62	273,853.67	9,446.37	3.45
V	0.04	0.07	173.05	0.05	0.10	210.01
Mn	313.21	264.29	84.38	472.94	245.14	51.83
Fe	1,785.62	671.39	37.60	1,315.81	595.54	45.26
Co	0.15	0.01	9.36	0.13	0.01	6.77
Ni	5.02	0.33	6.67	5.02	0.21	4.20

Cu	17.34	1.03	5.93	43.94	24.75	56.33
Zn	2,661.87	985.87	37.04	1,528.39	520.57	34.06
As	0.00	0.00	132.96	0.00	0.00	0.00
Se	0.64	0.18	27.45	0.77	0.03	3.39
Rb	1.88	0.28	15.01	2.28	0.33	14.50
Sr	153.22	10.72	7.00	196.79	24.63	12.52
Sn	0.08	0.03	37.91	0.08	0.01	14.36
Sn	0.17	0.01	4.90	0.17	0.01	4.41
Ba	587.60	240.59	40.94	519.16	135.49	26.10
Ba	12.76	2.17	17.00	20.61	19.21	93.25
Ce	0.39	0.10	25.19	0.55	0.16	28.50
Ce	2.13	0.01	0.26	2.14	0.02	0.93
Nd	0.19	0.05	24.26	0.12	0.05	41.02
Gd	0.15	0.05	36.48	0.17	0.03	17.67
Pb	71.07	12.19	17.16	98.57	32.80	33.28
Pb	0.00	0.00	0.00	0.00	0.00	0.00

SKP3-CEIE 94

Element	CRANIUM			FEMUR			
	Mean	SD	SD%	Mean	SD	SD%	
Al	798,138.21	830,601.39		104.07	175,270.03	196,361.38	112.03
P	88,918.16	21,402.05		24.07	88,093.29	8,582.07	9.74
K	771.95	14.42		1.87	786.27	7.37	0.94
Ca	252,911.36	40,147.24		15.87	279,490.20	17,936.52	6.42
V	0.01	0.01		197.40	0.06	0.05	83.80
Mn	360.95	272.11		75.39	212.14	85.14	40.14
Fe	2,236.78	842.31		37.66	5,135.64	1,332.50	25.95
Co	0.15	0.03		20.86	0.23	0.04	16.83
Ni	4.13	0.64		15.60	4.60	0.42	9.24
Cu	17.91	3.25		18.16	19.00	2.13	11.20
Zn	540.87	289.16		53.46	1,489.86	530.77	35.63
As	0.01	0.02		218.53	0.00	0.00	0.00
Se	0.50	0.08		15.12	0.54	0.04	8.02
Rb	1.37	0.30		21.54	2.17	0.52	23.73

Sr	226.89	31.48	13.88	200.60	14.36	7.16
Sn	0.07	0.03	44.87	0.13	0.02	13.81
Sn	0.15	0.02	15.30	0.18	0.01	7.08
Ba	646.52	194.40	30.07	784.27	466.54	59.49
Ba	30.83	40.82	132.39	12.10	0.38	3.16
Ce	0.46	0.15	31.84	0.26	0.17	66.43
Ce	2.15	0.03	1.45	2.21	0.07	3.23
Nd	0.18	0.05	25.64	0.23	0.12	51.18
Gd	0.12	0.03	24.54	0.17	0.05	30.90
Pb	90.79	15.38	16.94	85.62	6.75	7.88
Pb	0.00	0.00	136.93	0.00	0.00	0.00

Element	HUMERUS			TIBIA		
	Mean	SD	SD%	Mean	SD	SD%
Al	241,343.52	159,847.64	66.23	447,525.47	703,390.71	157.17
P	78,746.10	6,520.61	8.28	77,253.13	20,453.26	26.48
K	763.23	8.97	1.18	4,198.58	7,647.16	182.14
Ca	231,750.30	17,372.20	7.50	240,960.99	48,214.23	20.01
V	0.03	0.05	199.05	0.12	0.16	138.93
Mn	153.09	13.83	9.03	388.54	213.14	54.86
Fe	3,763.85	1,092.53	29.03	4,377.97	1,725.19	39.41
Co	0.19	0.03	16.76	0.19	0.07	38.32
Ni	3.59	0.36	9.98	4.04	0.86	21.36
Cu	14.75	0.60	4.08	17.03	1.40	8.23
Zn	869.92	242.86	27.92	1,139.95	311.74	27.35
As	0.00	0.00	13.98	0.00	0.00	85.27
Se	0.41	0.10	24.55	0.47	0.13	27.41
Rb	1.24	0.35	28.33	1.40	0.53	37.85
Sr	162.66	18.86	11.59	187.24	32.37	17.29
Sn	0.07	0.02	29.00	0.11	0.03	24.26
Sn	0.14	0.01	8.49	0.15	0.03	22.60
Ba	914.00	279.33	30.56	960.64	737.30	76.75
Ba	11.56	0.33	2.86	11.80	0.32	2.68

Ce	0.30	0.16	53.52	0.25	0.10	42.42
Ce	2.11	0.05	2.47	2.12	0.10	4.57
Nd	0.26	0.12	47.65	0.24	0.10	40.74
Gd	0.13	0.04	30.79	0.17	0.06	35.33
Pb	122.83	28.07	22.85	90.26	15.34	16.99
Pb	0.00	0.00	0.00	0.001	0.00	0

SKNP1-CEIE-94

Element	CRANIUM			FEMUR			
	Mean	SD	SD%	Mean	SD	SD%	
Al	360,236.11	799,689.19		221.99	3,755,568.35	1,423,515.55	37.90
P	106,533.48	20,009.08		18.78	91,491.38	24,247.31	26.50
K	299,112.90	13.34		0.00	785.61	15.08	1.92
Ca	296,922.25	40,944.03		13.79	288,222.97	45,940.92	15.94
V	0.76	0.93		122.42	0.91	1.04	114.27
Mn	111.28	80.98		72.78	91.75	71.76	78.22
Fe	1,953.20	615.96		31.54	1,274.41	174.11	13.66
Co	0.17	0.03		16.99	0.15	0.02	11.69
Ni	4.98	0.86		17.34	5.03	0.78	15.45
Cu	19.37	2.14		11.05	25.99	3.75	14.41
Zn	1,414.70	899.98		63.62	1,144.59	590.03	51.55
As	0.00	0.00		22.02	0.00	0.00	28.57
Se	0.48	0.11		23.77	0.51	0.12	23.37
Rb	1.44	0.49		34.02	1.20	0.47	38.93
Sr	258.82	45.37		17.53	235.45	11.83	5.03
Sn	0.09	0.02		25.59	0.12	0.05	41.80
Sn	0.19	0.04		18.77	0.18	0.03	17.62
Ba	782.89	584.48		74.66	796.40	532.99	66.92
Ba	228.80	371.61		162.41	11.25	0.20	1.81
Ce	0.62	0.20		32.24	0.31	0.05	16.07
Ce	2.25	0.04		1.82	3.28	2.23	67.97

Nd	0.20	0.15	74.45	0.19	0.10	50.34	
Gd	0.10	0.04	44.45	0.11	0.02	20.08	
Pb	95.53	30.68	32.11	89.73	12.76	14.22	
Pb	0.00	0.00	0.00	0.00	0.00	0.00	
Element	HUMERUS			ULNA			
Al	Mean	SD	SD%	Mean	SD	SD%	
P	1,336,766.41	2,215,511.47		165.74	4,529,893.74	748,403.51	16.52
K	109,575.77	4,193.47		3.83	88,982.05	14,662.37	16.48
Ca	787.73	5.38		0.68	118,870.37	237,478.42	199.78
V	304,426.34	4,920.83		1.62	291,931.76	18,190.68	6.23
Mn	0.11	0.13	120.74	0.62	0.59	95.86	
Fe	56.76	30.64	53.99	389.07	248.19	63.79	
Co	1,427.20	470.22	32.95	2,231.07	1,496.36	67.07	
Ni	0.16	0.02	14.57	0.15	0.03	22.64	
Cu	5.20	0.12	2.39	5.23	0.22	4.14	
Zn	22.21	1.20	5.40	28.05	5.97	21.30	
As	2,759.65	1,437.28	52.08	4,901.24	4,192.02	85.53	
Se	0.00	0.00	13.98	0.00	0.00	28.83	
Rb	0.46	0.07	14.40	0.37	0.13	35.17	
Sr	1.52	0.34	22.11	1.73	0.54	31.21	
Sn	257.83	18.65	7.23	346.93	72.57	20.92	
Sn	0.12	0.04	31.53	0.15	0.03	16.82	
Ba	0.19	0.01	2.90	0.18	0.02	9.38	
Ba	1,039.50	596.66	57.40	646.28	358.63	55.49	
Ce	11.41	0.41	3.59	16,005.41	22,065.85	137.86	
Ce	0.47	0.02	4.68	0.54	0.14	26.47	
Nd	2.24	0.05	2.39	2.19	0.04	1.82	
Gd	0.14	0.07	52.14	0.10	0.06	59.40	
Pb	0.08	0.01	11.59	0.15	0.05	31.44	
Pb	77.27	15.82	20.47	129.04	27.55	21.35	
Element	0.00	0.00	0.00	0.00	0.00	0.00	

SKNP2-CEIE 43

Element	CRANIUM			FEMUR			
	Mean	SD	SD%	Mean	SD	SD%	
Al	4,221,723.73	1,270,957.84		30.11	4,467,202.45	632,354.57	14.16
P	97,272.38	20,819.03		21.40	98,455.34	17,199.98	17.47
K	779.32	10.21		1.31	785.10	10.15	1.29
Ca	282,283.85	34,724.95		12.30	294,639.34	40,028.46	13.59
V	0.28	0.25		87.61	0.48	0.44	93.09
Mn	141.09	90.23		63.95	126.54	179.59	141.92
Fe	918.11	274.37		29.88	1,182.46	489.70	41.41
Co	0.13	0.02		16.37	0.14	0.01	8.38
Ni	4.79	0.72		14.98	5.01	0.79	15.75
Cu	16.72	1.46		8.71	19.02	2.20	11.57
Zn	725.03	380.45		52.47	1,931.12	1,265.31	65.52
As	0.00	0.00		16.11	0.00	0.00	#DIV/0!
Se	0.56	0.11		20.55	0.61	0.12	20.40
Rb	1.43	0.09		6.10	1.31	0.53	40.58
Sr	154.57	22.84		14.78	168.54	31.51	18.69
Sn	0.13	0.04		27.73	0.11	0.04	37.84
Sn	0.18	0.02		13.60	0.18	0.03	14.68
Ba	974.31	207.53		21.30	638.79	228.43	35.76
Ba	10.97	0.10		0.87	11.63	0.51	4.39
Ce	0.41	0.09		22.78	0.37	0.10	27.47
Ce	2.13	0.03		1.59	2.15	0.03	1.20
Nd	0.20	0.10		51.75	0.22	0.11	50.10
Gd	0.09	0.02		24.72	0.10	0.04	36.36
Pb	65.15	14.41		22.12	72.24	9.22	12.76
Pb	0.00	0.00		0.00	0.00	0.00	136.93

Element	HUMERUS			TIBIA			
	Mean	SD	SD%	Mean	SD	SD%	
Al	4,452,686.29	1,434,266.58		32.21	4,259,356.99	1,039,741.66	24.41
P	92,997.90	21,197.49		22.79	95,465.47	10,406.25	10.90
K	778.95	16.50		2.12	776.79	10.04	1.29

Ca	263,430.98	47,254.90	17.94	281,728.18	28,103.13	9.98
V	0.74	0.52	70.92	0.16	0.30	188.94
Mn	754.68	253.87	33.64	55.83	30.62	54.85
Fe	3,669.71	1,050.44	28.62	968.57	549.72	56.76
Co	0.18	0.02	8.80	0.13	0.03	20.27
Ni	4.46	0.92	20.70	4.68	0.65	13.94
Cu	19.74	1.69	8.58	17.14	1.80	10.51
Zn	2,842.07	1,257.04	44.23	761.94	307.84	40.40
As	0.00	0.00	15.21	0.15	0.20	137.34
Se	0.37	0.17	45.79	0.58	0.11	18.91
Rb	1.13	0.31	27.58	1.44	0.34	23.53
Sr	177.57	33.00	18.59	134.78	16.31	12.11
Sn	0.12	0.03	24.08	0.09	0.02	25.65
Sn	0.16	0.03	20.23	0.18	0.02	10.30
Ba	742.09	170.41	22.96	1,043.42	627.16	60.11
Ba	11.99	0.38	3.16	61.06	111.05	181.87
Ce	0.35	0.08	23.15	0.26	0.03	12.32
Ce	2.14	0.03	1.62	2.14	0.03	1.55
Nd	0.17	0.10	61.00	0.34	0.09	26.46
Gd	0.20	0.03	13.30	0.08	0.02	28.11
Pb	106.08	19.66	18.53	79.64	6.86	8.62
Pb	0.00	0.00	0.00	0.00	0.00	0.00

SKNP3-CEIE25

Element	Mean	SD	SD%	Mean	SD	SD%
Al	4,195,941.18	1,412,723.09	33.67	7,463,833.94	2,076,960.14	27.83
P	75,558.80	5,949.60	7.87	82,433.13	20,757.76	25.18
K	769.38	8.68	1.13	780.02	19.12	2.45
Ca	241,726.11	22,675.89	9.38	263,993.66	52,010.19	19.70
V	0.03	0.04	141.72	0.31	0.30	97.83
Mn	75.82	46.85	61.79	74.33	31.44	42.30
Fe	2,457.91	785.67	31.96	4,139.65	1,275.95	30.82

Co	0.15	0.03	20.15	0.20	0.06	28.74
Ni	4.01	0.57	14.30	4.36	0.97	22.18
Cu	20.30	2.60	12.80	35.82	11.42	31.87
Zn	720.77	353.00	48.98	685.84	266.02	38.79
As	0.01	0.03	207.63	0.06	0.13	219.63
Se	0.55	0.07	13.12	0.54	0.13	24.30
Rb	1.56	0.21	13.51	1.92	0.24	12.51
Sr	189.88	28.40	14.96	204.47	36.51	17.86
Sn	0.08	0.03	29.74	0.11	0.03	26.62
Sn	0.15	0.01	9.89	0.16	0.03	20.28
Ba	696.94	306.75	44.01	695.13	357.68	51.46
Ba	13.60	4.55	33.43	17.31	8.08	46.68
Ce	0.36	0.13	36.37	0.56	0.31	55.34
Ce	2.14	0.03	1.51	2.15	0.05	2.20
Nd	0.35	0.12	34.89	0.21	0.16	75.29
Gd	0.09	0.04	41.14	0.09	0.03	28.61
Pb	59.97	10.37	17.28	77.34	23.40	30.25
Pb	0.00	0.00	0.00	0.00	0.00	0.00

Element	Mean	SD	SD%	Mean	SD	SD%
Al	5,632,389.49	2,233,802.99	39.66	9,787,371.35	1,185,810.15	12.12
P	73,895.33	24,703.17	33.43	78,534.42	27,187.44	34.62
K	5,401.26	7,481.18	138.51	2,307,404.18	5,127,627.45	222.22
Ca	232,847.85	63,189.02	27.14	269,171.56	42,881.84	15.93
V	0.07	0.13	187.05	1.61	1.89	117.75
Mn	53.63	10.28	19.17	145.00	109.32	75.40
Fe	3,411.16	663.41	19.45	6,992.50	3,507.99	50.17
Co	0.17	0.04	24.88	0.24	0.04	16.55
Ni	3.89	1.13	29.04	4.84	0.26	5.38
Cu	27.44	10.08	36.72	40.47	18.45	45.58
Zn	1,330.32	579.75	43.58	5,501.88	9,555.40	173.68
As	0.03	0.06	214.56	0.00	0.00	#DIV/0!
Se	0.55	0.16	28.80	0.48	0.03	6.52

Rb	1.65	0.13	7.91	2.24	1.19	53.03
Sr	163.61	39.18	23.95	232.67	19.30	8.30
Sn	0.09	0.02	26.51	0.16	0.05	32.78
Sn	0.14	0.04	26.98	0.16	0.03	19.23
Ba	636.36	100.37	15.77	813.08	201.92	24.83
Ba	11.81	0.18	1.52	3,932.51	5,503.04	139.94
Ce	0.20	0.10	48.54	0.60	0.18	30.51
Ce	2.13	0.04	1.71	2.23	0.07	3.27
Nd	0.25	0.13	53.86	0.17	0.14	85.15
Gd	0.09	0.02	18.34	0.18	0.14	81.31
Pb	67.95	21.58	31.76	102.36	12.15	11.87
Pb	0.00	0.00	0.00	0.00	0.00	#DIV/0!

MEAN, SD, SD% OF INDIVIDUALS

Element	SKP1			SKP2		
	MEAN	SD	SD%	MEAN	SD	SD%
P	90,079.66	6,377.39	7.08	91,231.74	7,283.06	7.98
Ca	266,612.05	18,194.10	6.82	273,527.50	14,477.51	5.29
Mn	194.10	120.84	62.25	239.41	97.92	40.90
Fe	2,792.08	1,721.25	61.65	2,065.09	1,128.27	54.64
Co	0.12	0.03	22.40	0.14	0.03	20.45
Ni	4.23	0.03	0.64	4.51	0.55	12.18
Cu	36.84	15.96	43.32	35.23	19.14	54.34
Zn	1,346.21	787.77	58.52	1,331.11	964.10	72.43
Sr	207.92	14.97	7.20	203.35	14.52	7.14
Ba	660.33	93.74	14.20	642.49	106.18	16.53
Ba	229.55	347.26	151.28	281.10	406.12	144.47
Nd	0.21	0.16	72.63	0.27	0.14	51.82
Gd	0.11	0.05	47.70	0.10	0.06	59.32
Pb	375.47	74.43	19.82	411.27	24.81	6.03

SKP3

SKNP1

Element	MEAN			SD			SD%		
	MEAN	SD	SD%	MEAN	SD	SD%	MEAN	SD	SD%
P	59,209.77	51,615.73	87.17	99,145.67	10,412.40	10.50			
Ca	181,549.13	157,871.57	86.96	295,375.83	7,007.81	2.37			
Mn	170.70	133.34	78.11	162.21	152.91	94.27			
Fe	1,627.36	1,659.60	101.98	1,721.47	447.16	25.98			
Co	7.57	12.84	169.70	0.16	0.01	5.25			
Ni	3.38	2.40	70.96	5.11	0.13	2.45			
Cu	42.97	13.95	32.48	23.90	3.87	16.20			
Zn	1,123.38	1,209.81	107.69	2,555.04	1,716.22	67.17			
Sr	139.18	115.17	82.75	274.76	49.31	17.95			
Ba	396.42	334.35	84.34	816.27	163.54	20.03			
Ba	306.85	388.49	126.61	4,064.22	7,961.45	195.89			
Nd	24.43	41.75	170.92	0.16	0.05	28.69			
Gd	15.99	27.47	171.80	0.11	0.03	26.81			
Pb	284.38	230.26	80.97	97.89	22.12	22.60			

Element	SKNP2			SKNP3			SD		
	MEAN	SD	SD%	MEAN	SD	SD%	MEAN	SD	SD%
P	96,683.07	11,235.68	11.62	66,189.44	58,230.27	87.98			
Ca	294,860.35	8,489.39	2.88	198,786.82	172,265.70	86.66			
Mn	179.19	182.60	101.90	180.03	182.00	101.09			
Fe	1,644.23	513.93	31.26	1,228.08	1,115.95	90.87			
Co	0.15	0.01	3.31	1.85	2.94	158.72			
Ni	5.15	0.11	2.11	4.29	1.59	37.11			
Cu	25.42	2.96	11.65	22.15	5.92	26.74			
Zn	2,935.16	1,884.46	64.20	2,576.02	2,422.26	94.03			
Sr	280.07	58.98	21.06	207.57	170.15	81.97			
Ba	827.39	198.43	23.98	568.61	514.15	90.42			
Ba	5,342.69	9,234.19	172.84	5,404.24	9,181.35	169.89			
Nd	0.15	0.05	30.89	9.64	16.49	171.01			
Gd	0.11	0.04	30.79	9.01	15.41	170.99			
Pb	98.68	27.02	27.38	76.30	53.23	69.76			

